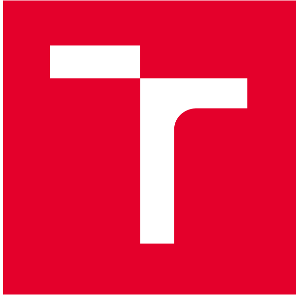

BRNO UNIVERSITY OF TECHNOLOGY

VYSOKÉ UČENÍ TECHNICKÉ V BRNĚ

FACULTY OF MECHANICAL ENGINEERING

FAKULTA STROJNÍHO INŽENÝRSTVÍ

INSTITUTE OF PHYSICAL ENGINEERING

ÚSTAV FYZIKÁLNÍHO INŽENÝRSTVÍ

PREPARATION AND PROPERTY MEASUREMENTS OF GAN NANOCRYSTALS ON SI(111) 7X7

PŘÍPRAVA A MĚŘENÍ VLASTNOSTÍ GAN NANOKRYSTALŮ NA SI(111) 7X7

MASTER'S THESIS

DIPLOMOVÁ PRÁCE

AUTHOR Bc. Jakub Šťastný

AUTOR PRÁCE

SUPERVISOR doc. Ing. Jindřich Mach, Ph.D.

VEDOUCÍ PRÁCE

BRNO 2025

BRNO UNIVERSITY OF TECHNOLOGY
FACULTY OF MECHANICAL ENGINEERING

Assignment Master's Thesis

Institut:	Institute of Physical Engineering
Student:	**Bc. Jakub Šťastný**
Degree programm:	Physical Engineering and Nanotechnology
Branch:	no specialisation
Supervisor:	**doc. Ing. Jindřich Mach, Ph.D.**
Academic year:	2024/25

As provided for by the Act No. 111/98 Coll. on higher education institutions and the BUT Study and Examination Regulations, the director of the Institute hereby assigns the following topic of Master's Thesis:

Preparation and property measurements of GaN nanocrystals on Si(111) 7x7

Brief Description:

GaN is a direct–transition semiconductor that appears to hold great promise for the semiconductor industry. This material can be produced by a unique low–temperature process in which low–energy nitrogen ions interact with atomic beams of gallium (Ga). The low temperature of the process allows the growth of ultrathin nanocrystals (2D) on a Si(111)7x7 substrate. The setting of the physical conditions of the experiment plays an important role in their growth.

Master's Thesis goals:

1) Conduct a research study on the topic of 2D GaN and its assumed properties.
2) Carry out a series of depositions of GaN nanocrystals on a Si(111) 7x7 substrate for different physical properties of the incident ions
nitrogen.
3) Carrying out structural and optical analysis of prepared samples (AFM, SEM, Ramanova spectroscopy, photoluminescence,...)
4) perform experiments to transfer GaN nanocrystals

Recommended bibliography:

MANIŠ, Jaroslav, Jindřich MACH, Miroslav BARTOŠÍK, et al. Low temperature 2D GaN growth on Si(111) 7 × 7 assisted by hyperthermal nitrogen ions. Nanoscale Advances. 2022, 4(17), 3549-3556. ISSN 2516-0230. Dostupné z: doi:10.1039/D2NA00175F

MACH, Jindřich, Jakub PIASTEK, Jaroslav MANIŠ, et al. Low temperature selective growth of GaN single crystals on pre-patterned Si substrates. Applied Surface Science. 2019, 497. ISSN 01694332. Dostupné z: doi:10.1016/j.apsusc.2019.143705

Deadline for submission Master's Thesis is given by the Schedule of the Academic year 2024/25

In Brno,

L. S.

prof. RNDr. Tomáš Šikola, CSc. Director of the Institute	doc. Ing. Jiří Hlinka, Ph.D. FME dean

Summary

This thesis examines the growth of two-dimensional gallium nitride (2D GaN) nanocrystals on Si(111) substrate with 7x7 surface reconstruction using the Low-Temperature Droplet Epitaxy (LTDE) method. 2D GaN holds promise for optoelectronic applications, but its synthesis remains challenging. The study focuses on how the incident angle of nitrogen ions and their energy during the postnitridation process influence nanocrystal growth.

Characterisation using SEM, AFM, Raman, PL, CL, 4D-STEM, XPS, and UHV-SEM revealed that these parameters could significantly affect morphology and optical properties. A key finding is the well-defined etching of the Si(111) 7×7 surface in the place of triangular GaN nanocrystals, caused by nitrogen ion impact and high temperature.

Abstrakt

Tato diplomová práce zkoumá růst dvoudimenzionálních nanokrystalů nitridu gallitého (2D GaN) na substrátu Si(111) s povrchovou rekonstrukcí 7x7 pomocí nízkoteplotní kapkové epitaxe (LTDE). 2D GaN vykazuje potenciál pro optoelektronické aplikace, ale jeho příprava je stále problematická. Tato studie se zabývá vlivem úhlu dopadu dusíkových iontů a jejich energie v průběhu procesu postnitridace na růst nanokrystalů.

Charakterizace pomocí SEM, AFM, Ramana, PL, CL, 4D-STEM, XPS a UVS-SEM odhalila, že tyto parametry by mohly důrazně ovlivňovat morfologii a optické vlastnosti. Klíčovým objevem je přesné leptání povrchu Si(111) 7x7 na místě trojúhelníkových nanokrystalů GaN, způsobeno dopadem dusíkových iontů a vysokou teplotou.

Keywords

2D GaN, Si(111), surface reconstruction, LTDE, nanocrystal growth, nitridation, etching

Klíčová slova

2D GaN, Si(111), povrchová rekonstrukce, LTDE, růst nanokrystalu, nitridace, leptání

STASTNY, J. *Preparation and property measurements of GaN nanocrystals on Si(111) 7x7.* Brno University of Technology, Faculty of Mechanical Engineering, Brno 2025. 84 s. Supervised by doc. Ing. Jindřich Mach, Ph.D.

I hereby declare that I have written my master's thesis on the topic of *Preparation and property measurements of GaN nanocrystals on Si(111) 7x7* independently, under the supervision of doc. Ing. Jindřich Mach, Ph.D. and using the literature and other sources of information all listed in the bibliography. Additionally, I declare that this work was reviewed with the assistance of ChatGPT, a large language model developed by OpenAI, and Grammarly, an AI-powered writing assistant. These tools were used solely for improving grammar and stylistic purposes.

Bc. Jakub Šťastný

I would like to express my sincere gratitude to my supervisor, doc. Ing. Jindřich Mach, Ph.D., for the professional guidance throughout my work. I would also like to thank the whole graphene group, especially Ing. Vojtěch Mikerásek and Ing. Jakub Piastek, Ph.D., for helping me with the XPS and UHV-SEM experiments. I would also like to thank my colleague Bc. Viktor Bajo for the 4D-STEM measurements. Last but not least, I want to give my gratitude to my family and friends who supported me throughout my whole life and continue even to this moment.

CzechNanoLab project LM2023051 funded by MEYS CR is gratefully acknowledged for the financial support of the measurements/sample fabrication at CEITEC Nano Research Infrastructure.

Bc. Jakub Šťastný

Contents

Introduction **3**

1. Two-dimensional materials **5**
1.1. Properties of 2D materials . . . 5
1.1.1. Tunning the properties of 2D materials . . . 6
1.1.2. Examples of 2D materials and their properties . . . 8
1.2. Applications and limitations of 2D materials . . . 11
1.3. Preparation of 2D materials . . . 13
1.3.1. Mechanical exfoliation . . . 13
1.3.2. Chemical vapor deposition . . . 15
1.3.3. Physical vapor deposition . . . 16
1.3.4. Molecular beam epitaxy . . . 16
1.4. Transfer of low-dimensional structures . . . 17
1.4.1. Wet-transfer . . . 18
1.4.2. Dry-transfer . . . 19

2. Two-dimensional Gallium Nitride **24**
2.1. Properties of 2D GaN . . . 24
2.2. 2D GaN preparation methods . . . 26
2.2.1. Migration-enhanced encapsulation growth . . . 27
2.2.2. Graphene-oxide-assisted synthesis . . . 28
2.2.3. Growth of 2D GaN single crystals on liquid metals . . . 29
2.2.4. Two-step method . . . 30
2.2.5. Plasma-enhanced chemical vapor deposition . . . 31
2.2.6. Sonochemical exfoliation . . . 33
2.2.7. Low-temperature droplet epitaxy . . . 33

3. The preparation of 2D GaN via low-temperature droplet epitaxy (LTDE) **36**
3.1. The preparation of Si(111) 7×7 . . . 36
3.2. The deposition and postnitridation process . . . 38

4. Characterisation of LTDE-grown GaN nanocrystals **39**
4.1. The effect of different postnitridation angles . . . 39
4.2. The effect of different ion energies . . . 44
4.2.1. Evolution of chemical composition . . . 44
4.2.2. Morphology of GaN nanostructures . . . 46
4.2.3. Optical and structural characterisation . . . 49
4.3. Investigation of the Si(111) 7×7 surface etching . . . 51
4.3.1. Time-dependent postnitridation . . . 52
4.3.2. Thermal annealing of GaN nanostructures . . . 55

5. The transfer of GaN nanocrystals **58**

Conclusion **62**

Literature **64**

List of abbreviations **82**

Introduction

Bulk materials, such as silicon, have dominated the semiconductor industry for decades. However, with the rapid development of electronic and optical nanodevices, these materials are increasingly unable to meet the growing demand for higher performance and smaller dimensions [1, 2]. This has driven the search for novel materials with extraordinary physical and chemical properties.

Since the first successful isolation of a monolayer of graphite, known as graphene, in 2004 [3], two-dimensional (2D) materials have attracted considerable attention as potential alternatives to conventional bulk materials [4, 5]. Their unique electrical, optical, and mechanical properties, combined with their atomic-scale thickness, make them promising for a wide range of scientific and industrial applications, including nanoelectronics, optoelectronics, medicine, and renewable energy [6–17]. Moreover, many of their properties can be tailored to suit specific applications.

Beyond graphene, other 2D materials such as phosphorene [18, 19], transition metal dichalcogenides (TMDs) [20–22], and particularly transition metal nitrides (TMNs) [23–25], have shown great promise due to characteristics such as wide bandgaps and high thermal stability [18, 20, 23]. Among TMNs, two-dimensional gallium nitride (2D GaN) stands out with a tunable bandgap ranging from 3.1 eV to 5.6 eV [26], making it a strong candidate for ultraviolet (UV) nano-optical applications [27, 28].

The first synthesis of 2D GaN was achieved via graphene encapsulation in 2016 [29]. However, due to the presence of the encapsulating layer, the resulting 2D GaN nanostructures are difficult to transfer and integrate into nanodevices. To address this limitation, numerous growth methods have since been developed to produce high-quality, large-area gallium nitride (GaN) thin films and nanocrystals [26, 27, 30–32]. Each technique presents its own set of advantages and drawbacks, including the requirement for high temperatures, the low quality of the resulting nanostructures, or the use of toxic precursors, all of which complicate the synthesis process.

To overcome these challenges, our research group has developed a novel method called low temperature droplet epitaxy (LTDE) [28], which enables the growth of high-quality GaN nanocrystals under ultra-high vacuum (UHV) conditions. This technique offers precise control over the growth parameters while avoiding many of the issues associated with conventional high-temperature methods.

Manis et al. utilised the LTDE growth method to synthesise crystalline 2D GaN nanostructures on Si(111) substrates exhibiting the 7×7 surface reconstruction [28]. This reconstruction plays a crucial role in the growth process, as it facilitates the surface transformation necessary for the formation of nanocrystals. The resulting nanostructures differ structurally from bulk wurtzite GaN, confirming the theoretically predicted 2D configuration. Their chemical composition was investigated using x-ray photoelectron spectroscopy (XPS) and energy-dispersive x-ray spectroscopy (EDX).

However, the growth process is highly sensitive to various parameters, including the base pressure in the UHV chamber, the energy of nitrogen ions, the particle flux from

the sources, the substrate temperature, and the incident angle of nitrogen ions during the nitridation of gallium.

To further investigate these factors, I focused on the influence of ion incidence angle in my bachelor's thesis [33]. Using the same LTDE growth procedure, I synthesised 2D GaN nanocrystals on Si(111) 7×7 substrates and analysed how the angle of nitrogen ion incidence affects both the dimensions and preferential growth direction of the resulting structures. Notably, when the ion beam was aligned perpendicular to the substrate surface during nitridation, etching effects were observed, resulting in nanometer-deep holes formed beneath the nanocrystals.

In comparison to the bachelor's thesis, this work focuses primarily on the influence of nitrogen ion energy on the growth of GaN nanocrystals, aiming to further deepen the understanding of the LTDE process. In addition, it investigates the effect of ion-induced etching on both the nanocrystals and the underlying substrate. Structural characterisation was performed using scanning electron microscopy (SEM) and atomic force microscopy (AFM). The optical response of LTDE-grown GaN nanostructures was analysed via Raman spectroscopy, photoluminescence (PL), and cathodoluminescence (CL) while their chemical composition was examined using XPS. Additionally, the structure of GaN nanocrystals was studied using four-dimensional scanning transmission electron microscopy (4D-STEM). Together, these techniques provide a comprehensive insight into how growth conditions affect the structure, properties, and stability of 2D GaN nanocrystals. To enable electrical measurements and facilitate the integration of 2D GaN nanocrystals into devices, a dry-transfer process onto a SiO_2 substrate was performed, exploring several different techniques.

The structure of this thesis is organised as follows:

The first chapter focuses on the importance of 2D materials for advanced applications. It introduces the general properties of 2D materials and provides several examples of commonly studied representatives. In addition, it discusses the methods by which these properties can be tuned to suit specific applications. Existing applications that already utilise 2D materials are also reviewed. Finally, the chapter presents an overview of the typical preparation methods for 2D materials and transfer techniques, which are crucial for their integration into nanodevices.

The second chapter discusses the key properties of 2D GaN, both those theoretically predicted and those experimentally measured. It also compares the bulk structure of GaN with its 2D form and shows the potential applications of 2D GaN nanostructures. In the second part, various methods for the growth of GaN thin films and nanocrystals are described, highlighting their main advantages and disadvantages. Finally, the LTDE method is introduced and compared to these techniques, as it is the primary approach used in this work.

In the third chapter, the LTDE method adopted for this work is described, including the modifications made to the growth parameters. The entire LTDE growth process is outlined step-by-step, beginning with the preparation of the Si(111) substrate and the formation of the 7×7 surface reconstruction, followed by the deposition of Ga droplets, and concluding with the postnitridation process.

The fourth chapter focuses on the analysis of the nanostructures grown by the LTDE method. As the work on my bachelor's thesis continued even after graduation to complete the experiments on the effect of the nitrogen ion incident angle on 2D GaN nanocrystals, these results are presented first. The main part of this thesis is then introduced, focusing on the effect of nitrogen ion energy on the growth of 2D GaN. This analysis combines topography measurements (SEM, AFM), evaluation of surface cleanliness and chemical composition via XPS, optical characterisation using Raman spectroscopy, photoluminescence (PL), and cathodoluminescence (CL), and crystalline structure using 4D-STEM. In addition, the experiments exploring the ion-induced etching of GaN nanocrystals and the Si(111) substrate are discussed.

The final chapter presents the experiments focused on the dry-transfer of 2D GaN nanocrystals onto a SiO_2 substrate. Different transfer techniques were tested, including the use of transparent adhesive tape, polydimethylsiloxane (PDMS) stamps, and common nail polish, and their effectiveness is compared and discussed.

1. Two-dimensional materials

With the rapid advancement of the electronics and optoelectronics industries, we are increasingly approaching the physical and technological limits of existing materials [1, 2]. The continuous miniaturisation of electronic devices and the growing demand for higher performance drive scientists worldwide to explore novel materials with unique, outstanding, and tunable physical properties. Among these, 2D materials have emerged as particularly promising candidates.

A pivotal moment in materials science occurred in 2004 when A. K. Geim and K. S. Novoselov experimentally demonstrated the existence of graphene [3]. Their groundbreaking discovery earned them the 2010 Nobel Prize in Physics [34]. The isolation of a graphene monolayer through mechanical exfoliation reignited interest in two-dimensional (2D) materials, which are distinguished by their unique internal structure and exceptional properties [24, 35, 36]. Although the existence of 2D materials had been predicted in the previous century [37], free-standing monolayers were long considered thermodynamically unstable [3, 38]. The discovery of graphene disproved these assumptions and opened the door to the exploration of other van der Waals materials, such as transition metal dichalcogenides (e.g. molybdenum disulfide) [20–22], phosphorene [18, 19], or transition metal nitrides [23–25].

Despite the immense potential of 2D materials, their synthesis and integration into practical applications remain challenging [39]. However, several fabrication techniques have been developed to address these obstacles, such as mechanical exfoliation [3, 40–42], chemical vapor deposition (CVD) [43–45], or molecular beam epitaxy (MBE) [45], and some applications have already been demonstrated, for example single-layer molybdenum disulfide (MoS_2) transistor [46], or high sensitivity detectors of visible or UV light [8]. This chapter explores the key physical properties of 2D materials, current synthesis methods, and their existing applications across various scientific and technological fields. In the last part, methods to transfer 2D materials will be described.

1.1. Properties of 2D materials

The characteristics of 2D materials differ significantly from their bulk counterpart. Their structure consists of only a few atomic layers, each with strong covalent in-plane bonding, held together by weak van der Waals interactions [7, 22]. This low-dimensional nature gives rise to distinct electronic, optical, and mechanical properties, making 2D materials highly attractive for advanced applications.

One of the most defining characteristics of these materials is their electronic band structure, which determines their electronic and optical behaviour [47, 48]. With the exception of undoped graphene, which exhibits unprecedented properties, most 2D materials are semiconductors or insulators [18, 20, 23]. The nature of their bandgap directly influences conductivity and optical absorption, making them promising candidates for nanoelectronics and optoelectronics. Furthermore, 2D materials display remarkable me-

chanical properties, including flexibility, strength, and elasticity due to their atomically thin structure [49, 50]. However, all of these properties are highly dependent on the material quality and cleanliness, as impurities and defects can significantly alter their behaviour. By precisely controlling the synthesis process, it is possible to tailor their properties, unlocking a wide range of possibilities for advanced technological applications.

1.1.1. Tunning the properties of 2D materials

Beyond the intrinsic properties of 2D materials, they offer exceptional tunability. Several factors influence their characteristics, including material thickness, defects, doping, impurities, and strain, all of which will be discussed in the following section.

A major distinction exists between a single monolayer and multiple stacked layers, as even a slight increase in thickness can significantly alter the material's electrical, optical, and mechanical behaviour [51, 52]. Depending on the material, reducing its thickness can lead to a transition from an indirect to a direct bandgap (or the other way around), along with a change in bandgap width [53–55].

Defects in the crystalline structure are generally considered undesirable due to their uncontrollable and unpredictable influence on material properties [56]. Figure 1 shows a few examples of these defects and dislocations. However, through precise engineering, these defects can be exploited to fine-tune material characteristics. For example, vacancies (missing atoms in the crystalline structure) can modify the electrical and chemical properties of the material by inducing an electric potential that alters the electron distribution [57, 58]. Purposefully engineered vacancies in 2D materials have been shown to enhance their electrochemical activity, making them promising electrocatalysts for hydrogen evolution [59].

Another approach to modifying 2D material properties is doping, which involves incorporating a controlled amount of impurities (dopants) into the material [47]. Doping plays a crucial role in electronic device fabrication, allowing for the adjustment of key properties such as carrier mobility. However, doping 2D materials and van der Waals heterostructures (layered 2D heterostructures) remains challenging, as the introduction of foreign particles can damage the atomically thin layer [61]. To address this issue, researchers are developing advanced techniques, such as remote-controlled charge transfer from molecular dopants [62] and laser-assisted doping [63]. Despite efforts to achieve a clean synthesis, unwanted impurities are inevitable. The objective is to minimise their presence while ensuring that only the desired dopants remain.

Strain engineering offers another method for tailoring the properties of 2D materials. Without the external strain applied, most 2D materials share a honeycomb-like Bravais lattice defined by primitive unit cells and a set of basis atoms [47]. However, applying external strain deforms this lattice, leading to macroscopic changes that influence the material's microscopic properties, including its electronic band structure [64–67]. For instance, density functional theory (DFT) calculations predict that increasing tensile strain in a MoS_2 monolayer results in a decreased bandgap width, and even suggest that a transition from semiconductor to metallic behaviour could be achieved under extreme strain

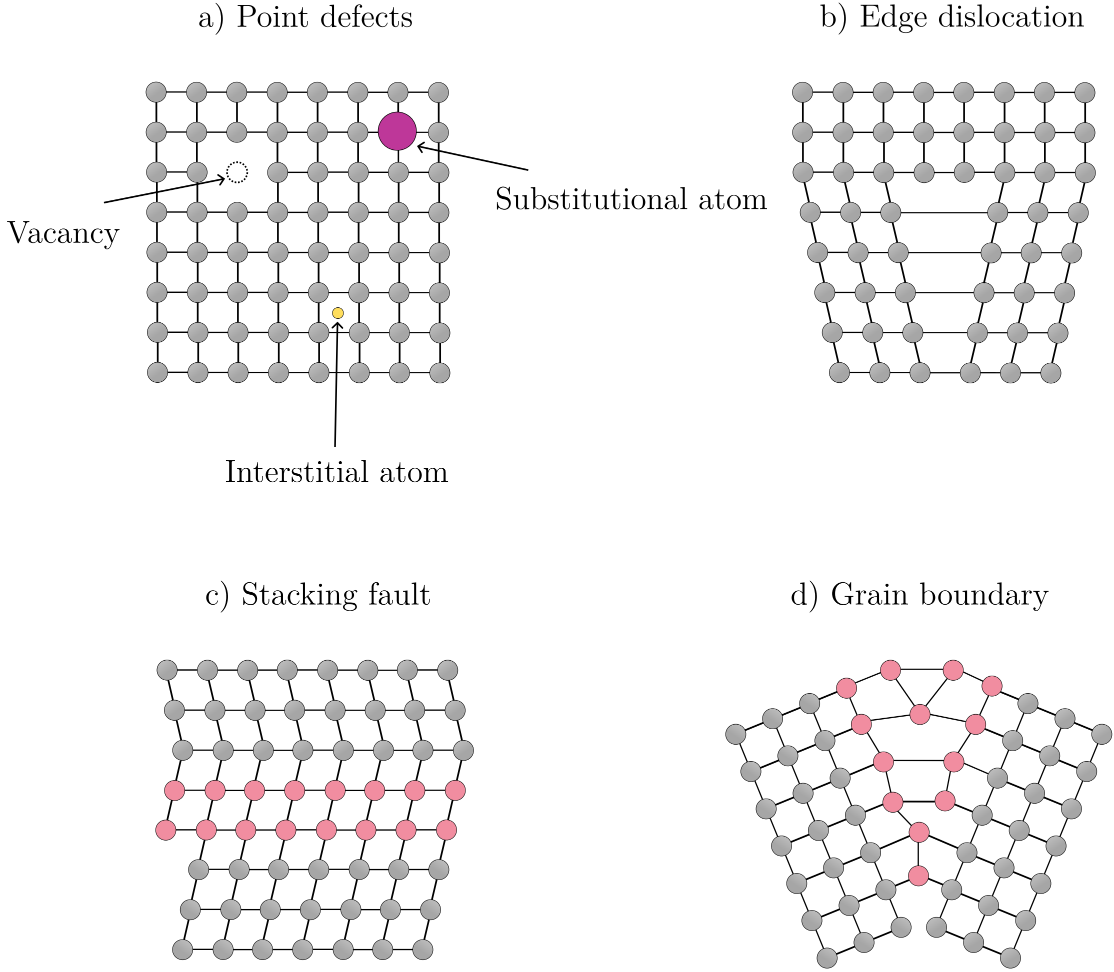

Figure 1: The schematic of crystalline defects and dislocations: a) point defects, b) edge dislocation, c) stacking fault, d) grain boundary. Adapted from [60].

[68]. Similarly, for graphene, the application of external strain can induce a bandgap in its otherwise gapless electronic structure, overcoming a major limitation for optoelectronic applications [69].

Even with their unique properties, free-standing monolayers of 2D materials are often challenging to utilise directly [70, 71], because they are commonly incorporated into van der Waals heterostructures, where they interact with other 2D or bulk materials [51, 52, 71]. Interface engineering expands the potential applications of 2D materials, as different stacking configurations yield distinct heterostructure properties. However, this process tunes the properties of the heterostructure rather than the 2D material itself. The interface between a 2D material and its substrate is particularly crucial for material growth. If the lattice constant of the substrate differs significantly from that of the 2D material, the resulting monolayer may exhibit poor quality, or may not form at all [72, 73]. Thus, the choice of substrate is critical in ensuring high-quality material synthesis.

By employing the aforementioned techniques, researchers can design customised materials tailored for specific applications. The extraordinary intrinsic properties and versatile tunability of 2D materials make them one of the most exciting topics in modern materials science.

1.1.2. Examples of 2D materials and their properties

Since the discovery of graphene, numerous other 2D materials have been identified, characterised, and integrated into various applications, and many more are still being discovered today. Some of the most prominent 2D materials include graphene [3], graphene-like materials (such as phosphorene [18], silicene [74], and germanene [75]), transition metal dichalcogenides (TMDs) [76], and transition metal nitrides (TMNs) [24]. Their fundamental properties will be discussed in the following sections.

However, it is important to note that the reported properties of 2D materials can vary significantly due to differences in growth methods, measurement techniques, and theoretical calculation approaches. These variations may lead to inconsistencies in reported values and characteristics for the same material, highlighting the need for careful interpretation and standardised methodologies in experimental and theoretical studies.

Graphene

A single layer of graphite, composed of carbon atoms arranged in a honeycomb lattice, is considered the marvel of 2D materials. Its unique combination of exceptional electronic and mechanical properties makes graphene stand out. In its electronic band structure, the conduction and valence bands meet at a single point known as the Dirac point [47]. Near this point, the energy bands form a conical shape, and the charge carriers behave like massless relativistic particles with an effective speed of $c_{ef} \sim 10^6$ m/s [35]. This relativistic-like behaviour of electrons gives rise to remarkable phenomena such as the anomalous quantum Hall effect [77, 78].

Graphene exhibits extremely high electron mobility at room temperature, typically exceeding $2\,000\,\mathrm{cm^2/V\cdot s}$ [35]. Due to its large lateral extension and strong field-effect response, graphene can be contacted relatively easily [3, 35]. With recent advancements in graphene preparation techniques, the purity and crystalline quality of monolayers have improved significantly, further enhancing carrier mobility, often surpassing $200\,000\,\mathrm{cm^2/V\cdot s}$ [79, 80]. These outstanding electrical properties, combined with the ease of tuning the Fermi level through doping, make graphene a highly promising material for applications in field-effect transistors (FETs) [81–83].

When reduced to a single atomic layer, graphite becomes highly transparent, with transparency decreasing linearly with thickness [35]. The unique combination of high electrical conductivity, mechanical strength, chemical stability, and optical transparency makes graphene an ideal candidate for transparent electrodes in devices such as solar cells [13, 84, 85]. Graphene also has extraordinary mechanical properties, it possesses a Young's modulus of approximately 1 000 GPa and exhibits high flexibility [86, 87].

Graphene analogues

A few years after the experimental isolation of graphene, a wide range of graphene-like materials was discovered. One of the earliest was phosphorene, a monolayer of black phosphorus, which shares the same honeycomb lattice structure as graphene but differs

significantly in geometry due to its nonplanar, ridged surface [18, 19, 88]. Phosphorene exhibits two principal crystallographic orientations: armchair and zigzag. Its intrinsic anisotropy governs its electrical, optical, chemical, and mechanical properties, making it particularly attractive for next-generation nanodevices [18, 19].

Like other 2D materials, phosphorene features a tunable bandgap width ranging from 0.3 eV [18] to 2.0 eV [36]. It offers a balanced set of material properties that often addresses the limitations of other 2D systems. For example, while graphene exhibits the highest carrier mobility among 2D materials, its zero bandgap width results in a low on-off current ratio [18], hindering its use in FETs. Phosphorene, on the other hand, combines moderate carrier mobility of approximately $1\,000\,\mathrm{cm}^2/\mathrm{V}\cdot\mathrm{s}$ [18, 36, 89] at room temperature with a high on-off ratio in the range of 10^3 to 10^5 [90], making it an ideal candidate for FETs, solar cells, and other optoelectronic devices.

Silicene [74] and germanene [75] (monolayer forms of silicon and germanium, respectively) have also gained significant attention due to their semiconducting behaviour and potential to exhibit the quantum spin Hall effect [75, 91, 92]. Their structures are reminiscent of phosphorene, leading to anisotropic material properties [74, 75]. However, both silicene and germanene are chemically unstable in ambient conditions and degrade rapidly once removed from UHV environments [93, 94]. Despite this limitation, techniques such as passivation or encapsulation have been developed to stabilise these materials [95, 96], enabling their use in various nanodevices.

Transition metal dichalcogenides

Two-dimensional forms of TMDs are promising alternatives to graphene and may even surpass it in some applications, thanks to their remarkable versatility, which spans from metallic (e.g., niobium disulfide (NbS_2) and vanadium diselenide (VSe_2)) to insulating (e.g., hafnium disulfide (HfS_2)) [76, 97, 98] behaviour. The monolayer structure of TMDs with the general formula MX_2 (where M is a transition metal from groups IVB to VIII and X corresponds to S, Se, or Te) [97] consists of three atomic layers bonded in an X–M–X configuration via covalent bonds. These monolayers are typically a few ångströms thick and are stacked by van der Waals interactions, making isolation of individual layers feasible [97].

TMDs feature a tunable band structure that varies with the number of layers. Their broad compositional variety results in a rich palette of electrical, optical, and mechanical properties. A well-known example is MoS_2, first described by L. Pauling in 1923 [37], which has a direct bandgap of 2.16 eV in monolayer form [99]. In contrast, bulk MoS_2 exhibits an indirect bandgap of 0.88 eV [76]. Metallic phases of 2D TMDs offer excellent electrical conductivity and act as efficient trapping sites for photogenerated charges—properties that are advantageous in photocatalysis, where they can enhance quantum efficiency [98].

Mechanically, TMD monolayers rank among the most flexible yet stiff materials known. Compared to their bulk counterparts, ultrathin TMD films typically exhibit a higher Young's modulus and greater breaking strength, owing to the reduced number of defects

and stacking faults [22]. Furthermore, TMDs are ideal candidates for strain engineering [76, 100]. Tensile strain applied to these materials modifies key characteristics such as the bandgap, charge carrier localisation, and effective mass, allowing for fine-tuning of their physical properties for targeted applications [76, 100].

Transition metal nitrides

The group of TMNs is primarily known for its wide bandgap properties [22, 24, 101]. Key representatives include boron nitride (BN) [24], aluminium nitride (AlN) [102], indium nitride (InN) [103], and GaN [29]. GaN, being the primary focus of this thesis, is discussed in detail in Chapter 2.1.

These TMNs share several structural characteristics. They all adopt a stable honeycomb lattice similar to that of graphene, consisting of alternating nitrogen and metal atoms (B, Al, Ga, or In) [22, 101]. Strong in-plane covalent bonds ensure structural integrity, while weak van der Waals forces act between the layers. The bandgap width, in the absence of defects and impurities, decreases with increasing atomic mass from approximately 5.95 eV for hexagonal boron nitride (h-BN) [24, 104] to around 1.2 eV [105] for hexagonal indium nitride (h-InN), spanning from excellent insulators to semiconductors. While h-BN has been widely studied and implemented, 2D AlN and InN have primarily been investigated theoretically, with experimental realisations remaining a challenge [102, 103].

Bulk boron nitride is notable for its exceptional properties: high mechanical strength, chemical and thermal stability, and low dielectric constant, making it a superb electrical insulator [106, 107]. These characteristics have led to widespread applications including thermal management in electronics, lubricants, adhesives, cosmetics, and water purification [101, 107–109].

Hexagonal boron nitride (h-BN) is the most stable form of BN [110]. Unlike graphene, h-BN is a polar material due to the difference in electronegativity between B and N atoms, which gives rise to anisotropic properties [111]. The strong B–N bonding contributes to its outstanding mechanical durability and thermal insulating capabilities [111]. h-BN is also chemically inert, making it ideal for protective coatings in aggressive environments [107, 112, 113]. Moreover, it is biocompatible, opening opportunities for medical and biological applications [107].

The bandgap width of h-BN, which ranges from approximately 4.0 eV to 6.0 eV [24, 111] depending on thickness and defects, can be modulated through doping or defect engineering. The monolayer typically exhibits a direct bandgap of around 6 eV [114], placing it among the strongest 2D insulators. Despite having low absorption in the (250 – 900) nm wavelength range, h-BN shows significant absorption in the deep ultraviolet (UV) region (200 – 220) nm [115, 116].

Finally, monolayer h-BN boasts a remarkable Young's modulus close to 1.0 TPa [114], placing it among the stiffest known materials on par with diamond [117].

1.2. Applications and limitations of 2D materials

The driving force in nanotechnology continues to be the semiconductor industry, still predominantly reliant on silicon [1, 2]. However, the search for a next-generation material that could surpass silicon and further advance semiconductor devices is ongoing. Among the strongest contenders are 2D materials [4, 5]. With their exceptional properties, including high carrier mobility, tunable bandgaps, large on-off ratios, mechanical strength, and chemical resistance, 2D materials are poised to revolutionise fields such as nanoelectronics, optoelectronics, biomedicine, surface coatings, and chemical sensing [52].

Despite their remarkable potential, the practical application of 2D materials faces several challenges. One of the most significant hurdles lies in the complexity of their synthesis. The growth of high-quality, stable 2D materials requires precise control over critical parameters such as surface flatness, cleanliness, and defect density. Moreover, many 2D materials are highly sensitive to environmental exposure. Although they are often synthesised in UHV conditions to ensure ideal growth, these materials frequently degrade, corrode, or undergo phase segregation once removed from such controlled environments.

To address these limitations, researchers are developing advanced growth techniques and protective strategies, as discussed in Chapter 1.3. These efforts are crucial for enabling the practical deployment of 2D materials across various industries. This section will explore both the current and emerging applications of 2D materials, alongside the remaining obstacles to their broader integration into technology.

The most common way to harness the unique properties of 2D materials is through the fabrication of van der Waals heterostructures, stacks of atomically thin layers held together solely by weak van der Waals forces [51]. By the combination of different monolayers in a defined sequence, it is possible to engineer artificial materials with tailored and often novel electronic, optical, or mechanical properties. These heterostructures enable functionalities that are unachievable in individual layers alone. However, the vast potential of such layered systems is constrained by current fabrication methods, including limitations in growth techniques, the complexity of transferring delicate nanocrystals or nanosheets, and, to some extent, the creativity of the researchers designing them.

The core components of most semiconductor-based nanodevices are field-effect transistors. FETs are three-terminal devices composed of source, drain, and gate electrodes [118]. A semiconductor channel connects the source and drain, while a dielectric layer insulates the channel from the gate. The voltage applied to the gate modulates the flow of electrons through the channel, thereby controlling the current between the source and drain. However, as the channel length is reduced in pursuit of device miniaturisation, short-channel effects become dominant [48]. One major consequence is an increase in off-state currents, where charge carriers continue to leak through the channel despite the application of a suppressive gate voltage, leading to current leakage [6]. To mitigate these effects, novel materials and device architectures are being explored. The integration of 2D materials into such systems enhances their performance, reduces device dimensions,

and enables new functionalities, making them promising candidates for next-generation nanoelectronics.

The 2D materials commonly used in FET devices include graphene, h-BN, TMDs, phosphorene, and silicene. While graphene exhibits exceptional carrier mobility, its intrinsic zero bandgap width limits its use in FETs without additional doping or bandgap engineering. In contrast, materials such as MoS_2 and phosphorene are more suitable, as they can be isolated in monolayer form with minimal surface roughness and a low density of dangling bonds. When combined with h-BN as a dielectric layer, these materials exhibit almost no interface traps, further enhancing device performance. Key material properties essential for FET applications include high carrier mobility, a large on-off switching ratio, and strong drive current, criteria that TMDs, phosphorene, and silicene fulfil. Notably, the first single-layer MoS_2 transistor demonstrated a carrier mobility of approximately $200\,\mathrm{cm^2/V \cdot s}$ [46] and an impressive on-off ratio of 10^8 [46], underscoring the potential of 2D materials for advanced nanoelectronic devices.

Arranging transistors into arrays creates complex circuits known as integrated circuits, which are fundamental to the semiconductor industry. A significant milestone in the integration of 2D materials into these circuits was the development of a 1-bit processor, composed of 115 2D material-based transistors [7]. This breakthrough highlights the potential of 2D materials in practical applications. Moreover, recent advances have made it possible to fabricate large-scale and flexible FET arrays [119]. In addition, high-density memristors based on 2D materials have been developed, offering promising capabilities for information storage.

The diverse bandgap widths of 2D materials make them ideal for broadband photodetection. Narrow bandgap 2D materials, with bandgap energies lower than 1 eV, are well-suited for infrared detection. TMDs such as MoS_2, tungsten disulfide (WS_2), molybdenum diselenide ($MoSe_2$), and their heterostructures hold promise for infrared optoelectronic applications [15]. The wide bandgap materials like gallium sulfide (GaS), gallium selenide (GaSe), or germanium selenide (GeSe), on the other hand, present excellent potential for highly sensitive visible and UV detection [8]. The spectrum of wavelengths that 2D material-based photodetectors can detect spans from 0.3 THz to 10^{15} THz, covering the range from infrared to near UV.

In addition to light detection, 2D materials are also utilised in light-emmiting devices (LEDs). Their wide spectrum of diverse materials meets the specific requirements of optoelectronic devices. By creating such stacked devices containing graphene, phosphorene, or TMDs, researchers aim to improve charge transport and extraction, performance, and interface stability [9].

Renewable energy is currently a widely discussed issue, and nanodevices capable of harvesting light from the Sun are being rapidly developed. The implementation of 2D materials plays a crucial role in enhancing the performance of solar cells and energy storage nanodevices. Transparent conductive electrodes are key components of photovoltaics, as they determine the amount of light that passes onto the photoactive layer. Unlike conventional electrodes, the transportation of generated charge carriers to the external circuit is ensured by the electrical conductivity of the transparent electrode. 2D material-

based electrodes do not suffer from low flexibility and high structural defects, and their tunable optical and electrical properties offer unique solutions to the limitations of current green energy devices [10].

Detection of biomolecules is the cornerstone of disease diagnostics, environmental monitoring, or food safety [11, 12]. Electrochemical biosensors, which are based on conventional FETs, benefit from the enhanced performance of transistors, thus increasing the effectiveness of biosensors. This is another crucial application of 2D materials. As the medical and environmental fields progress rapidly, the requirements for biosensors are growing. These devices must offer high selectivity, sensitivity, and stability while maintaining cost-effective qualities that 2D materials can provide. Graphene, TMDs, and phosphorene are actively being explored for biosensing applications [13]. For example, a single-layer MoS_2 demonstrates extraordinary sensitivity for detecting trace amounts of hydrogen peroxide (H_2O_2), which are secreted by A549 cancer cells in vivo [14].

Composite materials based on graphene or h-BN exhibit exceptional mechanical properties, such as enhanced tensile strength and elasticity. These polymeric composites proved effective for high-strength applications [16]. Additionally, graphene has shown the ability to delay the diffusion process during combustion in gases, significantly reducing flammability [120]. This property has led to the use of graphene as a coating material for fabrics, improving their fire resistance [17].

1.3. Preparation of 2D materials

The preparation of free-standing low-dimensional nanostructures or films presents numerous challenges, with various factors influencing the final outcome. To address these challenges, several techniques have been developed. Broadly speaking, the preparation of 2D materials follows one of two main approaches: top-down or bottom-up.

The top-down approach involves reducing a bulk material into a low-dimensional form by exploiting the weak van der Waals interactions between layers. Its simplicity and cost-effectiveness make it an attractive option, often preserving the intrinsic properties of the material. However, this approach may introduce structural imperfections or limit scalability [121].

In contrast, the bottom-up approach constructs 2D nanostructures and films atom by atom or molecule by molecule, enabling greater control over structure and composition. Nevertheless, the requirements for bottom-up synthesis are much more demanding. Factors such as material purity, temperature, substrate type, crystalline structure, and pressure play a crucial role in determining the success of the growth process [121].

In the following sections, key methods for the isolation and synthesis of 2D materials, such as mechanical exfoliation, CVD, and MBE, will be discussed.

1.3.1. Mechanical exfoliation

The mechanical exfoliation, being the first successful method used to isolate a stable monolayer of graphite, remains the simplest method to prepare various 2D materials [3].

The genius of exploiting the weak van der Waals interactions between layers is achieved by applying Scotch tape to the surface, exerting a normal force, and leaving multiple layers of the material on the tape. By repeatedly applying the normal force onto the bulk surface, the material gets thinner and thinner until only a monolayer, at best, a few layers remain. The schematic of the mechanical exfoliation process is shown in Figure 2. Exfoliating the monolayers from the bulk material results in high-quality, clean, and large-area 2D flakes. Not only graphene but also other graphene-like materials are prepared using this method, such as MoS_2 or tungsten diselenide (WSe_2) [40].

Mechanical exfoliation, as elegant and easy as it seems, has numerous limitations. The thickness of the final flake is almost uncontrollable, and one must be skilled and lucky enough to obtain a homogeneous monolayer. Additionally, the exfoliation process is time-consuming and labour-intensive, which complicates the implementation of this method into the industry. To overcome these challenges, multiple modifications and setups were introduced. For example, Jayasena et al. [42] suggested trimming the bulk material into a pyramid shape and embedding it in epoxy. Afterwards, a sharp diamond wedge

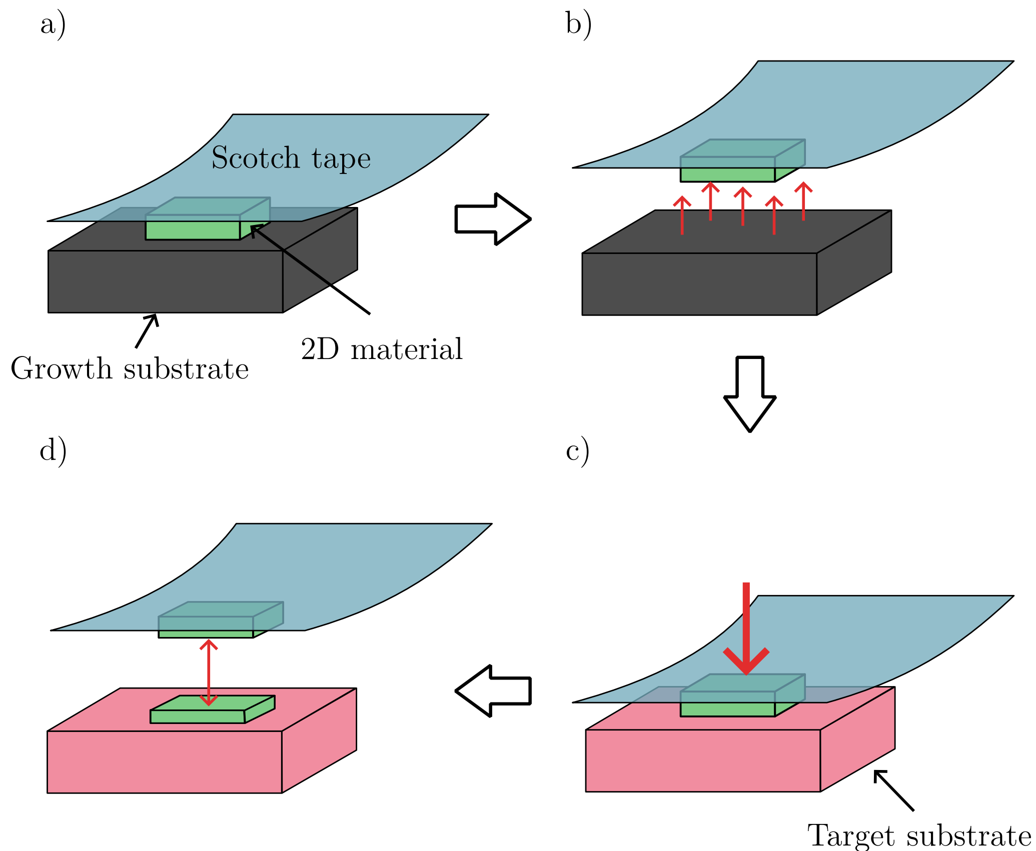

Figure 2: The mechanical exfoliation process: a) Scotch tape is applied on the bulk material on the growth substrate. b) The pickup is performed by lifting the tape from the surface. c) The tape with the bulk material is placed on the target substrate. d) By repeatedly sticking the tape onto the target substrate, the bulk material is thinned down to a 2D material. Adapted from [122].

mounted on the ultrasonic oscillation system exfoliates monolayers from the pyramid-shaped material.

To enable the large-scale production of 2D material flakes, a method utilising sonication was developed. This method is based on dispersing graphite powder in specific organic solvents followed by sonication and centrifugation, resulting in a low-concentration graphene dispersion. This exfoliation method proved successful, however, it exhibits two vital imperfections. The number of defects in the monolayer is higher than desired, and the sonication process does not affect all areas equally, creating flakes of different thicknesses [41].

Many other useful methods of acquiring single-layer materials inspired by mechanical exfoliation are being developed, such as the ball milling technique [123] or fluid dynamics method [41]. Where one approach fails to satisfy the expectations, the other one fulfils them, and the other way around. Nevertheless, mechanical exfoliation is still the essential and commonly used top-down technique for the preparation of monolayers.

1.3.2. Chemical vapor deposition

A leading technique for the bottom-up growth of 2D materials is CVD. The fundamental principle of the CVD method involves the adsorption of volatile precursor molecules onto a heated substrate, undergoing a chemical reaction, creating a thin film or a thin flake [43–45]. The schematic of the CVD system is shown in Figure 3. There is a strong correlation between the parameters set in CVD and the properties of the final 2D materials. Parameters such as the temperature of the substrate, chamber pressure, source-substrate distance, and gas molecule flow rate greatly influence the thickness, size of the nanostructures, morphology, and orientation. Therefore, precise control of these parameters is crucial for achieving the desired 2D nanostructure. Unlike the conventional CVD methods to grow silica, tungsten, etc., the approaches were modified to grow high-quality, large-area 2D materials. The modification of the CVD method called metal-oxide chemical vapor deposition (MOCVD) [124] will be mentioned in the following text.

MOCVD is a technique that enables the growth of large-area thin 2D films on various substrates using metal-oxide precursors such as trimethylgallium or trimethylaluminum.

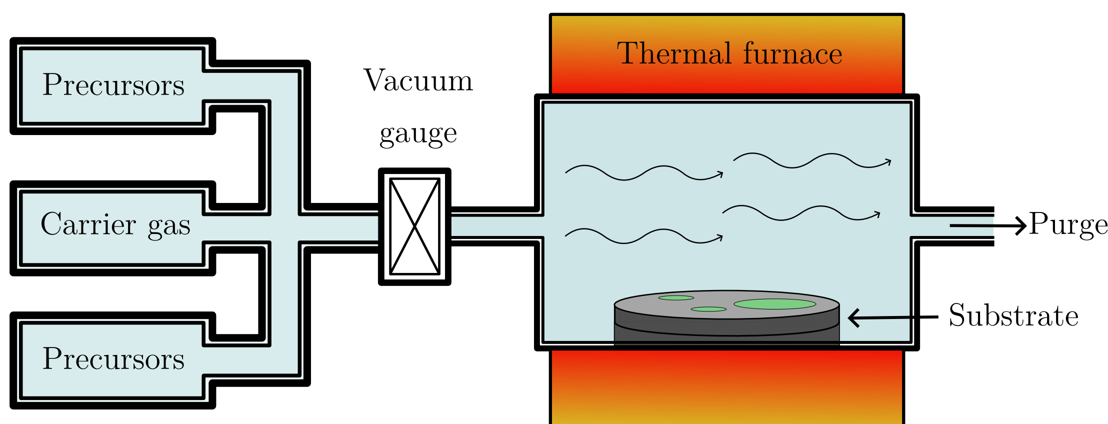

Figure 3: The schematic of CVD system. Adapted from [44].

The advantages of such metal-oxide precursors are reasonable vapor pressures for CVD growth at room temperature, high purity, cost-efficiency, and low toxicity. Nonetheless, many metal-oxide precursors that meet the purity and vapor pressure expectations are highly reactive, even pyrophoric. The toxicity and reactivity of some precursors require for cautiousness while growing the 2D materials via the MOCVD method. Therefore, using the MOCVD approach requires special safety measures, making the 2D material growth process more complicated and expensive. Similar to the CVD method, precursor molecules decompose and are adsorbed on the heated substrate surface. Afterwards, they fully decompose and are desorbed. The particles move around forming thin nanostructures and films, replicating the crystalline structure of the substrate. The growth of highly oriented, large-area MoS_2 and WSe_2 was achieved, and the MOCVD method is considered to be the most favourable 2D material growth method for industry [45, 124].

1.3.3. Physical vapor deposition

A different technique based on vapor deposition called physical vapor deposition (PVD) is an alternative for the growth of high-quality oxide films in a high-vacuum environment [125]. The growth is realised via pulse laser deposition (PLD), or sputtering. The laser energy is a key parameter for the vaporisation of the target. Typically, UV lasers with a wavelength of around 248 mm are used. The PLD approach is best suited for insulators because of the high reflectivity and thermal conductivity of semiconductors and metals, which results in low energy adsorption from the laser into the substrate. Therefore, this technique proved to be efficient in the growth of amorphous BN films as well as graphene and TMDs. On the other hand, sputtering PVD uses ion bombardment of the high-purity target instead of a laser. The incoming ions interact with the target surface atoms, creating a vapor of solid material at low temperature. The major advantage of the sputtering approach is that the 2D material can be directly grown from its bulk equivalent. This method is favourable for the growth of WS_2, $MoSe_2$, and other TMDs [45, 125].

1.3.4. Molecular beam epitaxy

MBE is a bottom-up technique used for the epitaxial growth of thin films and nanostructures of various 2D materials. The schematic of the MBE system is shown in Figure 4. Epitaxial growth is the process of depositing 2D films with a crystalline structure similar to a substrate. The growth is realised inside a UHV chamber, and the substrate is heated to the desired temperature. The material to be deposited onto the substrate located in effusion cells is heated, creating a beam of molecules. These molecules have a high mean free path, resulting in minimum collisions between the particles. The precursors reach the substrate and react together, creating the desired thin films or nanostructures. Thin films of molybdenum ditelluride ($MoTe_2$) or MoS_2 were successfully developed by the MBE approach. Additionally, TMDs at the wafer scale were grown by MBE as well as a monolayer of h-BN [45].

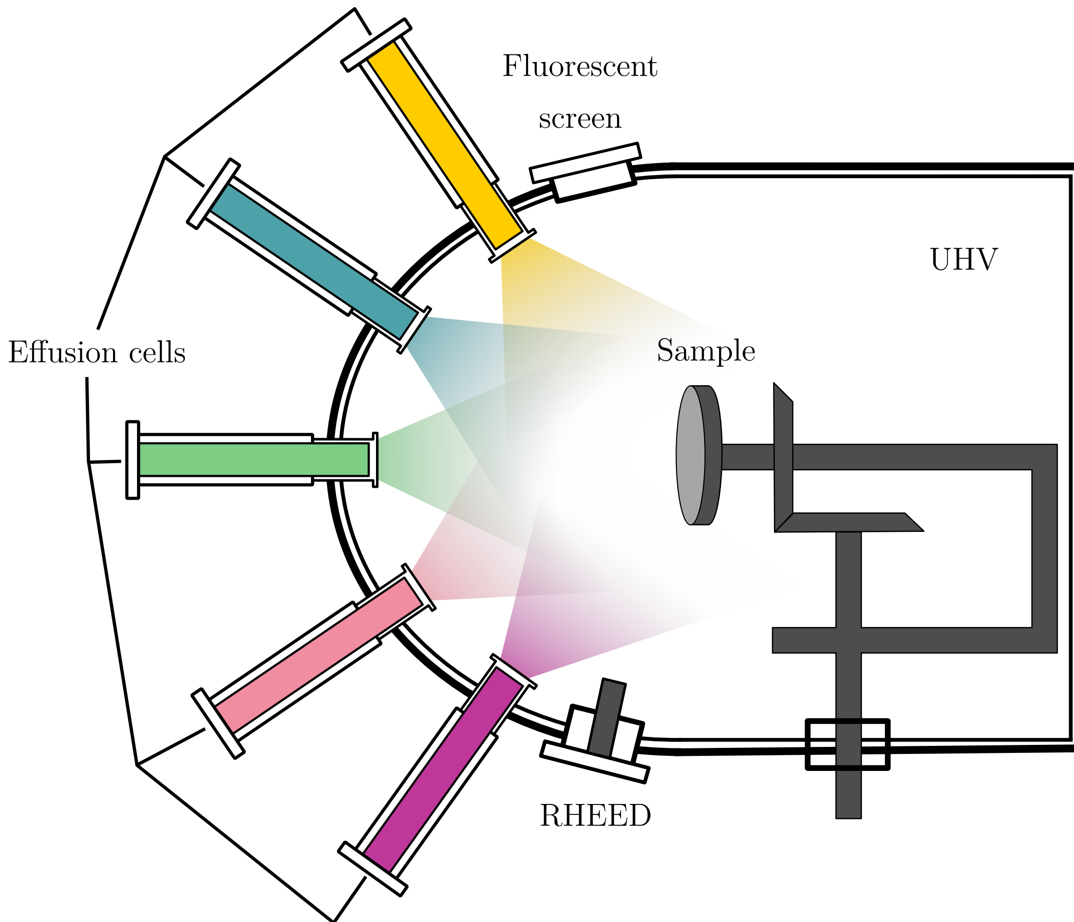

Figure 4: The schematic of the MBE system with reflection high-energy electron diffraction and a fluorescent screen to detect the RHEED signal for precise control over the thickness of the deposited layers. Adapted from [33].

MBE exhibits several advantages for the large-area, high-quality thin films and nanostructures. The UHV environment ensures a high mean free path of deposited particles and minimises the impurities that could appear during the growth process. Additionally, UHV enables the use of in-situ electron diffraction techniques to monitor the growth of 2D materials and the state of the substrate surface. The high-purity precursors placed in effusion cells are vital for the low-defect thin films. Lastly, the very slow deposition rate of precursors (generally a few Å per minute) allows for precise control over the thickness of the final film or nanostructure. Although the MBE approach proved to be effective in the epitaxial growth of 2D materials, it is mostly used for research and development purposes. The requirements for UHV systems are difficult to fulfil, and the growth is sensitive to various factors, which complicates the industrial applications.

1.4. Transfer of low-dimensional structures

Even though 2D materials can be grown directly on various substrates, the original growth substrate is often unsuitable for further use, for example, due to its conductive properties. As a result, thin films often need to be transferred onto a different substrate for subsequent

characterisation, device fabrication, or integration into van der Waals heterostructures [51, 52]. The material must be carefully detached from the original substrate and transferred without introducing additional impurities, defects, or mechanical damage. The transfer process is therefore a crucial step in the fabrication of high-quality 2D material-based devices, and the efficiency of the transfer has a direct impact on the electrical, optical, and mechanical integrity of the material.

There are two primary methods for transferring 2D materials: wet-transfer and dry-transfer. In the wet-transfer approach, the material is typically covered by a polymer support layer and released from the original substrate through chemical etching or dissolution [126]. This method is widely used due to its simplicity and effectiveness. However, etching solutions can sometimes damage or contaminate the 2D material, and the transfer process may introduce residues or wrinkles, which reduce the final quality of the thin films or nanostructures. On the other hand, dry-transfer methods minimise the use of chemical solutions and rely instead on mechanical or thermal release mechanisms [126–128]. As a result, dry-transferred materials often exhibit fewer impurities and less structural damage, making this approach particularly suitable for the fabrication of van der Waals heterostructures, where high-quality interfaces are crucial. Each method offers distinct advantages and presents different challenges, depending on the intended application. The specific techniques and uses of both approaches will be described in the following sections.

1.4.1. Wet-transfer

In the wet-transfer approach, the sample is covered by a polymer protective layer, and the 2D material is removed from the substrate by chemical etching or dissolution. A polymer commonly used in the wet-transfer of 2D materials is polymethyl methacrylate (PMMA) [129, 130]. The process of 2D material transfer using the PMMA layer is shown in Figure 5. The polymer serves as a protective barrier, preventing mechanical damage to the delicate 2D structure during handling [126]. In the first step, a layer of PMMA is spin-coated onto the synthesised 2D material on the original substrate, fully covering the surface. The substrate is then immersed in an etching solution, which removes the substrate material and releases the PMMA film with the 2D material attached, allowing it to float freely in the solution [126].

Next, the PMMA/2D material stack is transferred to deionised (DI) water to rinse away residual etchants. The floating film is then carefully scooped onto the target substrate, aligning it as needed. Finally, the PMMA is removed, typically using an organic solvent such as acetone, leaving the 2D material adhered to the desired substrate [126].

This method enables the transfer of 2D materials onto virtually any desired target substrate, as the protective PMMA layer minimises mechanical damage during handling [126]. Moreover, it has been reported that large-area transfers, up to 4-inch wafer-sized films, can be achieved, making the technique promising for industrial-scale applications [131, 132]. However, a major drawback lies in the incomplete removal of residual PMMA, which can remain on the surface even after solvent treatment [133]. These residues may

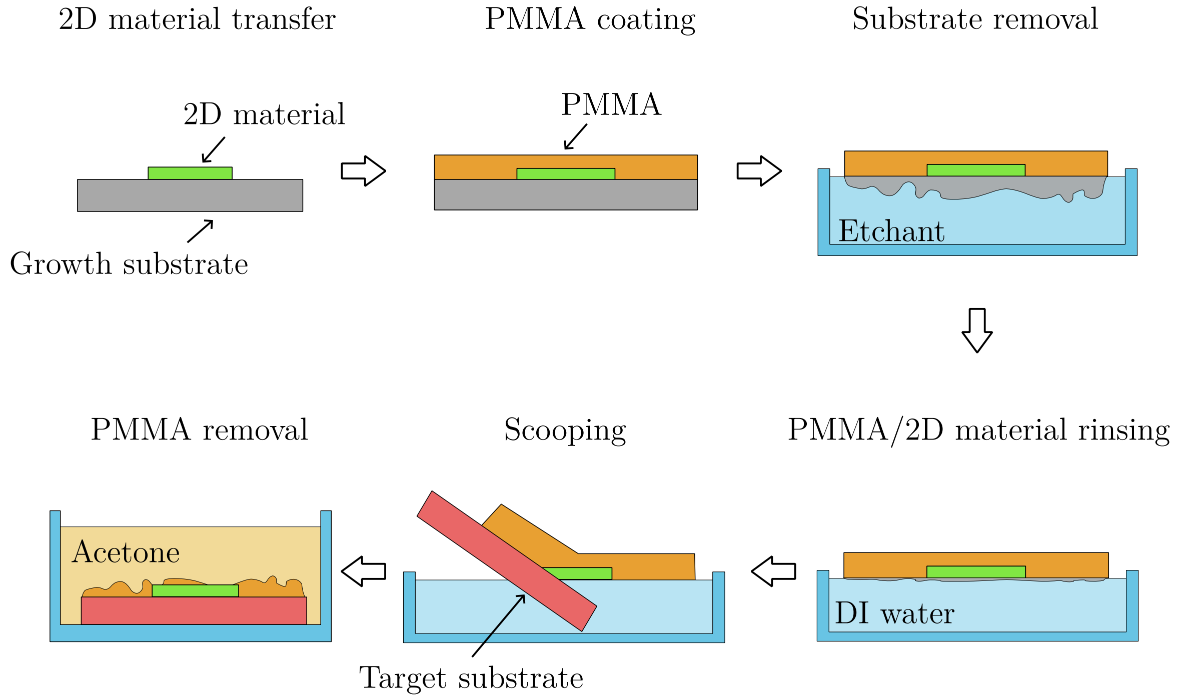

Figure 5: Schematic of wet-transfer process using PMMA protective layer. Adapted from [126].

degrade the electrical and optical properties of the transferred material, limiting its performance in sensitive applications.

To achieve complete removal of PMMA residues, additional processing steps are often required. Various strategies have been proposed to enhance the electrical and optical properties of transferred 2D materials, including extra etching stages, surface treatments, solvent concentration control, and thermal annealing [134–136]. However, each of these steps increases the overall complexity of the wet-transfer process and may limit the choice of compatible target substrates [126]. Despite these efforts, PMMA residues are rarely eliminated entirely, which continues to pose a challenge for high-performance device applications.

The use of alternative polymers, such as pentacene [137], polyvinyl alcohol [138], or polyvinyl carbonate [139], as protective layers in place of PMMA has been explored. Nonetheless, these polymers often form strong bonds with the 2D material, making the complete removal extremely challenging [126]. In some cases, polymer molecules may also unintentionally dope the material, leading to unwanted alteration of its properties. More recently, a residue-free wet-transfer method utilising paraffin [140] and rosin [141] has been introduced. Despite its promising results, the residue-free transfer requires additional solvents and is limited to smaller transfer areas, rendering it unsuitable for large-scale or industrial applications [126].

1.4.2. Dry-transfer

In contrast to the wet-transfer approach, dry-transfer methods do not require the use of liquid solvents, thereby minimising contamination of the 2D material. These tech-

niques rely on mechanical forces, thermal release, or van der Waals interactions to pick up and relocate the material. It exploits the difference in adhesion between the original and target substrates—if the 2D material adheres more strongly to the target substrate, the transfer proceeds with minimal mechanical damage. Because dry-transfer techniques avoid direct solvent exposure, they are especially well-suited for applications that demand high structural integrity and clean interfaces, such as the fabrication of van der Waals heterostructures or sensitive electronic devices [126–128].

Polydimethylsiloxane transfer

The commonly used polymer for dry-transfer methods is polydimethylsiloxane (PDMS), a representative viscoelastic material. PDMS is widely chosen due to its combination of elasticity, flexibility, and transparency, which makes it well-suited for handling 2D materials. By leveraging the elastic properties of PDMS stamps, 2D materials can be transferred by applying pressure to the growth substrate, which causes the 2D material to adhere to the stamp. Once on the PDMS stamp, the material can be precisely positioned onto a target substrate with minimal damage [126, 142, 143].

The surface energy of both substrates and the transfer medium plays a crucial role in the transfer process. The lower the surface energy of the transfer medium compared to that of the target substrate, the higher the probability that the 2D material will adhere to the target substrate, detaching from the PDMS stamp [126]. PDMS exhibits low surface energy, which greatly increases the likelihood of the 2D material adhering to the target substrate [144]. Conversely, increasing the surface energy of PDMS enhances its adhesion to the 2D material on the original substrate, improving the pickup probability. Several variations of this technique have been developed to optimise the transfer process. For example, to increase the surface energy of the PDMS, thus the adhesion to the MoS_2 film, dimethyl sulfoxide (DMSO) molecules can be vaporised onto the PDMS stamp surface at high temperatures [145]. Once the PDMS stamp containing the MoS_2 film is brought into contact with the target substrate, the temperature is increased to 70 °C, restoring the natural low surface energy of the PDMS. This allows the MoS_2 film to remain on the target substrate with minimal residues and without the need for solvents.

However, the inherently low surface energy of PDMS complicates the transfer process, as its adhesion to 2D materials may be weaker than that of the growth substrate [128]. To overcome this limitation, the introduction of an intermediate layer is often necessary. A commonly used interlayer is polyvinyl alcohol (PVA), which is attached to the PDMS stamp and serves as the primary support layer, while PDMS provides secondary structural support [146]. Since PVA lacks viscoelastic properties, it cannot ensure uniform contact and transfer on its own. Therefore, the secondary support of PDMS becomes indispensable, yet this layered setup introduces additional complexity to the overall transfer process [128].

Transparent nail polish transfer

While the dry-transfer of 2D materials using PDMS with additional support layers has proven effective, it presents a significant limitation: the inability to transfer small areas or individual nanostructures with precision [147]. To overcome this challenge, a modified technique enabling selective transfer has been developed. Interestingly, this method utilises a commercially available nail polish as an adhesive layer [147, 148].

Nail polish significantly improves the probability of successful pickup from the growth substrate, as its adhesion to 2D materials surpasses that of a plain PDMS stamp [147]. However, if not removed properly, it may leave behind residues that could affect the quality of the transferred material. Despite its seemingly unconventional nature, the method has shown promising results in the precise transfer of high-quality 2D nanostructures such as BN [147] or silver telluride (Ag_2Te) flakes, which I successfully transferred during my Erasmus at CIC Nanogune in San Sebastian.

The dry-transfer process using nail polish, described in Figure 6, proceeds as follows: A small piece of PDMS stamp is placed on a glass slide and secured in position using transparent tape. Then, using a sharp wire or toothpick, a droplet of transparent nail polish is extracted and deposited onto the tape covering the PDMS stamp. The viscoelastic nature of the PDMS allows for precise control over the contact between the substrate and the nail polish droplet. The glass slide is then placed on a hot plate and baked at 90 °C for several minutes to cure and harden the droplet, creating an exceptionally sticky surface [147].

Once prepared, the glass slide is mounted onto a manipulator, enabling precise movement along the x, y, and z axes. Under an optical microscope, the droplet is aligned with the desired flake or nanostructure on the growth substrate. The glass slide is slowly lowered to make contact with the sample, and the stage temperature is gradually increased. For a successful transfer, the nanostructure must be fully enveloped in the nail polish. This can be achieved by lowering the glass slide further or by increasing the stage temperature to approximately 40–50 °C. Once the nanostructure is fully covered, the temperature is reduced and the glass slide is swiftly and continuously lifted, causing the 2D material to detach from the growth substrate [147].

After the pickup, the slide is baked again at 90 °C to reflow the nail polish. The glass slide is then remounted onto the manipulator, and the nanostructure, visible through the transparent droplet, is aligned with the desired location on the target substrate. By carefully lowering the glass slide, contact is established, and the stage is heated to facilitate coverage of the nanostructure by the droplet. Once the coverage is complete, the temperature is decreased, allowing the nail polish droplet to delaminate naturally and adhere to the target substrate. The nail polish is then dissolved in acetone, leaving minimal residue and completing the transfer process [147].

Polymer-free transfer

While polymer-based transfer techniques, such as those utilising PMMA or PDMS, offer reliable support during the transfer process, they often introduce unwanted residues

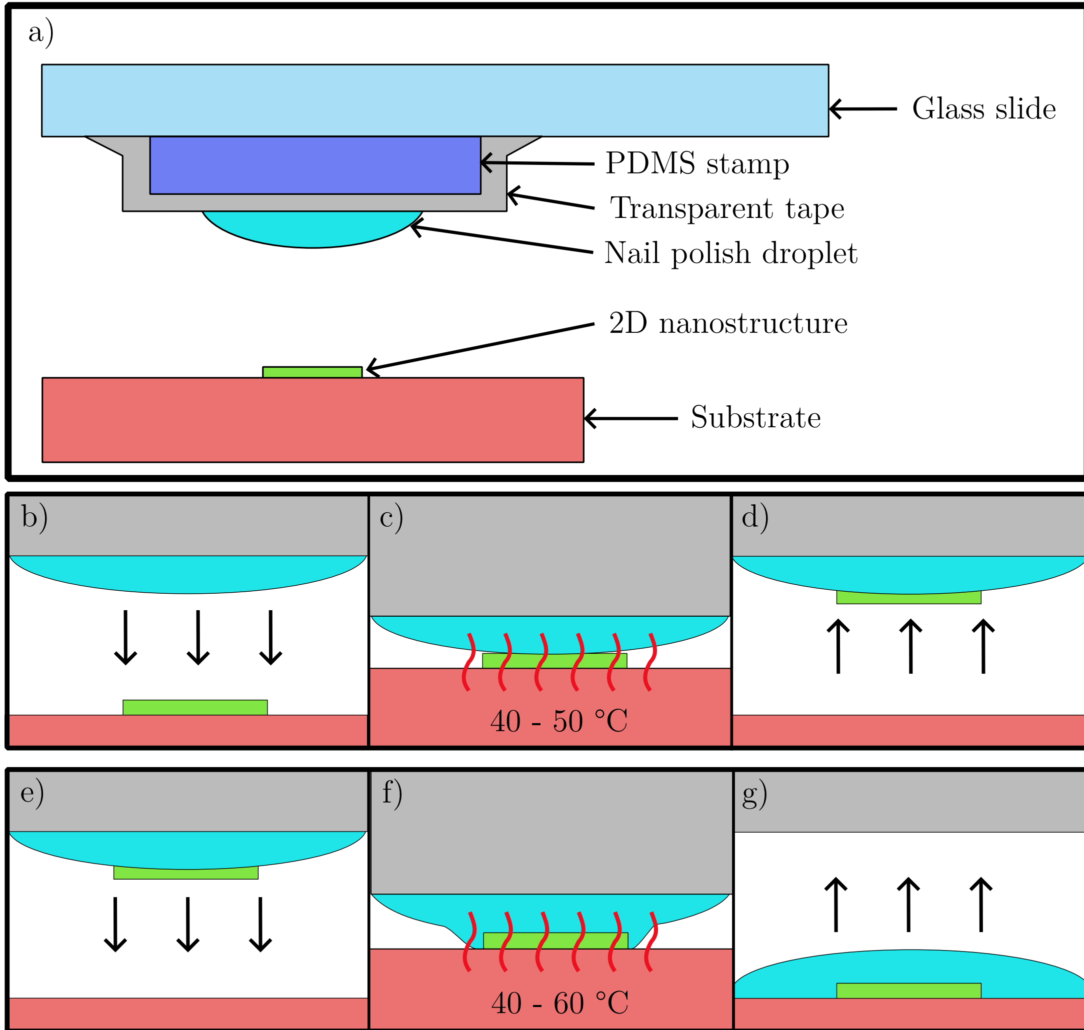

Figure 6: Scheme of dry-transfer using nail polish as an intermediate layer: a) Overview of the components used for the transfer. b–d) Pickup process: The glass slide is lowered to bring the nail polish droplet into contact with the 2D material. The stage is then heated to around 40–50 °C to facilitate adhesion. After heating, the glass slide is retracted, lifting the 2D nanostructure adhered to the nail polish droplet. e–g) Transfer to the target substrate: The nanostructure is aligned with the desired position on the target substrate. The glass slide is then lowered, bringing the droplet into contact with the surface. Heating the stage to 40–60 °C causes the droplet to delaminate. Finally, the glass slide is retracted, leaving the droplet and the 2D nanostructure on the target substrate. [147]

that degrade the electrical, optical, or structural quality of the 2D materials [133]. To overcome these challenges, polymer-free transfer methods have been developed [149–151]. These techniques eliminate the need for sacrificial support layers, therefore minimising contamination and preserving the intrinsic properties of the transferred materials [126].

Polymer-free transfer approaches typically rely on direct mechanical delamination, electrostatic interactions, or the use of surface tension forces to pick up and release 2D materials. Although these methods may require more careful alignment and handling, they offer the advantage of producing ultra-clean interfaces, making them particularly suitable for high-performance devices and sensitive heterostructure assemblies [126].

In summary, this chapter highlighted the unique tunability of 2D materials and introduced several widely studied representatives. Their key applications, limitations, and common synthesis methods were reviewed, along with various transfer techniques. The following chapter will focus on 2D GaN, examining its intrinsic properties and fabrication methods.

2. Two-dimensional Gallium Nitride

From the family of group III-nitrides emerges a fascinating material whose 2D form was discovered only recently [29], GaN. In its bulk form, GaN is one of the most important semiconductor materials of the modern era, renowned for its exceptional properties [152–154]. With a wide direct bandgap of 3.4 eV [153, 155], GaN emits visible blue light, making it indispensable in optoelectronic applications [156–158]. Without GaN, the invention of colored LEDs would not have been possible. In recognition of this achievement, the Nobel Prize in Physics was awarded in 2014 to the inventors of GaN-based blue LEDs [159].

While bulk GaN continues to receive widespread attention, the study of its 2D counterpart is still in its early stages. The first successful synthesis of 2D GaN was achieved in 2016 via the migration-enhanced encapsulated growth (MEEG) method [29], which is described in detail in Chapter 2.2.1. Since this initial discovery, many other methods have been developed to achieve thin films and nanocrystals of 2D GaN [26–28, 30–32], each with its own advantages and challenges, which this chapter describes in detail.

Because the synthesis of high-quality 2D GaN remains complex, experimentally determining its intrinsic properties has proven challenging. As a result, theoretical models play a crucial role in shaping our current understanding of its behaviour. These predictions are essential for assessing the material's potential in nanoelectronic and optoelectronic applications. Accordingly, the following sections provide a comprehensive overview of both the predicted and experimentally measured physical and chemical properties of 2D GaN, followed by a detailed discussion of fabrication methods.

2.1. Properties of 2D GaN

Similar to other 2D materials, 2D GaN is anticipated to exhibit unique electrical, optical, and mechanical properties [29, 160, 161]. However, it is important to consider that the properties of 2D GaN are highly dependent on the method of its growth. Impurities and defects in the crystalline structure can significantly affect the material's characteristics. Similarly, theoretical predictions of these properties are subject to the calculation methods used, which can lead to differing results.

The 2D GaN comes from the TMDs group, sharing similarities in crystalline structure with other representatives. In contrast to its bulk counterpart, which exhibits the wurtzite structure [162], 2D GaN exhibits the typical hexagonal structure with strong in-plane covalent bonds both in thin films and nanocrystals [161, 163, 164]. However, Kolobov et al. suggest that the honeycomb structure applies only for the monolayer of GaN [163]. Multiple layers exhibit an 8|4 bonding pattern referred to as Haeckelite [163, 164]. The comparison of bulk, monolayer, and few-layer-thick GaN is shown in Figure 7. In contrast to the planar honeycomb structure of the GaN monolayer, Haeckelite is not planar, and the Ga and N atoms are distributed in sublayers. It exhibits two main crystallographic orientations: armchair and zigzag, the same as phosphorene. In the top view (x-y plane), they still show the hexagonal structure, but in the side view (x-z plane),

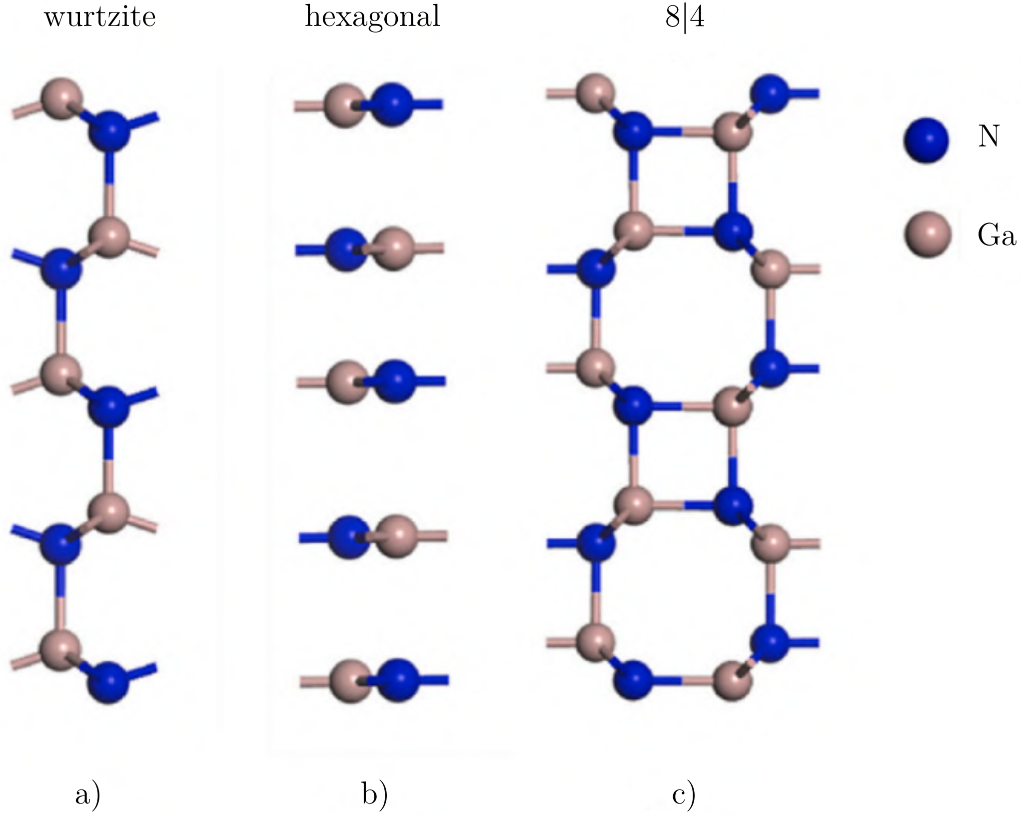

Figure 7: Comparison of GaN crystalline structures in side view (x-z plane): a) wurtzite (bulk), b) hexagonal (monolayer), c) 8|4 haeckelite (few layers thick). Adapted from [164].

they form octagonal and square rings. This means that the layers are connected with covalent bonds and not van der Waals interactions, making it difficult to obtain a GaN monolayer, in contrast to natural 2D materials such as h-BN or graphene [163, 164].

It is reported that synthesized 2D GaN nanocrystals exhibit a larger interlayer distance of (3.15 ± 0.09) Å [28] than that of wurtzite GaN in the range of 2.59 Å [165] to 2.70 Å [31]. The lattice parameter of (3.29 ± 0.13) Å [28] also convincingly differs from the bulk GaN (3.18 Å) [166].

The thickness of the nanostructure and the crystallographic orientation dictate the mechanical properties of low-dimensional GaN [164]. The resistance to elastic and shear deformation is represented by Young's modulus E and shear modulus G, respectively. The layer modulus γ determines the material's resistance to stretching. The Poisson's ratio μ indicates the resistance to shear strain, and the anisotropic factor A represents the anisotropy magnitude. All the values for the monolayer and a few layers of GaN for both crystallographic orientations are shown in Table 2.1.

For a structure to be stable, it needs to satisfy the Born criteria [167] for shear modulus $G > 0$. Both monolayer and multilayer structures fulfil these criteria, thus, their stability is theoretically ensured [160]. With the increasing thickness of GaN, Young's modulus

Table 2.1: Mechanical properties of monolayer and multilayer GaN from [160].

	G (N/m)	E_{armchair} (N/m)	E_{zigzag} (N/m)	μ_{armchair}	μ_{zigzag}	γ (N/m)	A
1 layer	25.24	105.10	105.04	0.47	0.47	98.45	0.71
2 layers	40.57	175.97	145.53	0.24	0.20	102.81	0.62
3 layers	50.65	247.71	189.57	0.34	0.26	155.25	0.60
4 layers	66.46	335.65	248.34	0.30	0.23	197.30	0.57
5 layers	81.24	413.75	300.59	0.30	0.22	240.28	0.57

increases for both crystallographic directions. The layer and shear modulus increase with the number of layers as well, suggesting the elasticity of multilayered GaN. The anisotropy factor A decreases with the GaN thickness, indicating a possible elastic anisotropy caused by different values of Young's and shear modulus in armchair and zigzag directions.

As with other TMDs, an ultrawide bandgap was expected for 2D GaN [29, 163, 164]. The bandgap is a key parameter that determines the material's electrical and optical properties. Therefore, numerous ab initio calculations, including DFT [163], density of states (DOS) [29], and other first-principles methods, have been employed to characterise the bandgap of 2D GaN. Depending on the computational approach used, reported bandgap values range from 3.1 eV [26] to 5.6 eV [26], spanning a range from semiconducting to insulating behaviour. All experimentally confirmed values, obtained via UV–vis spectroscopy or ellipsometry measurements, fall within this range [26, 27, 32]. The variability in bandgap values is primarily attributed to the coexistence of different structural phases and the varying number of atomic layers in the material [29]. Lower bandgap values are often associated with highly defective 2D GaN or multilayered stacks [32]. Compared to bulk GaN, which has a direct bandgap of 3.4 eV [153, 155], the 2D form typically exhibits a wider gap, while still maintaining a direct transition [26].

Other calculations uncovered that the strong inherent polarisation field present in the 2D GaN causes the amplification of the quantum-confined Stark effect (effect of an external electrical field on the absorption and emission of light) [161]. As a result, the bilayer of 2D GaN emits light of the same wavelength as bulk GaN. However, the monolayer of GaN emits in the deep UV region, and the uniaxial in-plane strain enables the emission of linearly polarised light at room temperature for both monolayer and multilayer 2D GaN [161].

2.2. 2D GaN preparation methods

To achieve well-defined, high-quality GaN nanosheets or nanocrystals, the preparation process plays a crucial role. The growth mechanism directly influences the resulting properties of the nanostructures, making the choice of a specific method highly dependent on the intended application. Since research on 2D GaN is still in its early stages, current efforts are primarily focused on synthesising nanostructures suitable for characterising

electrical, optical, and mechanical properties, rather than targeting specific device integration.

A variety of growth methods have been explored for the synthesis of low-dimensional GaN. These methods share a common feature: the bottom-up approach. Due to the strong covalent bonding throughout the GaN crystal lattice, mechanical exfoliation is not feasible. As a result, top-down strategies commonly used for van der Waals materials like graphene or MoS_2 [3, 40] are not easily applicable to GaN, thus, the main focus is on bottom-up techniques that can be employed to fabricate its two-dimensional form. In this section, various methods used to grow GaN nanocrystals and free-standing nanosheets will be discussed.

2.2.1. Migration-enhanced encapsulation growth

In 2016, the first successful synthesis of 2D GaN was reported by Al Balushi et al. using a technique known as MEEG, in which graphene plays a crucial role as an encapsulating layer [29]. The low-dimensional GaN was grown on a SiC(0001) substrate. However, direct deposition of GaN onto the SiC surface results in the formation of bulk GaN islands due to the large lattice mismatch and unfavourable surface energy. To overcome this, the substrate surface is passivated prior to growth to promote Frank–van der Merwe (layer-by-layer) growth.

The first step of the MEEG process involves the synthesis of epitaxial graphene via the sublimation of silicon atoms from the surface of the SiC substrate. This epitaxial graphene is subsequently transformed into quasi-freestanding epitaxial graphene by hydrogenation. The hydrogen passivates the dangling bonds between the graphene buffer layer and the SiC substrate, effectively decoupling them and resulting in the formation of a second graphene layer. This treatment creates a low-energy interface that is suitable for the subsequent growth of 2D GaN [29].

Next, trimethylgallium ($Ga(CH_3)_3$) is introduced into the chamber at 550 °C. At this temperature, the precursor decomposes into Ga adatoms, which diffuse across the graphene surface and gradually intercalate into the low-energy interface. Once a sufficient Ga layer is formed, the temperature is increased to 675 °C, and ammonia (NH_3) is introduced into the chamber. The NH_3 decomposes into N atoms that also intercalate beneath the graphene, where they react with the intercalated Ga to form a GaN nanosheet. The whole growth process is shown in Figure 8.

After the MEEG process, the graphene layers remain on the substrate. However, graphene exhibits numerous defects, which act as intercalation sites for Ga atoms. The presence of these defects suggests strain or structural modifications, indicating interactions between the 2D GaN layer and the graphene. Additionally, the 2D GaN exhibits strong covalent bonding with the SiC substrate. As a result, transferring the thin GaN film onto other substrates becomes extremely challenging, which currently limits the applicability of MEEG-grown 2D GaN in device fabrication.

Interestingly, it has been suggested that MEEG-grown 2D GaN does not undergo oxidation upon exposure to air. During the ammonolysis step, nitrogen atoms are hy-

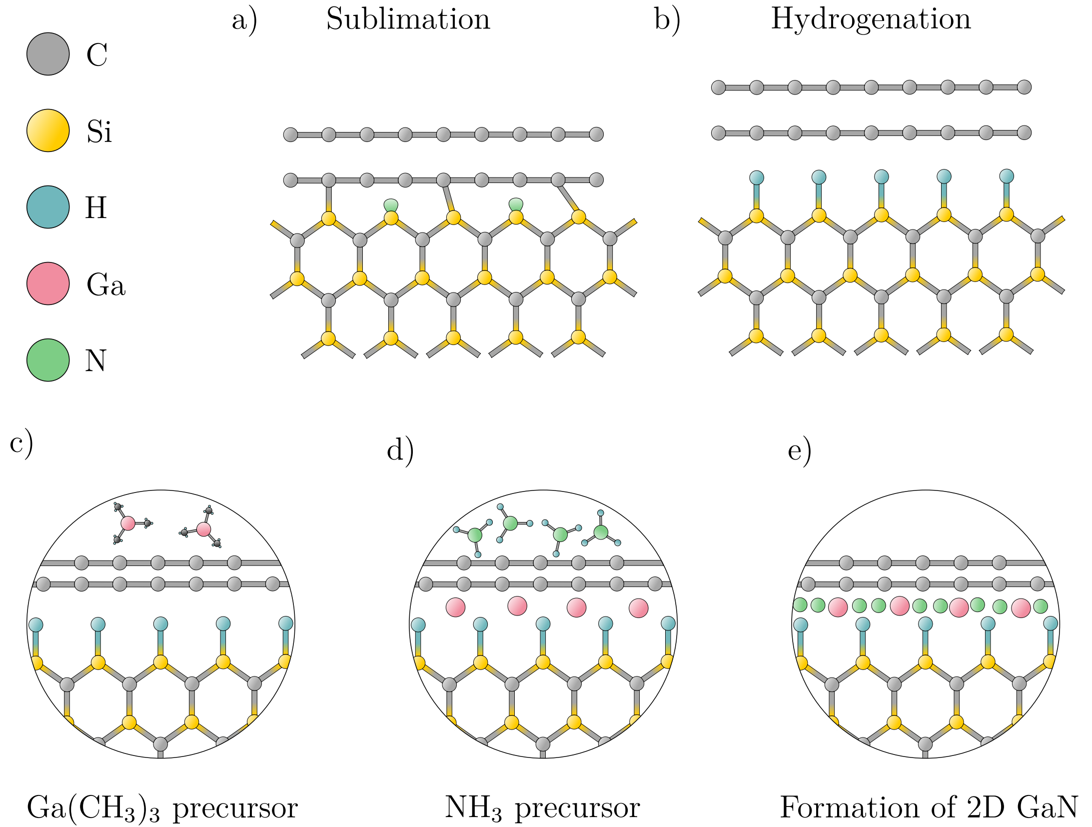

Figure 8: Schematic of MEEG method: a) the sublimation of Si atoms from the SiC surface creating bilayer graphene. b) the hydrogenation and formation of a low-energy graphene/SiC interface. c) introduction of $Ga(CH_3)_3$ precursor. d) intercalation of Ga atoms and introduction of NH_3 precursors. e) formation of 2D GaN at the graphene/SiC interface. Adopted from [29].

pothesised to replace hydrogen atoms at the Ga/SiC interface, effectively passivating high-energy surface sites. This substitution helps maintain charge neutrality and contributes to the ambient stability of the 2D GaN film [29].

2.2.2. Graphene-oxide-assisted synthesis

Inspired by the MEEG approach, a novel method for the synthesis of GaN nanosheets was developed by Changlong et al. specifically for application in lithium-ion batteries as an anode material [30]. Lithium-ion batteries require materials with high electrical conductivity and minimal volume change during insertion/desertion processes. 2D GaN exhibits properties that align well with these requirements, making it a promising candidate for next-generation battery technologies. In this method, GaN nanosheets are synthesised via a wet-chemical approach, using graphene oxide (GO) as a supporting substrate. The role of GO is crucial in the growth of GaN nanosheets, as it serves as a heterogeneous nucleus for the gallium oxyhydroxide (GaOOH).

The synthesis begins with the anchoring of GaOOH nanocrystals onto the surface of GO sheets. This is achieved through a homogeneous precipitation method, in which functional groups on the GO surface facilitate the attachment of GaOOH. To convert

the GaOOH layer into GaN, the composite is calcined at 600 °C in an NH_3 atmosphere, followed by thermal treatment in air [30]. A schematic representation of the graphene-oxide-assisted growth process is shown in Figure 9.

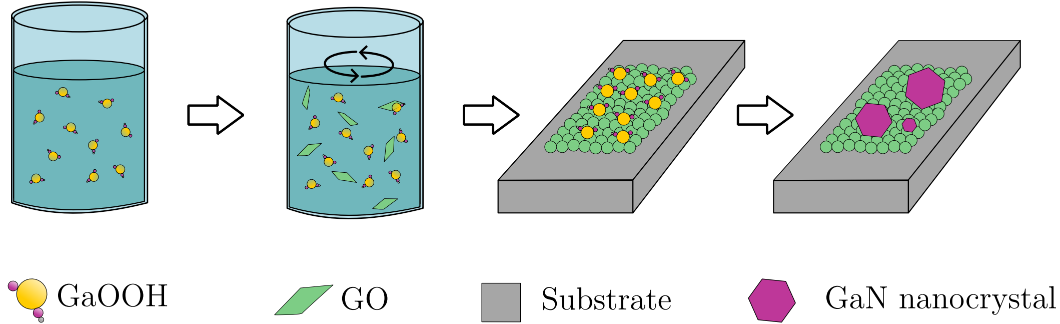

Figure 9: The schematic of graphene-oxide-assisted 2D GaN growth. Adopted from [30].

After the removal of the GO layers, uniform hexagonal GaN nanostructures remain, with lateral dimensions ranging from 1 µm to 5 µm. The formation of hexagonal wurtzite GaN was confirmed, with an average thickness of approximately 14.5 nm. The resulting 2D GaN nanostructures exhibit high discharge capacity and ultrahigh rate capability, both essential attributes for efficient lithium-ion battery performance [30].

2.2.3. Growth of 2D GaN single crystals on liquid metals

Although encapsulation-based methods allow for the synthesis of nanometer-thick GaN films, the investigation of their intrinsic physicochemical properties remains limited due to substrate interactions and encapsulation layers [29]. To address this, Yunxu et al. reported the growth of free-standing, single-crystal 2D GaN via a surface-confined nitridation reaction using CVD [31]. In this method, a tungsten foil serves as a substrate onto which liquid Ga is spread. Tungsten is widely regarded as a suitable platform for the growth of 2D materials [168, 169].

The process follows a procedure similar to that described in Section 1.3.2. The tungsten foil is used as the substrate, over which liquid gallium is spread. The tungsten foil is then placed into a CVD furnace and heated to elevated temperatures (approximately 1 080 °C). Urea (CH_4N_2O) is employed as the nitrogen source and is introduced into the furnace subsequently. Upon thermal decomposition, urea (CH_4N_2O) releases nitrogen species that react with the liquid gallium, leading to the formation of GaN nanocrystals at the confined surface [31].

Once the 2D GaN nanocrystals are synthesised, a wet-transfer method using PMMA as a support layer is employed. First, PMMA is spin-coated onto the sample surface, after which the remaining liquid Ga layer is selectively etched away using hydrogen chloride (HCl), as only the surface Ga atoms undergo nitridation. This step leaves only the GaN nanocrystals protected by PMMA. The PMMA/GaN stack is then transferred onto a

target substrate, and the PMMA layer is removed using acetone, leaving behind the 2D GaN nanocrystals on the target substrate.

This method successfully yields free-standing GaN single crystals with lateral dimensions of up to 50 µm and thicknesses as low as 4.1 nm. Structural analysis confirmed the formation of the typical wurtzite structure with a hexagonal plane [31]. While this method demonstrates a viable approach to the synthesis of 2D GaN, the CVD-based process involves high temperatures, precursors, and high-pressure conditions, all of which can introduce impurities or structural defects in the resulting nanocrystals [26, 27].

2.2.4. Two-step method

The growth of 2D GaN is often constrained by the choice of substrate, which complicates the transfer of nanocrystals or thin films to desired platforms. Furthermore, the crystalline structure of the substrate must closely match that of the target material; otherwise, lattice mismatch can introduce significant defects into the resulting GaN nanostructures. To address this issue, Hongyuan et al. proposed a modified hydrothermal reaction and ammoniation two-step method that enables the synthesis of 2D GaN without the need for a growth substrate [32].

In this approach, gamma gallium oxide (γ-Ga_2O_3) is employed as a precursor due to its crystalline structure, which facilitates in-situ exchange reactions with nitrogen atoms supplied by NH_3 gas. Moreover, hexagonal γ-Ga_2O_3 nanosheets are relatively easy to synthesise and offer a low-cost alternative, making this method attractive for scalable production.

The first step in the two-step method for growing GaN nanosheets is the synthesis of high-quality γ-Ga_2O_3 nanosheets via a hydrothermal reaction. An aqueous solution of gallium chloride ($GaCl_3$) is combined with hydrochloric acid and DI water in a beaker. Subsequently, CH_4N_2O, oxalic acid dihydrate ($C_2H_2O_4$+($2H_2O$)), and polyvinylpyrrolidone (PVP) are added to the solution. The mixture is thoroughly stirred and transferred into an autoclave. Urea plays a critical role in this step by inhibiting the formation of gallium hydroxide ($Ga(OH)_3$), which would otherwise interfere with the crystallisation of γ-Ga_2O_3. The hydrothermal reaction is carried out at 230 °C, yielding nanosheets with a thickness of approximately 10 – 20 nm.

In the second step, the synthesised γ-Ga_2O_3 nanosheets undergo ammoniation to form free-standing 2D GaN. The nanosheets are placed on a quartz boat in the centre of a tubular furnace, which is heated to 850 °C under a flow of NH_3 gas. The nitridation reaction facilitates the conversion of Ga_2O_3 to 2D GaN. After the reaction, the sample is cooled to room temperature under an argon flow. The complete synthesis process is illustrated in Figure 10.

The characterisation of the resulting 2D GaN nanosheets reveals a typical multilayer hexagonal stacking corresponding to the wurtzite GaN crystal structure. However, UV-vis spectroscopy measurements show an optical bandgap of 3.12 eV, which is lower than the theoretical predictions for 2D GaN [29] and even below the bulk GaN value of 3.4 eV [153, 155]. This discrepancy suggests the presence of a high density of defects, likely stem-

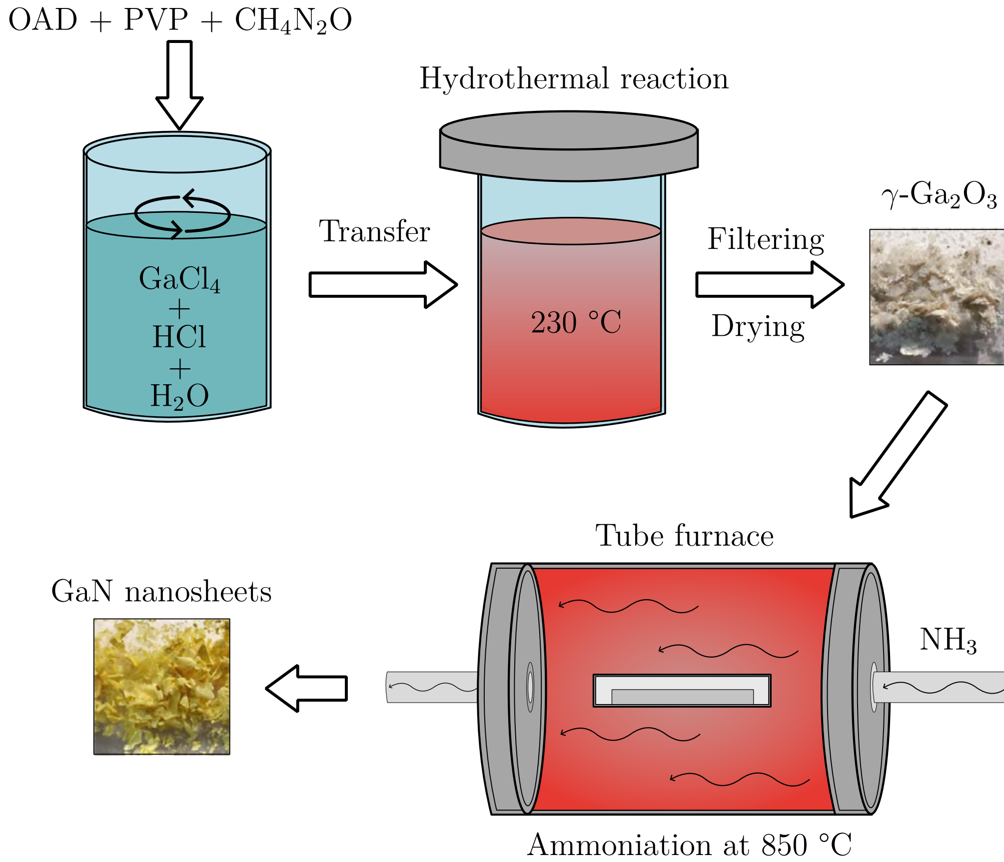

Figure 10: The schematic of the two-step method (the scale was not stated in the original article). Adopted from [32].

ming from stacking faults between GaN layers [32]. These structural imperfections can significantly influence the electronic band structure, potentially introducing defect states within the bandgap. Furthermore, the defects may serve as trapping sites for impurities introduced during the ammoniation process. While this two-step synthesis method offers a low-cost and substrate-independent route to 2D GaN, the resulting material quality remains a significant challenge for practical applications.

2.2.5. Plasma-enhanced chemical vapor deposition

Ammonia is commonly used as a nitrogen source in the growth of 2D GaN [29, 31, 32]. However, its extreme corrosivity and poor cracking efficiency present significant challenges [170, 171]. As a result, alternative nitrogen precursors that are non-pyrophoric, non-toxic, and non-corrosive are desirable for the growth of high-quality 2D GaN. Additionally, precise control over the thickness of GaN films and nanostructures remains a persistent challenge. To address these issues, Gehui et al. reported the synthesis of subnanometer-thick GaN films by utilising plasma in a plasma-enhanced chemical vapor deposition (PECVD) process [27].

The synthesis begins with two Si/SiO_2 wafers, which are first cleaned using sonication baths of acetone, isopropyl alcohol (IPA), and DI water. To ensure complete removal of organic residues and enhance surface purity, an oxygen plasma cleaning step is subse-

quently employed. A small droplet of liquid Ga is then placed on one of the wafers and compressed between the two pretreated surfaces on a hot plate at 50 °C, as schematically illustrated in Figure 11. Due to the oxygen plasma pretreatment, this process results in the formation of a thin Ga_2O_3 layer on the Si/SiO_2 wafer. The residual liquid Ga is removed using a cotton swab dipped in IPA [27].

The wafer bearing the thin Ga_2O_3 layer is then transferred into a PECVD chamber, where the nitridation process takes place. Instead of conventional NH_3, molecular nitrogen (N_2) is used as the nitrogen source. At a process temperature of approximately 800 °C, the Ga_2O_3 layer undergoes a nitridation reaction, converting into GaN. Following the nitridation, the system is cooled down to room temperature under an argon flow.

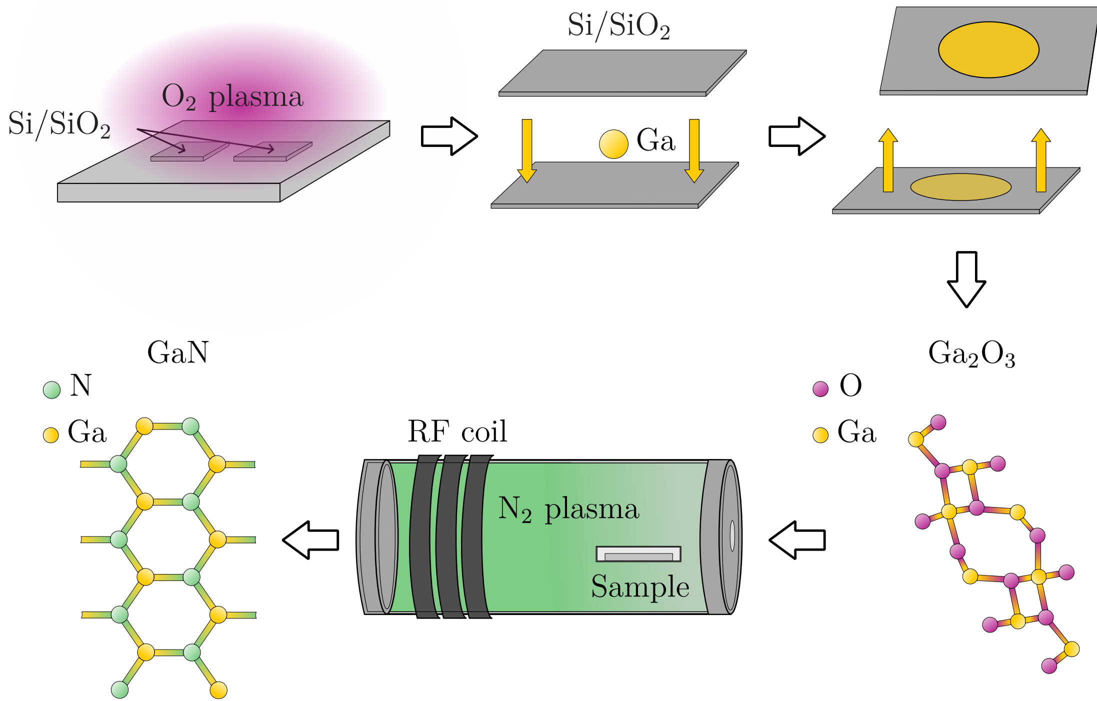

Figure 11: The schematic of the PECVD method. Adopted from [27].

Previous studies have suggested that the thickness of the GaN film corresponds to that of the Ga_2O_3 precursor layer, making it difficult to achieve precise control over the thickness-dependent properties of the final GaN film [168]. However, in this work, the resulting GaN film was found to have a thickness of approximately 0.8 nm, which corresponds to just two atomic layers of wurtzite GaN [27]. Interestingly, the final GaN thickness was observed to be significantly lower than that of the original Ga_2O_3 layer, for instance, an 8 nm thick Ga_2O_3 layer yielded a GaN film only 0.9 nm thick. This suggests that the nitridation process is accompanied by simultaneous etching.

The nitrogen plasma not only facilitates the nitridation of Ga_2O_3 but also etches the surface layer, enabling the formation of ultrathin GaN. This etching is highly time-dependent: it proceeds rapidly at first and slows down as the GaN film becomes thinner.

This slowdown is attributed to the increasing bond strength between GaN and the substrate, which limits further etching. Once the Ga reservoir is depleted, the growth of GaN ceases, and the film begins to degrade due to continued etching. Therefore, precise timing is critical. The process must be halted promptly to preserve a high-quality ultrathin GaN film.

Remarkably, the as-grown GaN film exhibits an ultrawide bandgap of 4.9 eV, significantly higher than values typically reported for GaN synthesised using ammonia. This indicates a high crystal quality and suggests that PECVD-grown GaN films are promising candidates for deep-UV optoelectronic applications. The PECVD technique thus offers a controllable, ammonia-free pathway for the growth of ultrathin, high-quality 2D GaN [27].

2.2.6. Sonochemical exfoliation

Even though the mechanical exfoliation of 2D GaN is infeasible due to the strong covalent bonding between its atomic layers, a modified sonochemical exfoliation technique has shown promising results in synthesising free-standing 2D GaN nanocrystals [26].

In this method, bulk GaN crystals are first ground into smaller fragments and subsequently dispersed in a solvent. The suspension is then subjected to ultrasonic treatment in a sonication bath for several hours. This process induces cavitation, leading to the separation of thin layers from the bulk material. The resulting mixture contains both residual bulk GaN and exfoliated monolayers or few-layer nanocrystals. To isolate the 2D sheets, the solution is centrifuged, and the supernatant, which contains the exfoliated GaN, is carefully collected using a micropipette [172].

The choice of solvent plays a critical role in the efficiency of exfoliation [26]. An effective solvent should closely match the surface energy between the GaN layers to facilitate exfoliation while preserving structural integrity. Sahu et al. investigated several solvents, including acetone, IPA, DI water, N N-dimethylformamide (DMF), and toluene. Among these, IPA yielded the most favourable results, producing the largest and most uniform free-standing GaN nanocrystals.

The exfoliated 2D GaN nanocrystals exhibit high purity, and their measured bandgap ranges from 4.7 eV to 5.3 eV, depending on their crystalline structure and thickness. These wide-bandgap values indicate strong quantum confinement and excellent optical properties. Consequently, 2D GaN produced via sonochemical exfoliation is considered a promising material for next-generation thermoplastic and piezoelectric devices, photodetectors, and emerging technologies such as 6G wireless communication [26].

2.2.7. Low-temperature droplet epitaxy

The droplet epitaxy (DE) method [173, 174], typically carried out in a standard MBE chamber, was adopted and modified by Manis et al. [28] for the growth of GaN nanostructures. One of the main advantages of DE lies in the precise control over the deposition environment, as only desired elements are introduced into the UHV chamber. More-

over, the accurate tuning of the deposition rate enables the fabrication of ultrathin GaN nanostructures. In their work, Manis et al. proposed a modified DE method for the low-temperature growth of GaN nanocrystals, known as LTDE [28]. This technique enabled the synthesis of planar, triangular GaN nanocrystals with a crystalline structure distinct from that of bulk wurtzite GaN and instead resembling the theoretical 2D GaN configuration.

The LTDE growth process consists of four key steps, as illustrated in Figure 12. The first step is the thermal annealing of the substrate. A single-crystal Si(111) substrate is used, which is typically covered with a native oxide layer several nanometers thick and may also contain surface impurities. Therefore, it is essential to anneal the substrate to remove both the oxide and contaminants.

Carbon impurities, commonly present on the surface, significantly hinder the growth of 2D GaN nanocrystals by distorting the substrate morphology. To eliminate these impurities and generate large, atomically flat terraces suitable for nanocrystal growth, a flashing routine is employed. The substrate temperature is rapidly increased to approximately 1250 °C for several seconds and then quickly decreased to 800 °C. This cycle is repeated multiple times until the surface is clean with large atom-high terraces. Importantly, this treatment induces the 7×7 surface reconstruction, which is reported to be the only Si(111) surface reconstruction compatible with the growth of 2D GaN nanocrystals.

Following the surface preparation, deposition of Ga atoms is carried out using an effusion cell. This results in the formation of small Ga droplets on the surface, which diffuse and merge into larger droplets. During this stage, the substrate temperature is maintained at 330 °C.

Subsequently, the postnitridation step is performed. The Ga droplets are exposed to a nitrogen atom/ion source at a steady temperature of 210 °C. As low-energy nitrogen ions ($E = 50\,\mathrm{eV}$) impinge on the droplets, N atoms diffuse across the droplet surface toward the liquid–solid interface, where they react with Ga to nucleate GaN. As the nanocrystal grows, the Ga reservoir is gradually consumed, and the growth ceases once the droplet is fully depleted.

The GaN nanocrystals grown by LTDE exhibit high structural purity, primarily due to the tightly controlled UHV conditions during the process. The triangular nanocrystals have a thickness in the range of 6–20 nm, depending on the miscut angle of the Si(111) substrate. Their crystalline structure corresponds to the theoretically predicted form of 2D GaN. As a result, the high-quality GaN nanocrystals fabricated by the LTDE method demonstrate considerable potential for future applications in nanoelectronics and optoelectronics [28].

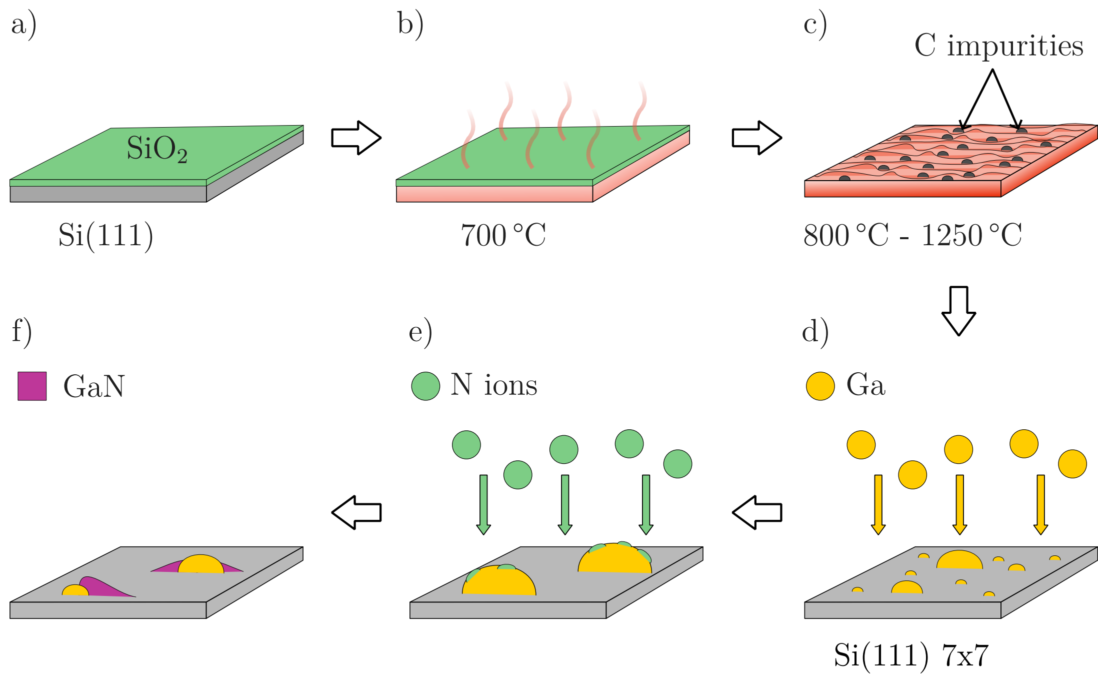

Figure 12: The schematic of LTDE method: a) Si(111) with native SiO_2 layer, b) annealing of the sample, c) flashing routine to align and clean the surface and creation of 7×7 surface reconstruction, d) deposition of Ga atoms, e) nitridation of Ga islands, f) growth of GaN nanocrystals.

3. The preparation of 2D GaN via low-temperature droplet epitaxy (LTDE)

As mentioned in Section 2.2.7, Manis et al. employed the LTDE method to grow high-quality GaN nanocrystals, demonstrating significant potential for future nanoelectronic and optoelectronic applications [28]. However, their synthesis relied on a single set of fixed parameters: nitrogen ions with an energy of 50 eV impinging at an angle of 35°, shown in Figure 13. The influence of different postnitridation angles was already explored in my bachelor thesis [33], revealing notable effects on the shape, size, and overall growth behaviour of the resulting GaN nanocrystals. Nevertheless, the nitrogen ion energy used in that work was relatively high, and at normal incidence (0°), the nanocrystals were etched away completely.

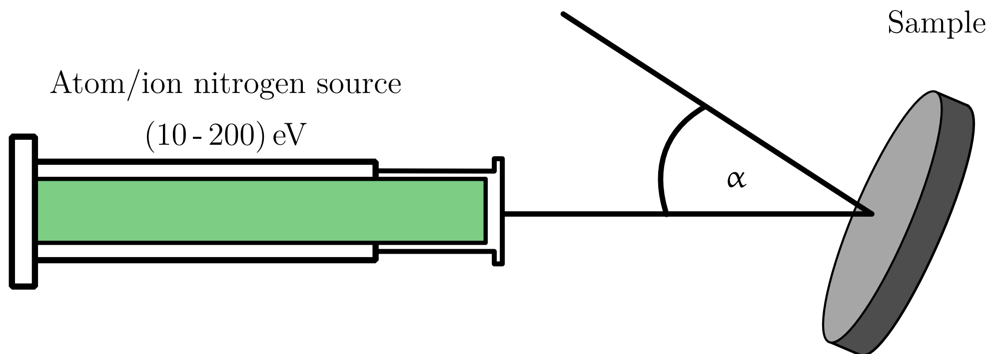

Figure 13: The angle (α) of the atom/ion nitrogen beam relative to the sample surface normal.

These findings highlighted the need for a more detailed investigation into the role of ion energy in the postnitridation process. This became the main focus of the present study. In the following section, the step-by-step procedure for preparing 2D GaN nanostructures using a modified LTDE approach, with a particular emphasis on varying the energy of nitrogen ions during the nitridation step, is described.

3.1. The preparation of Si(111) 7×7

The choice of substrate, and in particular, its surface orientation and quality, plays a critical role in governing the growth behaviour of GaN nanostructures. In order to replicate the experimental conditions reported in [28, 33], a comparable Si(111) substrate was used. However, due to material availability, a wafer with a slightly different miscut angle of 0.5° was selected, instead of the 0.2° and 4.0° wafers employed in the previous studies. The miscut angle of the Si substrate has been shown to exert a minor influence on the size and thickness of the resulting GaN nanostructures [28]. As a result, slight deviations in

the dimensions of the nanostructures produced in this work, compared to earlier reports, are anticipated.

The Si(111) substrate was mounted into the sample holder (see Figure 14 a), which is designed for direct current heating within the UHV apparatus. A schematic of the entire UHV system is shown in Figure 14 c). Before insertion into the system via the load-lock chamber, the substrate was cleaned using a flow of nitrogen. The sample was placed in the load-lock chamber, which was sealed and pumped to the UHV system's pressure (typically 10^{-7} Pa). It was then transferred from the storage chamber (Karusel) to the deposition chamber (Figure 14 b) using a magnetic manipulator. This complex UHV setup enables not only the clean and controlled growth of GaN nanocrystals, but also surface characterisation via low-energy electron diffraction (LEED) and chemical analysis through surface-sensitive XPS.

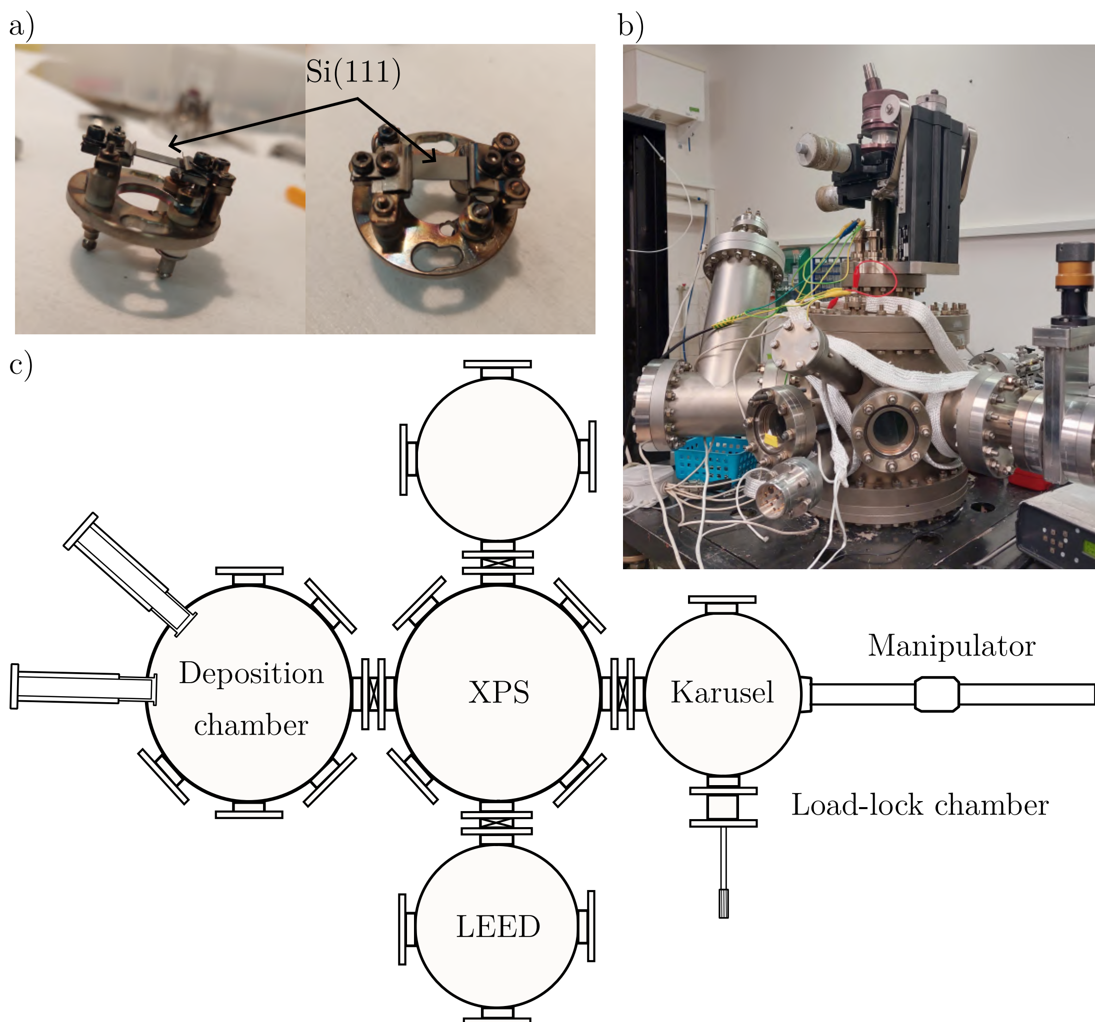

Figure 14: The UHV apparatus: a) the photography of the holder used for direct current heating of the sample, b) the photography of the deposition chamber used for LTDE growth, c) the schematic of the complex UHV apparatus with Karusel for sample storing, XPS chamber, and LEED chamber.

The electrical current running through the sample heated it up to 700 °C, as measured by an optical pyrometer. The sample was annealed at this temperature for at least 12 hours to fully remove the native SiO_2 layer. Following the annealing process, a flashing routine was applied. To achieve the Si(111) with 7×7 surface reconstruction, the sample was initially heated to 800 °C and then rapidly flashed to a maximum of 1380 °C, close to the melting point of silicon [175], before being quickly cooled back to the original temperature. This procedure was repeated for 40 cycles, each lasting one minute, while maintaining the chamber pressure below 2.0×10^{-6} Pa. After the final cycle, the sample was slowly cooled down, allowing the 7×7 surface reconstruction to form [28].

In addition to enabling the reconstruction, the flashing routine offers two key advantages: it flattens the surface, producing atomically flat terraces suitable for the growth of large-area nanostructures, and it removes SiC impurities, which would otherwise inhibit the formation of extended flat regions.

3.2. The deposition and postnitridation process

Once the Si(111) surface with the 7×7 reconstruction was prepared, the deposition of Ga atoms was carried out. Ga was deposited using an Omicron effusion cell onto the Si(111) substrate, forming small Ga droplets upon arrival. The atomically flat surface enabled the lateral diffusion of these droplets, which subsequently merged into larger Ga islands. Since a larger Ga reservoir is expected to result in the formation of larger GaN nanocrystals, ensuring an extremely smooth substrate surface is crucial. To enhance the mobility of Ga droplets and support their diffusion, the substrate temperature was maintained at 330 °C during deposition. The process lasted for 50 minutes, with the chamber pressure kept below 2.0×10^{-7} Pa throughout the procedure.

The postnitridation process is realised to obtain the GaN nanocrystals. The chamber is filled with N_2 molecules until the pressure reaches 1.0×10^{-4} Pa. Using the atom/ion nitrogen source developed by our group [176], nitrogen ions are generated and directed onto the substrate with low energy. The energy of ions used in this work was in the range of 20 eV to 50 eV. In comparison with the Manis et al. [28] experiment, the nitrogen source was perpendicular relative to the sample's surface. During the postnitridation, the sample was heated at 210 °C.

4. Characterisation of LTDE-grown GaN nanocrystals

To characterise the GaN nanocrystals grown by the LTDE method using different energies of nitrogen ions, several analytical techniques were employed during and after the synthesis process. First, XPS was used to verify the cleanliness of the substrate surface following the annealing and flashing routine (described in Chapter 3). As a surface-sensitive technique, XPS provides information on the chemical composition of the surface; therefore, spectra were also acquired after gallium deposition and after the postnitridation step. After removal from UHV conditions, the sample was inspected using an optical microscope, and its surface topography was further examined by SEM and AFM.

To investigate the optical properties of the GaN nanocrystals, Raman spectroscopy, PL, and CL were employed. Finally, to gain insight into the crystalline structure of the nanocrystals, 4D-STEM was used.

The influence of varying nitrogen ion energies during the postnitridation process on the resulting GaN nanostructures will be thoroughly discussed in the following sections. Additionally, the effect of the postnitridation angle will be analysed, thereby extending and completing the findings presented in my bachelor's thesis [33].

4.1. The effect of different postnitridation angles

In my previous work, which was based on the study by Manis et al. [28], the influence of the incident angle of nitrogen ions on Ga droplets was thoroughly investigated [33]. Multiple samples of GaN nanocrystals on Si(111) 7×7 surfaces were prepared and characterised using SEM and AFM. The nitrogen ion energy was kept constant at 40 eV throughout the experiments, and the time of deposition and postnitridation was 50 min and 120 min respectively. The Ga droplets were nitridised using ions with incident angles of 0°, 25°, 35°, 55°, and 80° (as illustrated in Figure 13), resulting in nanocrystals with varying shapes, sizes, and orientations.

Each resulting nanostructure consists of four distinct domains: the etched Si surface, the Ga/GaN interface, the GaN nanocrystal, and, if the Ga droplet was not fully consumed, the residual Ga. An example of a nanocrystal nitridised at 25°, along with its domain structure, is shown in Figure 15. This image corresponds well to the LTDE growth mechanism described in Section 2.2.7. The nitrogen ions impinge on the Ga droplet (region C + D) and initiate the formation of GaN clusters, which then slide down the droplet to the Si(111) substrate (region E), where they nucleate GaN (region B). As the GaN nanocrystal (region A) grows, the Ga droplet is gradually depleted in the direction of the nanocrystal, leaving behind a damaged Si surface (region D).

This damage results from a process known as meltback etching, in which Ga etches the Si(111) 7×7 surface, as reported by Manis et al. [28] and Khoury et al. [177]. Notably, meltback etching is not observed within the GaN nanocrystal itself, likely because the

reaction between Ga and the hyperthermal nitrogen ions dominates, delivering Ga directly to the Ga/GaN interface [28]. Furthermore, the nitrogen beam consists of both N^+ ions and N_2 molecules, which are believed to suppress meltback etching [177]. Therefore, meltback etching was observed only in regions shielded from direct nitrogen exposure.

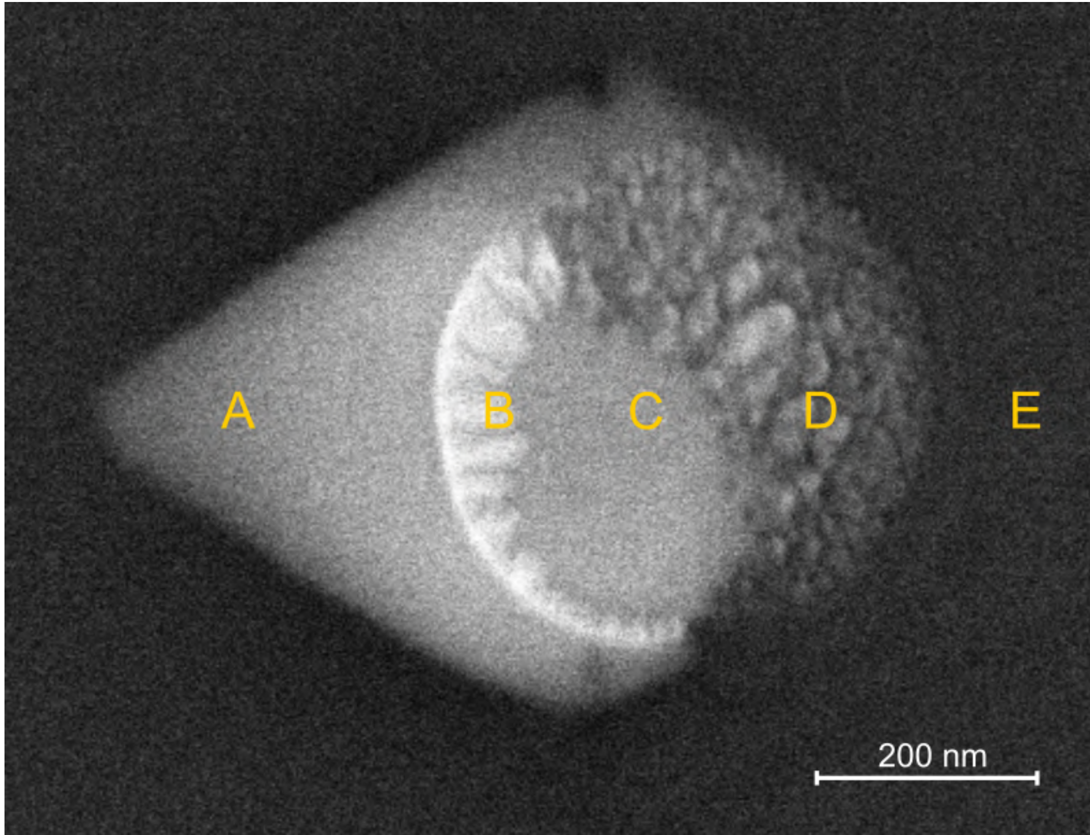

Figure 15: The SEM image of GaN nanocrystal nitridised at 25° with the highlighted domains: A) the triangular-shaped GaN nanocrystal, B) the Ga/GaN interface, C) the residual Ga, D) the etched Si substrate, E) the Si(111) substrate. Adapted from [33].

For incident angles greater than 25°, the growth of GaN nanocrystals was significantly suppressed: either only small nuclei were formed, or the Ga droplets remained unnitridised altogether. Consequently, the focus shifted to smaller incident angles, which had a more pronounced effect on the growth of LTDE-grown GaN nanocrystals. The primary differences between perpendicular incidence (0°) and an angle of 25° were observed in the size, orientation, and, most unexpectedly, the thickness of the resulting nanocrystals. Based on SEM contrast, the nanostructures formed at 0° appeared as holes in the substrate, which was confirmed by AFM measurements (see Figure 16). Instead of thin GaN nanocrystals, 2 – 4 nm deep holes were formed in the Si(111) substrate, exhibiting the same well-defined triangular shape as the 25° nanocrystals.

Interestingly, this etching of the substrate occurred only in regions where GaN nanocrystals had formed, suggesting a specific interaction between the nanocrystals and the Si(111) 7×7 surface. This phenomenon is unexpected, as the presence of N_2 molecules in the nitrogen beam should inhibit meltback etching [177]. To further investigate the formation of these triangular holes, additional experiments were conducted in which nitrogen ions

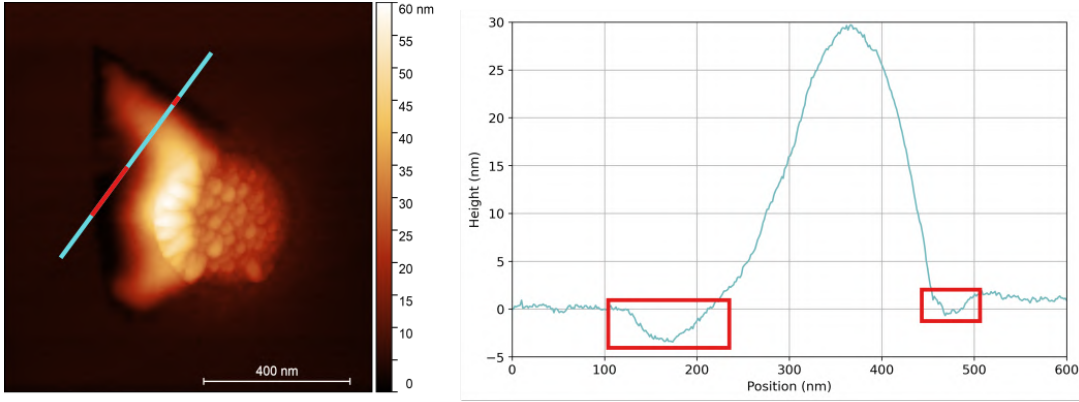

Figure 16: The AFM topography measurement of GaN nanostructure nitrided under the incident angle of 0°. The height profile uncovers the 2 to 4 nm deep holes in the Si(111) substrate on the edges of the GaN nanocrystal (highlighted by the blue lines and squares).

impacted Ga droplets at incident angles of 5°, 10°, and 15°. Figure 17 shows the SEM images of all different nitridation angles.

As previously mentioned, incident angles greater than 25° resulted in the formation of only small GaN nuclei. At 25°, the resulting nanocrystal was well-defined and exhibited no visible signs of damage. Nevertheless, its size was noticeably smaller compared to those formed at 0° nitridation angle, with maximal length reaching approximately 480 nm [33]. In contrast, nanostructures produced at normal incidence reached sizes of around 700 nm. Interestingly, the nanocrystal formed at a 5° incident angle had a size comparable to that of the 25° nanostructure, indicating that there is little to no direct correlation between the nitridation angle and the resulting nanostructure size. Instead, the final size appears to be primarily influenced by the quality of the Si(111) 7×7 surface, particularly its cleanliness and flatness, as well as the initial size of the deposited Ga droplet.

At a nitridation angle of 25° (as shown in Figure 17), the Ga droplet was not entirely depleted, suggesting that a longer nitridation time could be applied without compromising the integrity of the resulting nanocrystal. In contrast, for lower incident angles, the two-hour nitridation process was sufficient to fully consume the Ga droplet. However, the resulting nanostructures exhibited inhomogeneous contrast, indicating potential structural damage confirmed by AFM (see Figure 18).

Once the Ga reservoir was depleted, the thinnest regions of the GaN nanocrystal began to degrade. The borders of the nanocrystals were etched away, leaving only a faint outline of their original shape. However, for incident angles of 10° and 15°, AFM measurements revealed no substrate depressions deeper than 1 nm, suggesting that damage to the underlying Si(111) substrate was minimal. It was reported that for the incident angle of 0°, the damage to the Si(111) 7×7 surface was significantly higher [33].

Moreover, the AFM height profiles indicate that the Ga/GaN interface (region B in Figure 15) constitutes the highest point of the GaN nanostructure, reaching over 50 nm. This is consistent with the proposed growth mechanism, in which GaN clusters nucleate upon ion impact and subsequently slide down the Ga droplet to form the crystalline inter-

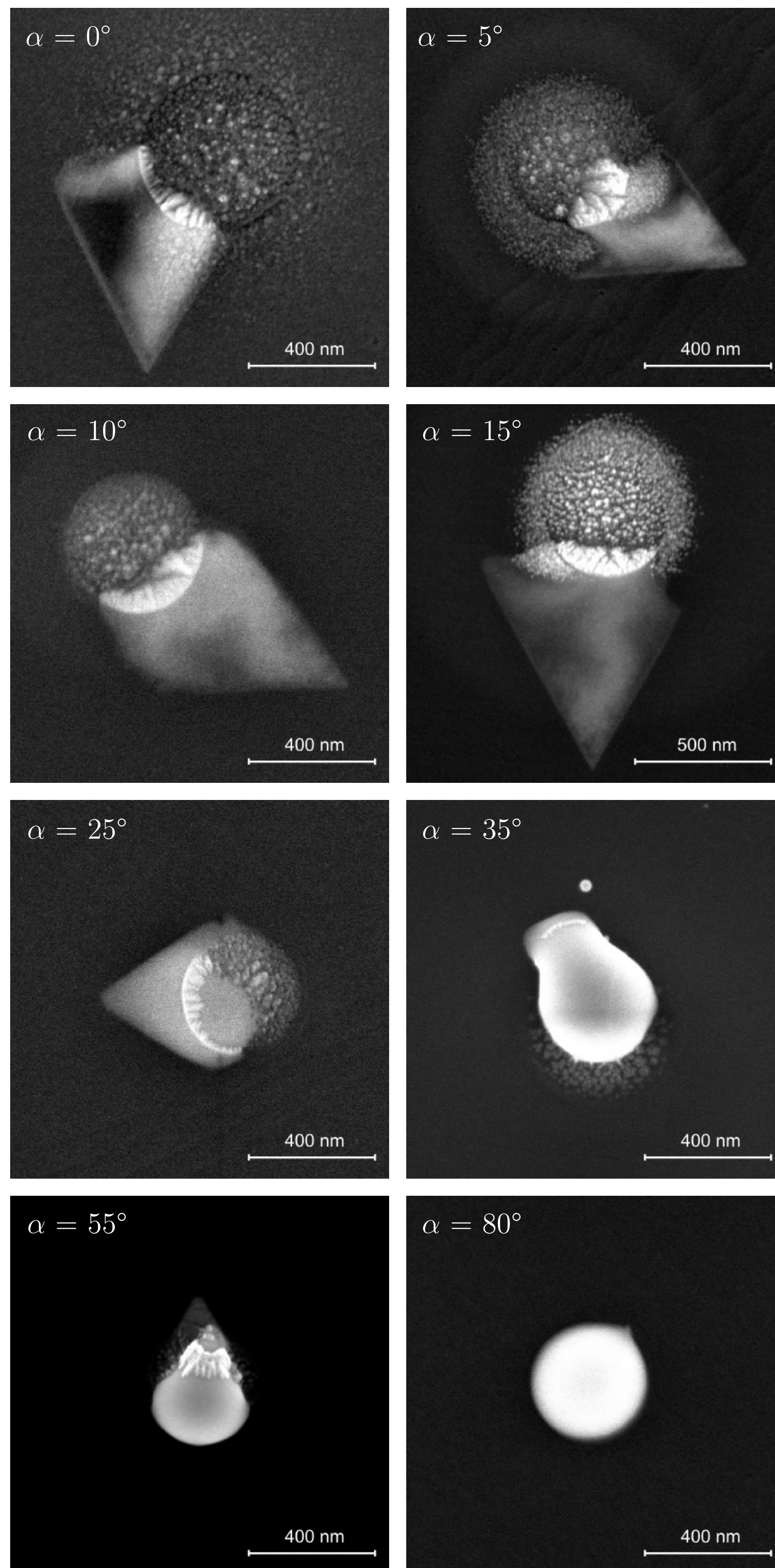

Figure 17: SEM images of GaN nanostructures nitridised under different incident angles α in the range of 0° to 80° (please note that 15° has a different scale). 0°, 25°, 35°, 55° and 80° were adapted from [33].

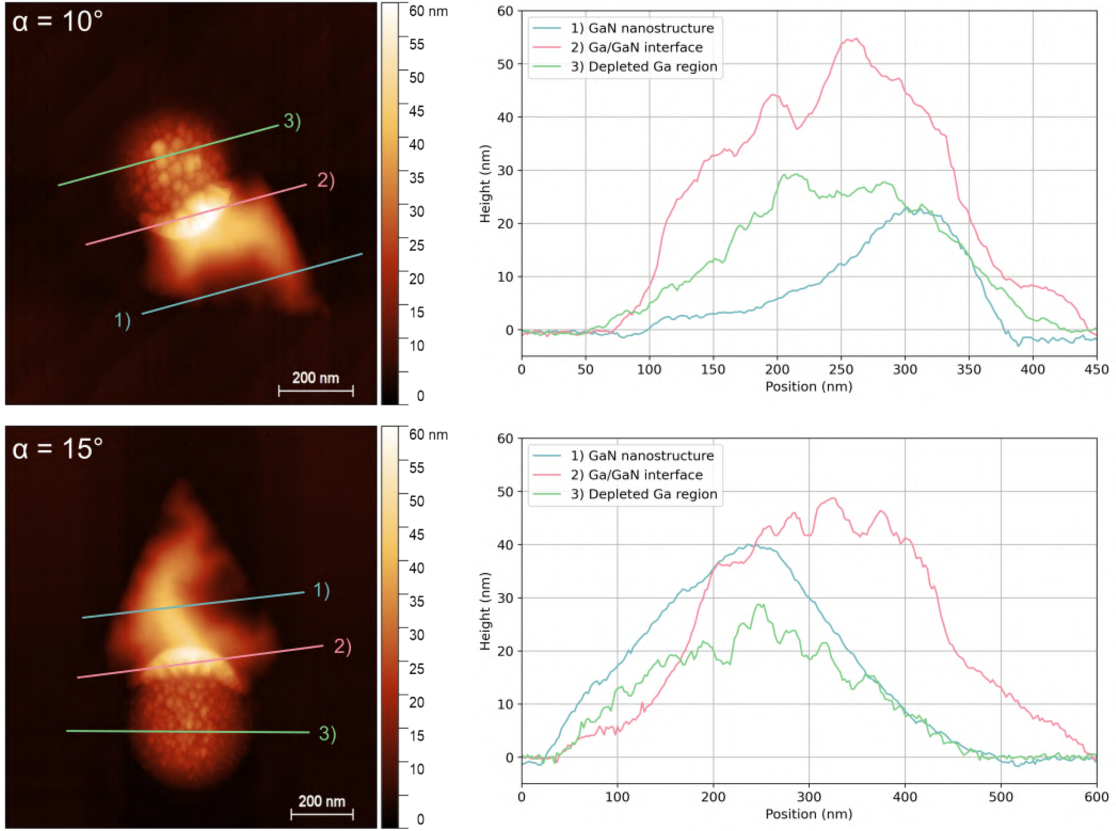

Figure 18: The AFM topography measurements of GaN nanostructures nitrided under the incident angle of 10° and 15° with extracted height profiles (colourful lines labelled with numbers) of damaged GaN nanocrystal, Ga/GaN interface, and a region of depleted Ga droplet.

face. The GaN nanocrystal then continues to grow from this elevated base. Consequently, the maximum height of the nanocrystal must remain below that of the Ga/GaN interface.

To summarise the key findings on the effect of nitrogen ion incident angle on the resulting GaN nanostructures, additional samples nitridised at 5°, 10°, and 15° were analysed, complementing the previously studied angles ranging from 0° to 80° [33]. While the maximal lengths of the nanostructures varied, no direct correlation with the nitridation angle was observed, instead, the size was primarily influenced by the quality of the Si(111) 7×7 surface and the shape of the nanostructure [33]. For incident angles below 25°, the two-hour nitridation process led to full depletion of the Ga droplet and subsequent degradation of the thinnest regions of the nanocrystals, resulting in shallow substrate etching. In contrast, the 25° sample retained some Ga residues, and the nanostructure remained intact and well-defined. These results indicate that at 50 eV nitrogen ion energy, higher incident angles slow down the nitridation process and thus better preserve the nanocrystal. Therefore, the angle of incidence primarily affects the nitridation rate, and comparable results may be achieved at different angles by adjusting the nitridation time.

4.2. The effect of different ion energies

The findings from the previous section provide a solid foundation for the following experiments, which investigate the effect of varying nitrogen ion energies (20 eV to 50 eV) on the formation and morphology of GaN nanostructures. All samples were prepared following the procedure detailed in Chapter 3, using nitrogen ions with the incident angle of 0° and kinetic energies of 20 eV, 30 eV, 40 eV, and 50 eV. The different ion energies are expected to influence both nanocrystal formation and surface etching, offering key insights into the mechanisms governing GaN nanocrystal growth and surface etching. This section follows the chemical evolution of the sample, its morphology, and its optical response across this energy range. Additionally, time-dependent postnitridation and thermal annealing experiments were conducted to clarify the processes responsible for the etching of the nanocrystals and the substrate.

4.2.1. Evolution of chemical composition

To monitor changes in the chemical composition during the growth process and to verify surface cleanliness, XPS measurements were performed after each step. The XPS system is integrated into the UHV chamber shown in Figure 14, allowing characterisation without exposing the sample to ambient atmosphere. The resulting spectra are presented in Figure 19, with the final spectrum after nitridation shown separately in Figure 20, highlighting the nitridation of Ga into GaN in greater detail.

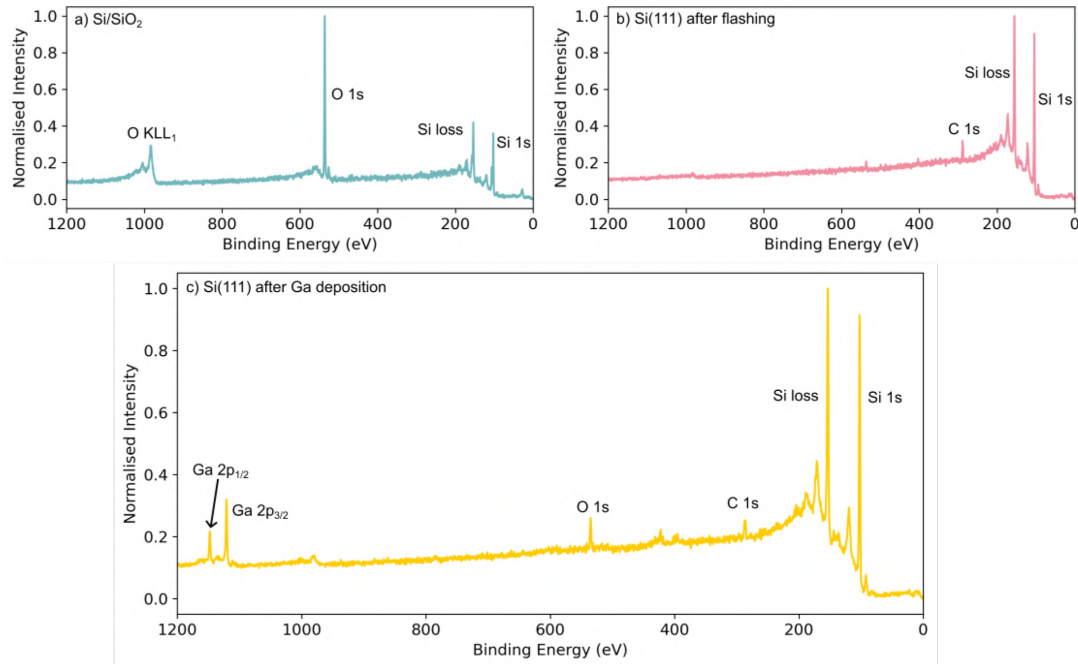

Figure 19: XPS measurements throughout the synthesis of GaN nanocrystals via LTDE method: a) the Si/SiO_2 substrate before annealing and flashing, b) the surface of Si(111) 7×7 after the annealing and flashing, c) the Si(111) 7×7 surface after the Ga deposition.

The surface of the Si(111) substrate is initially covered by a thin native oxide layer, as confirmed by two prominent oxygen peaks: O KLL_1 at 979.9 eV and O 1s at 532.0 eV. The peaks in the low-energy region correspond to the Si(111) substrate.

After prolonged annealing at 700 °C for at least 12 hours and multiple cycles of the flashing routine between 800 °C and 1380 °C, the XPS spectrum (Figure 19b) shows that the oxygen peaks (O KLL_1 and O 1s) were successfully removed from the Si(111) surface, with only minimal O 1s residues remaining. However, the C 1s peak indicates incomplete removal of carbon contaminants. These residual carbon impurities can degrade the surface quality, resulting in a rough morphology unsuitable for 2D GaN growth. To fully eliminate carbon, additional flashing cycles must be performed. Once the C 1s intensity is minimised, a clean and atomically flat surface is achieved, providing the necessary conditions for gallium droplet deposition.

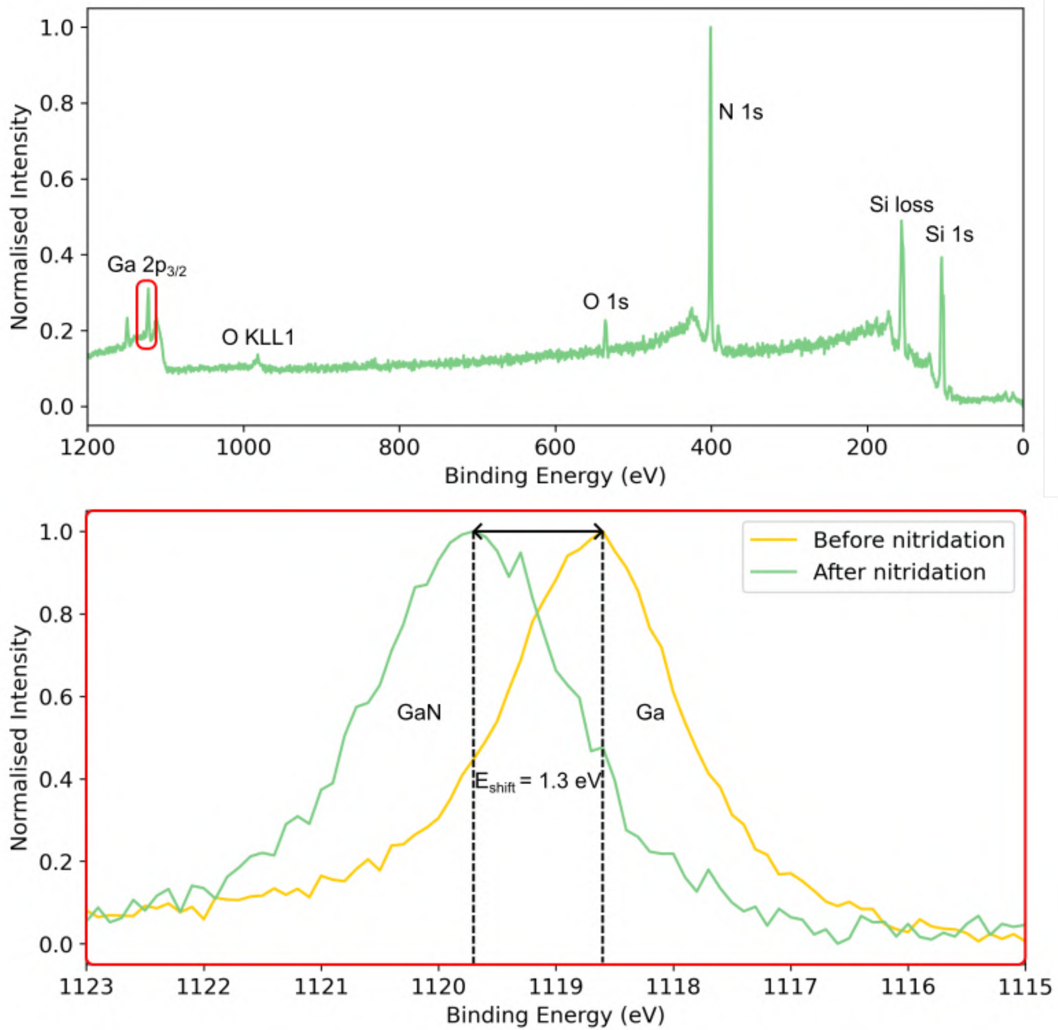

Figure 20: XPS spectrum of the Si(111) 7×7 surface after nitridation of Ga droplets. The red square highlights the Ga $2p_{3/2}$ peak, which is shown in detail in the accompanying spectrum. The observed shift in binding energy (E_{shift} = 1.3 eV) towards higher values indicates the formation of Ga–N bonds, confirming successful nitridation.

Following Ga deposition, the XPS spectrum (Figure 19c) reveals two key peaks: Ga $2p_{1/2}$ and Ga $2p_{3/2}$, confirming the presence of Ga droplets. Their relatively low intensities suggest limited surface coverage, which was later verified by SEM imaging. Notably, the O 1s peak reappears after Ga deposition, likely due to residual oxygen originating from the Ga effusion cell.

The XPS spectrum following the nitridation of Ga droplets is shown in Figure 20. The most notable change compared to the prenitridation spectrum is the emergence of a prominent N 1s peak, confirming the incorporation of nitrogen into the sample. Additionally, small increases in the intensities of O 1s and O KLL_1 peaks are observed, which can be attributed to residual oxygen present in the nitrogen gas lines. To minimise this contamination, the gas tubes should be annealed prior to each deposition process.

To verify that Ga nitridation occurred, the Ga $2p_{3/2}$ peak must be examined in detail. Upon successful nitridation, a slight shift of this peak toward higher binding energies is expected [28]. As shown in Figure 20, a shift of approximately 1.3 eV is evident when compared to the Ga $2p_{3/2}$ peak measured after Ga deposition, indicating the formation of Ga–N bonds. Thus, this XPS analysis confirms both the high surface purity of the Si(111) 7×7 substrate throughout the fabrication process and the successful nitridation of Ga droplets into GaN nanocrystals.

4.2.2. Morphology of GaN nanostructures

After the XPS measurements, the sample was removed from the UHV system for a quick inspection using an optical microscope. Although submicrometer-sized structures are generally hard to spot using optical microscopy, GaN nanocrystals exhibit strong contrast, particularly in dark-field imaging, making them distinguishable. This allows for a rapid assessment of surface coverage and identification of areas where GaN nanocrystals are present, as the surface is not necessarily uniformly covered.

However, to accurately determine the morphology of the GaN nanostructures, high-resolution imaging techniques such as SEM and AFM were employed. SEM images were acquired using a high-resolution FEI Verios 460L scanning electron microscope operated in immersion mode. The imaging was performed at an accelerating voltage of 5 kV with a beam current ranging from 25 to 50 pA. AFM measurements were performed using the Scanning Probe Microscope Bruker Dimension Icon equipped with ScanAsyst probes.

In Figure 21, GaN nanocrystals grown by the LTDE method using nitrogen ion energies ranging from 20 to 50 eV are shown. Throughout the experiment, the incidence angle of nitrogen ions was 0°, eliminating any preferential growth direction associated with ion incidence angle. The resulting nanocrystals exhibit shape variations that depend on both the surface and the ion energy. At 20 eV and 40 eV, the nanocrystals are poorly defined and do not exhibit the typical triangular morphology observed at other energies. In addition, they are smaller in size, with average lateral dimensions of approximately 260 nm and 400 nm, respectively.

These differences are attributed to insufficient surface preparation prior to Ga deposition, particularly ineffective flashing. In the SEM images, SiC impurities are clearly

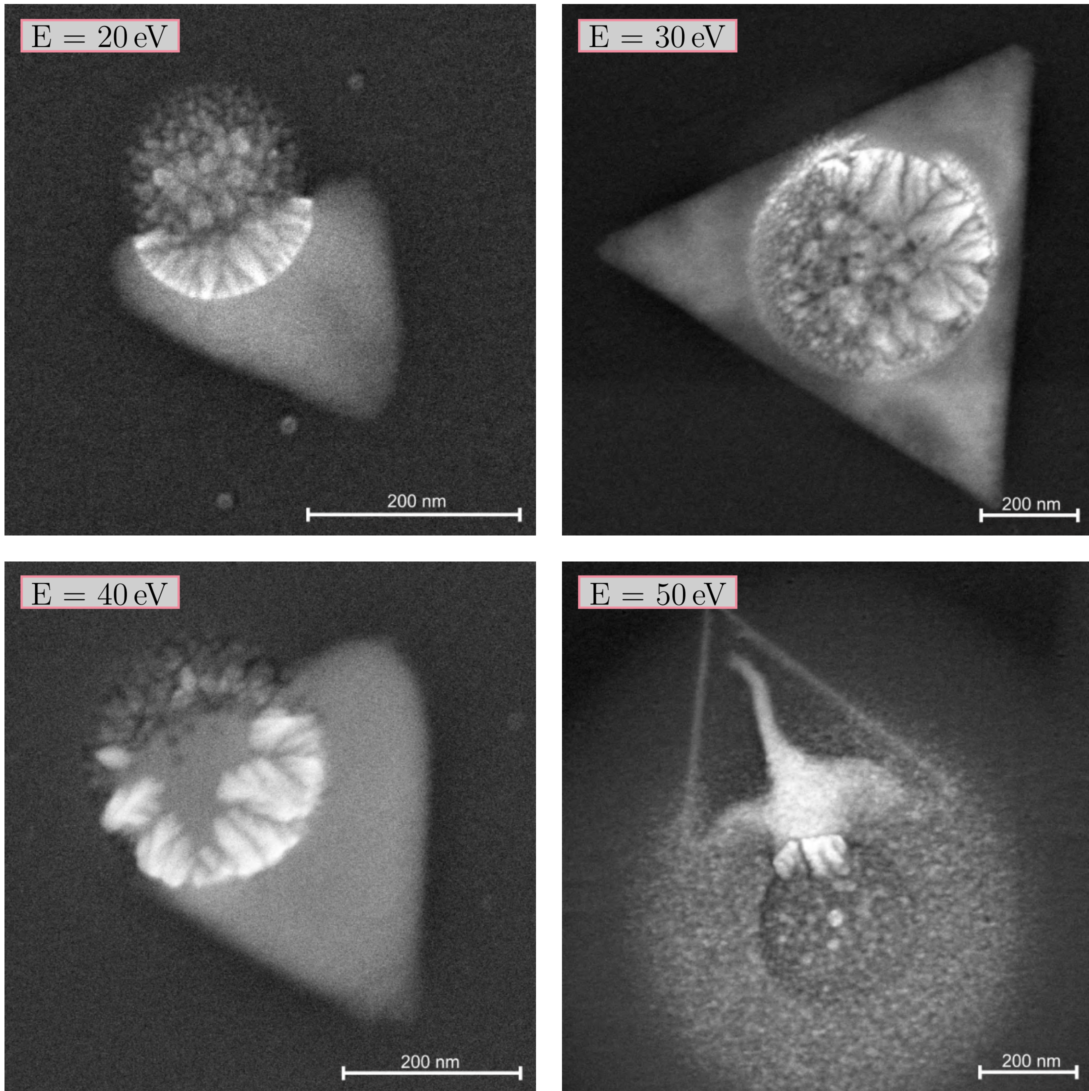

Figure 21: SEM images of GaN nanocrystals on Si(111) 7×7 grown by the LTDE method under the perpendicular incident angle of nitrogen ions.

visible, indicating that the flashing routine did not fully remove them. When the substrate is heated above 800 °C, the Si(111) surface begins to melt, forming large, atomically flat terraces that facilitate uniform GaN growth. However, the presence of residual impurities disrupts this process, leading to bent melting planes and the formation of small terraces with rough step edges. These features limit the diffusion of Ga droplets, preventing them from merging into larger reservoirs and ultimately resulting in the reduced size and irregular shape of the GaN nanocrystals.

In contrast, at 30 eV and 50 eV, the surface was clean and flat, providing suitable conditions for GaN nanocrystal growth. The resulting nanocrystals reached average lateral sizes of approximately 830 nm and 660 nm (shown in Figure 22), respectively. In this energy range, the ion energy plays a crucial role in both defining the crystal morphology and minimising surface damage. As shown in Figure 21, two key differences can be observed. The nanocrystal grown at 30 eV exhibits a well-defined triangular shape with no visible surface damage. Notably, it does not display the circular residual pattern often

left around the original Ga droplet, indicating minimal etching or redeposition effects during nitridation. In comparison, the nanocrystal formed at 50 eV does exhibit such a circular pattern, likely caused by a redeposited Ga layer originating from the Ga droplet impacted by nitrogen ions [33]. This redeposition causes the minor etching of the surface in the vicinity of the original Ga droplet, as Ga atoms are known to etch the Si(111) 7×7 surface [177]. Nevertheless, the higher ion energy and associated Ga redeposition did not inhibit the formation of well-defined GaN nanocrystals. To further clarify the origin of the triangular-shaped holes observed in the Si(111) 7×7 surface, two additional experiments were conducted and are discussed in Section 4.3.1 and Section 4.3.2.

In addition to their lateral dimensions, the vertical profiles of the GaN nanocrystals were investigated using AFM. The nanocrystals reached heights ranging from 29 nm to 40 nm (see Figure 22), depending primarily on surface quality and, consequently, the size of the Ga droplets. Therefore, the dimensions of the GaN nanostructures are not governed by the energy of the incident nitrogen ions. Additionally, these values are significantly higher than those reported by Manis et al. [28], who observed heights of 13–20 nm and 6–8 nm on Si(111) substrates with miscut angles of 0.2° and 4°, respectively. This discrepancy is likely due to differences in the substrate type used in this work, as the surface preparation procedures were otherwise comparable.

In principle, several strategies could be employed to reduce the height of GaN nanocrystals. Since the vertical dimension is largely determined by the initial Ga droplet size (this trend is visible in Figure 22), producing thinner Ga droplets could yield flatter nanocrystals. However, this approach was not explored further in this study to maintain consistency with the growth parameters reported by Manis et al. for the sake of reproducibility. Another possibility is to modify the shape of the nanocrystals post-growth through angled ion bombardment. In the PECVD method (see Section 2.2.5), subnanometer-thick GaN films were achieved by controlled nitrogen plasma exposure. If a similar effect could be replicated using low-energy nitrogen ions, it might be possible to produce thinner GaN nanostructures while preserving high crystalline quality.

The topography of a GaN nanocrystal nitridised by nitrogen ions with a kinetic energy of 50 eV is presented in Figure 23. In the depleted region, the Ga droplet is fully consumed, and the underlying Si(111) 7×7 surface exhibits noticeable damage. However, AFM measurements did not reveal any distinct holes in this area. Instead, the data indicate the presence of residual Ga that likely underwent nitridation, forming small, bulk-like GaN nanocrystals. In contrast, the region containing the GaN nanocrystal displays 4 nm-deep holes in the Si(111) 7×7 surface, shaped identically as the GaN nanocrystal. This is attributed to the nanocrystal's pyramid-like morphology, where the thinnest regions, located along the sides, are etched away faster, while the central strip and the Ga/GaN interface remain intact on the substrate. Notably, the thickness of these preserved regions slowly decreases, supporting the hypothesis that the GaN nanocrystal thickness could be further reduced through controlled ion bombardment.

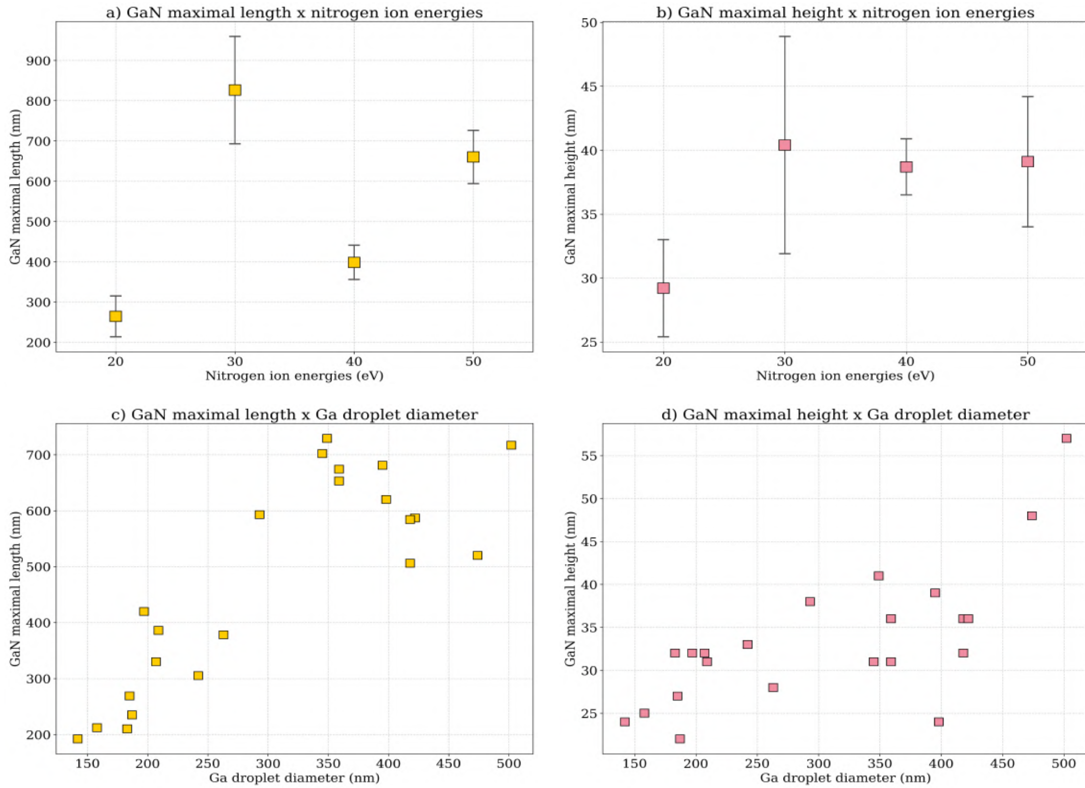

Figure 22: The maximal length and maximal height of GaN nanocrystals dependent on: a-b) nitrogen ion energy, c-d) Ga droplet diameter.

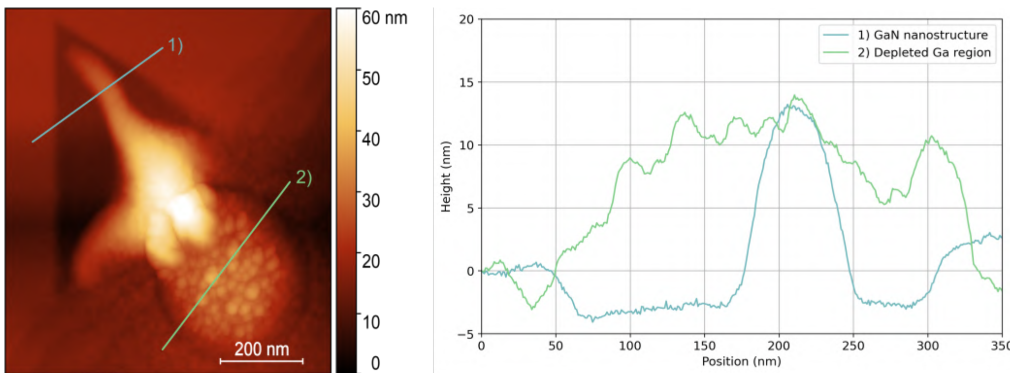

Figure 23: AFM image of GaN nanostructure nitridised by 50 eV ions with the extracted height profiles of: 1) GaN nanocrystal region and 2) depleted Ga region.

4.2.3. Optical and structural characterisation

Once the quality of the synthesised nanocrystals was confirmed by SEM and AFM, additional optical measurements were performed to investigate their structural and electronic properties. To assess crystallinity and identify potential defects, Raman spectroscopy was carried out using a Witec Alpha 300R. Two laser wavelengths were used: 355 nm (2–4 mW) and 633 nm (20–30 mW), enabling both surface-sensitive and deeper probing of the nanostructures. Photoluminescence (PL) spectroscopy was also conducted on the same instrument to determine the optical bandgap of the LTDE-grown GaN nanocrystals.

These measurements were conducted to obtain complementary insight into the electronic quality and possible quantum confinement effects within the nanocrystals.

The expected Raman peak exclusive to 2D GaN appears at 566.2 cm^{-1}, alongside three characteristic bulk GaN modes at 567.2, 560.7, and 529.3 cm^{-1} [31, 178]. However, none of these features were observed in our Raman spectra presented in Figure 24. The only prominent peak detected was at 520 cm^{-1}, corresponding to the silicon substrate. Similarly, the photoluminescence (PL) measurement yielded no detectable signal. This suggests that the LTDE-grown GaN nanocrystals are optically inactive under these conditions, or that their bandgap lies below the excitation energy of the 355 nm laser.

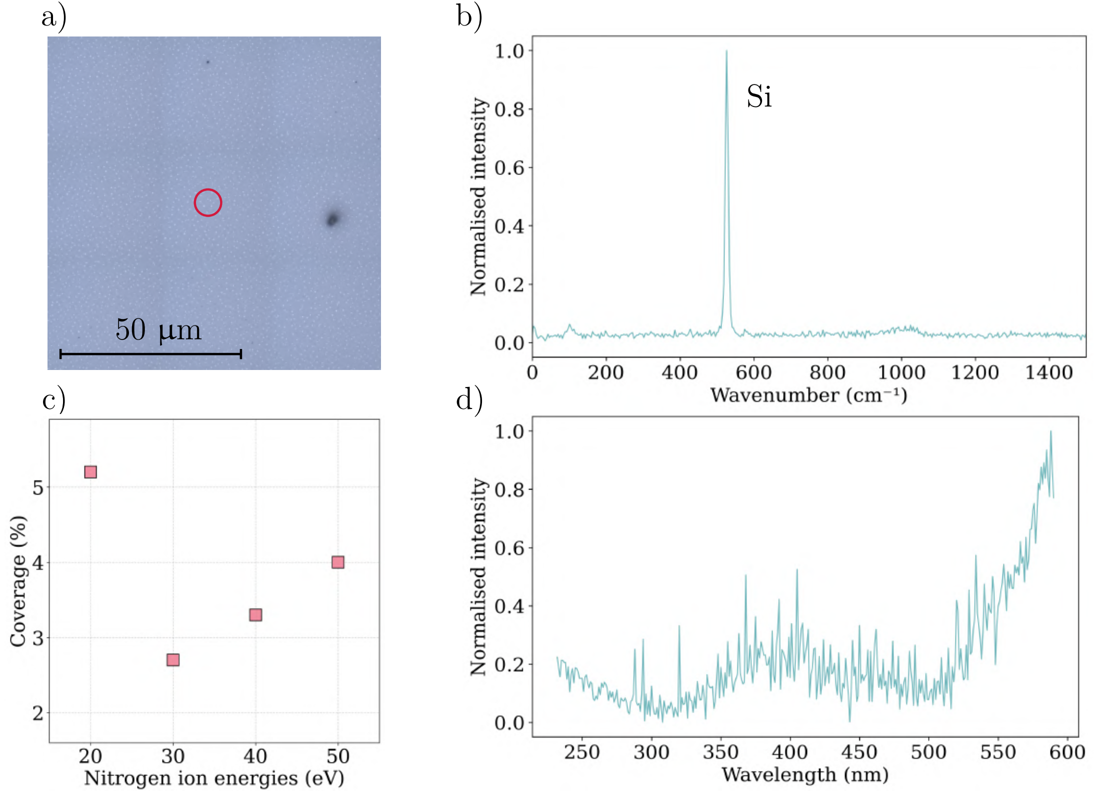

Figure 24: a) The optical image of GaN nanocrystals in bright-field with the red circle showing the area where b) the Raman spectrum was measured using the 355 nm laser. c) The comparison of nanocrystals coverage of the Si(111) 7×7 surface for different nitrogen ion energies. d) The PL spectrum obtained using the 224 nm laser.

Additional PL measurements were conducted at the Institute of Physics of the Czech Academy of Sciences in Prague to investigate the optical properties of the LTDE-grown GaN nanocrystals further. A 224 nm excitation laser was used to excite potential UV emission from the GaN nanostructures (see Figure 24). While a faint signal near the bulk GaN emission peak was observed, it was barely distinguishable from the noise. The low signal-to-noise ratio made it difficult to conclusively attribute the emission to the GaN nanocrystals. As a result, cathodoluminescence (CL) measurements were performed under various electron beam conditions to improve sensitivity. However, no detectable signal was observed, suggesting that the nanocrystals remain optically inactive or that their radiative efficiency is extremely low.

Another factor potentially contributing to the optical inactivity is the low surface coverage of GaN nanocrystals on the Si(111) 7×7 substrate. The highest observed coverage (shown in Figure 24), measured on the sample nitridised with 20 eV nitrogen ions, reached only 5.2 %, and this sample also exhibited poor surface quality and the smallest nanocrystal dimensions. In contrast, the sample with the best surface quality and nearly micrometre-sized nanocrystals had a coverage of just 2.7 %. Such limited coverage significantly reduces the overall volume of optically active material, which may explain the low or undetectable PL and CL signals.

Additionally, structural analysis of the GaN nanostructures was attempted using a 4D-STEM detector, developed within a TACR (Technology Agency of the Czech Republic) project in collaboration with AdvaScope and TESCAN, mounted on the FIB/SEM Tescan Amber II. The measurements were carried out by my colleague Bc. Viktor Bajo from Brno University of Technology. This technique enables the acquisition of diffraction patterns at each pixel of the scan, providing detailed information about the crystalline structure, such as symmetry and lattice parameters.

To enable electron transmission, thin lamellae (approximately 50 nm thick) had to be fabricated from the sample (see Figure 25). The whole lamellae fabrication process is thoroughly described in Bajo's work [179]. However, preparing suitable lamellae from the small and thin GaN nanocrystals proved highly challenging. No high-quality lamellae were successfully produced, and preserving the crystal structure during preparation was also problematic. As a result, no usable diffraction patterns could be obtained. At one point, a diffraction pattern from a small area of a presumed nanocrystal was acquired (see Figure 25b–c). However, only a few diffraction spots were visible, and the pattern exhibited a high level of noise, making it difficult to interpret. As a result, no meaningful structural information could be extracted.

In addition, precise targeting of individual nanocrystals during focused ion beam milling was difficult, preventing reliable determination of their thickness and lateral dimensions. Alternative techniques such as high-resolution transmission electron microscopy (HRTEM) or scanning tunnelling microscopy (STM) should be considered to explore the internal structure of these nanocrystals in future studies.

4.3. Investigation of the Si(111) 7×7 surface etching

Although intriguing, the etching of the Si(111) 7×7 surface is an undesirable effect, as interactions between the substrate and the GaN nanocrystals may limit their potential future applications. Until now, the only known mechanism for the etching of this surface has been meltback etching induced by Ga [177]. However, previous reports indicate that this process should not occur in the vicinity of triangular GaN nanocrystals [28]. This discrepancy suggests the presence of an alternative etching mechanism, which has not yet been described in the literature.

The experimental results suggest that the surface etching occurs only in cases where the Ga reservoir is fully depleted, indicating that the etching process begins after the

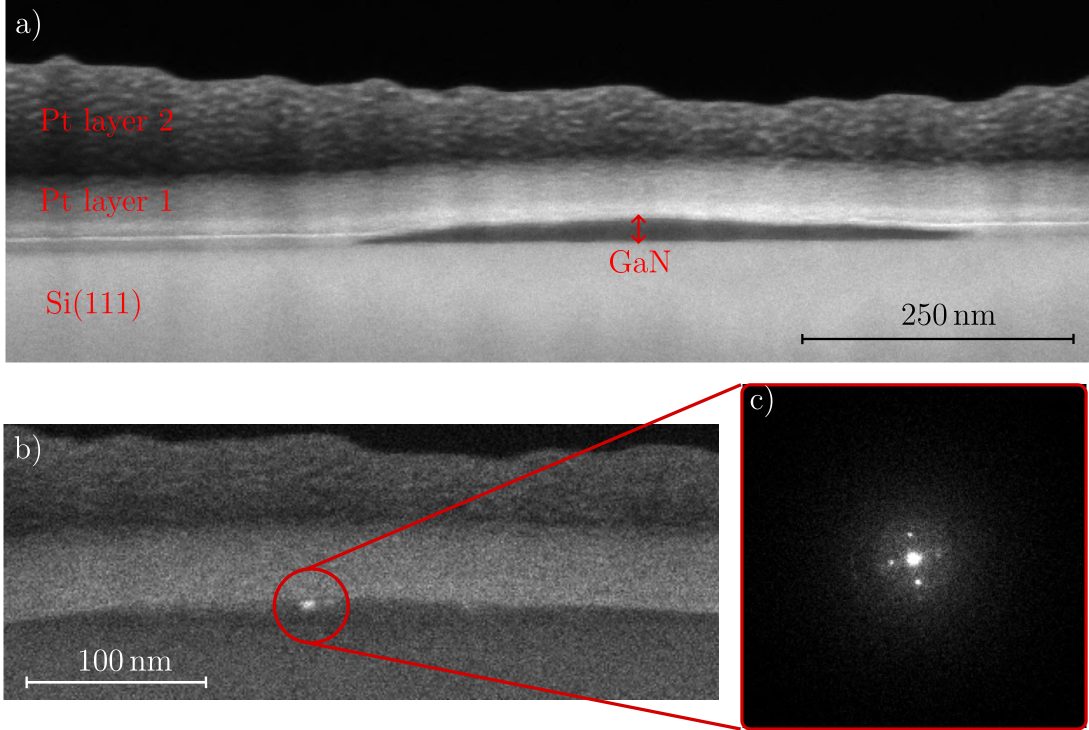

Figure 25: 4D-STEM lamella prepared with two protective platinum layers deposited by electron (Pt layer 1) and ion (Pt layer 2) sputtering. a) Bright-field image showing the lamella structure. (b) Magnified view indicating the point from which the diffraction pattern in (c) was acquired.

growth of the GaN nanocrystals has stopped. The etching is most prominent at the thinnest regions of the nanocrystals, with the resulting holes extending no deeper than 4 nm into the Si(111) substrate. This phenomenon was primarily observed in samples nitridised with 50 eV nitrogen ions. At lower ion energies, although the nanocrystals exhibited structural damage, no substrate etching was detected. Throughout the nitridation process, the temperature was maintained at 210 °C. The incidence angle of the nitrogen ions also proved to be a critical factor: while higher angles (10°–15°) led to significant damage to the GaN nanocrystals, they did not result in deep etching of the underlying silicon surface.

To investigate the nature of this phenomenon, two additional experiments were conducted. The first involved time-dependent nitridation to determine when the etching initiates and to estimate the speed of the etching process. The second experiment focused on thermal annealing to evaluate the influence of temperature on the stability of the GaN nanostructures. Both experiments are discussed in the following sections.

4.3.1. Time-dependent postnitridation

To explore the etching mechanism of GaN nanocrystals, the duration of the nitridation step was reduced from two hours to one hour, with the expectation that the LTDE-grown GaN nanostructures would display different stages of surface and nanocrystal damage (see Figure 26). The energy of the nitrogen ions was 50 eV, and the other parameters

remained unchanged throughout the experiment as described in Chapter 3. Surprisingly, the nanostructures showed a comparable degree of damage to both the GaN nanocrystals and the Si(111) 7×7 surface, indicating that the etching initiates rapidly and slows down significantly once specific regions of the nanocrystals are etched. The holes in the surface were deeper than ever before, reaching almost 10 nm. Notably, the central strip and the areas surrounding the Ga/GaN interface remained largely intact and exhibited a high resistance to further etching. In comparison with the profiles illustrated in Figure 23, the profiles shown in Figure 27 exhibit a relatively unchanged thickness of these regions, implying that these unetched parts possess stronger or more stable bonding. Furthermore, the whole Ga reservoir was depleted after one hour of nitridation by 50 eV ions, therefore, the nitridation process is much faster than initially thought, and the nitridation time was further lowered for the following experiments.

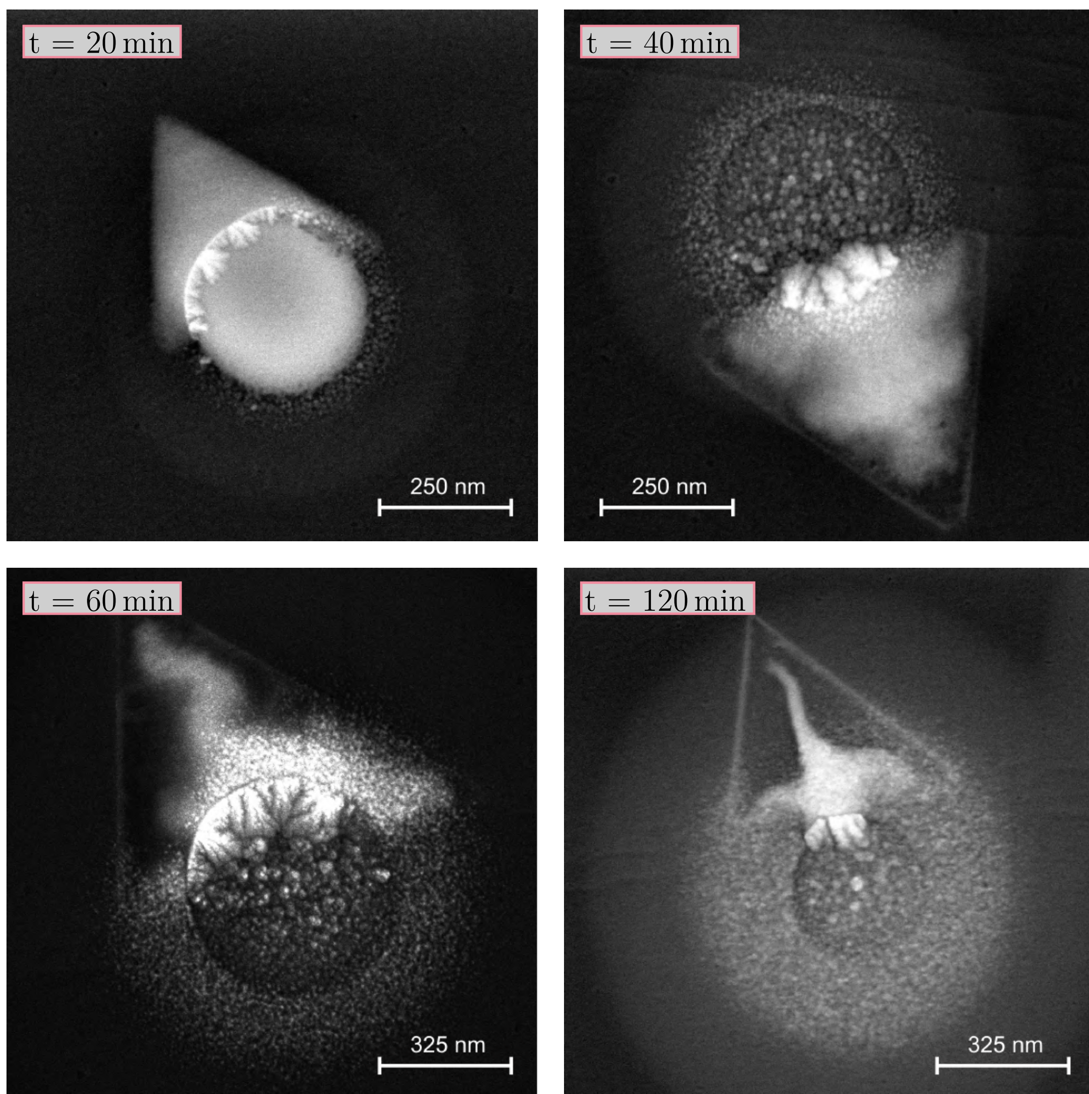

Figure 26: SEM images showing different stages of GaN nanocrystal development as a function of nitridation time: 20, 40, 60, and 120 minutes.

After reducing the nitridation time to 40 minutes, the GaN nanocrystal appeared to be in the early stages of the etching process, shortly after the Ga reservoir was depleted. The

edges of the nanocrystal showed significant damage, however, no holes in the surface in the place where the GaN nanocrystal was synthesised were detected in the AFM measurement in Figure 27.

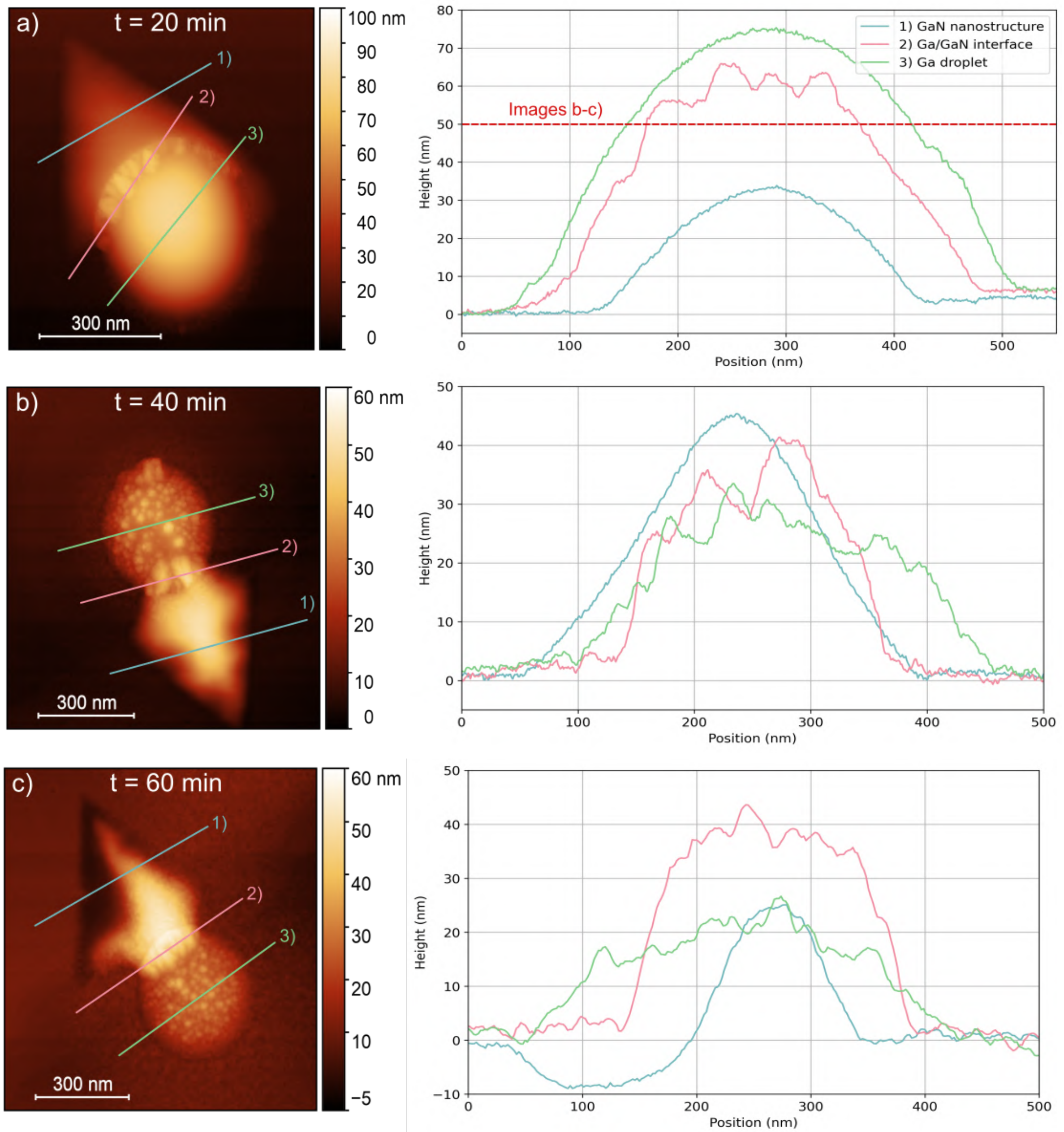

Figure 27: Topography measurements (AFM) of GaN nanostructures nitridised for different times with extracted height profiles: a) 20 minutes, b) 40 minutes, c) 60 minutes. In the c) height profile, a significant hole on the substrate is noticeable.

In contrast, the sample nitridised for 20 minutes displayed a well-defined GaN nanocrystal with no noticeable morphological damage. The Ga reservoir remained partially intact, supporting the hypothesis that etching begins only after the Ga droplet is fully converted into the GaN nanocrystal.

SEM and AFM analysis of the GaN nanostructures revealed notable trends in their morphology. The lateral size of the nanostructures increases with longer nitridation times, while the height remains comparable across samples in the unetched regions. This confirms that the initial Ga droplet height determines the maximum thickness of the resulting GaN nanocrystal. Interestingly, even after the Ga reservoir is depleted, lateral growth continues: nanostructures nitridised for 40 and 60 minutes exhibit mean maximum lengths of approximately 573 nm and 758 nm, respectively. Since the visible nanocrystals reach just over 500 nm in length, this suggests that etched nanostructures can be tens of nanometers larger than their unetched counterparts. We hypothesise that the etching process extends the nanostructure edges, indicating that the GaN crystal may grow into the substrate, forming a buried wedge-like feature. Although not directly observable by SEM or AFM, such a wedge could destabilise the overlying Si(111) structure, making it more susceptible to ion or thermal etching.

These findings provide valuable insights into the growth mechanism of GaN nanocrystals on the Si(111) 7×7 surface and have significantly reduced the required preparation time. However, further experiments are needed to investigate the possibility of in-depth growth of the GaN nanostructures in more detail.

4.3.2. Thermal annealing of GaN nanostructures

To investigate the effect of temperature on pre-synthesised GaN nanostructures, a ultra-high vacuum scanning electron microscope (UHV-SEM) experiment was conducted. This setup allows for precise control of the sample temperature and enables in situ imaging of the nanostructures during thermal annealing. A sample nitridised for 20 minutes was selected for this study, as thermal treatment could influence both the GaN nanocrystals and the residual Ga droplet. The sample was mounted on a calibrated ceramic plate and inserted into the UHV-SEM chamber. The sample was indirectly heated by the electrical current flowing through the ceramic (pyrolytic boron nitride (PBN)) plate.

Temperature was expected to play a critical role not only in potential etching processes but also in the stability and evolution of the nanostructures. In particular, changes in the dimensions and morphology of the nanocrystals were anticipated.

Heating began at low temperatures, as the threshold for morphological changes in the nanostructures was initially unknown. The sample was incrementally heated to specific temperatures and held for five minutes at each step to monitor any signs of structural changes. Up to 490 °C, no noticeable modifications were observed. However, once the temperature exceeded 500 °C, a contrast change in the SEM image indicated an onset of morphological transformation, as shown in Figure 28. The longest edge of the nanocrystal began to disappear.

As the temperature was gradually increased, this defect propagated across the nanocrystal. Upon reaching 600 °C, a rapid degradation of the GaN nanocrystal occurred, leaving only the stable central region of the GaN nanocrystal and the area around the Ga/GaN interface intact. The annealing continued up to 620 °C, at which point even these stable regions were removed, leaving behind a triangular pit in the Si(111) substrate.

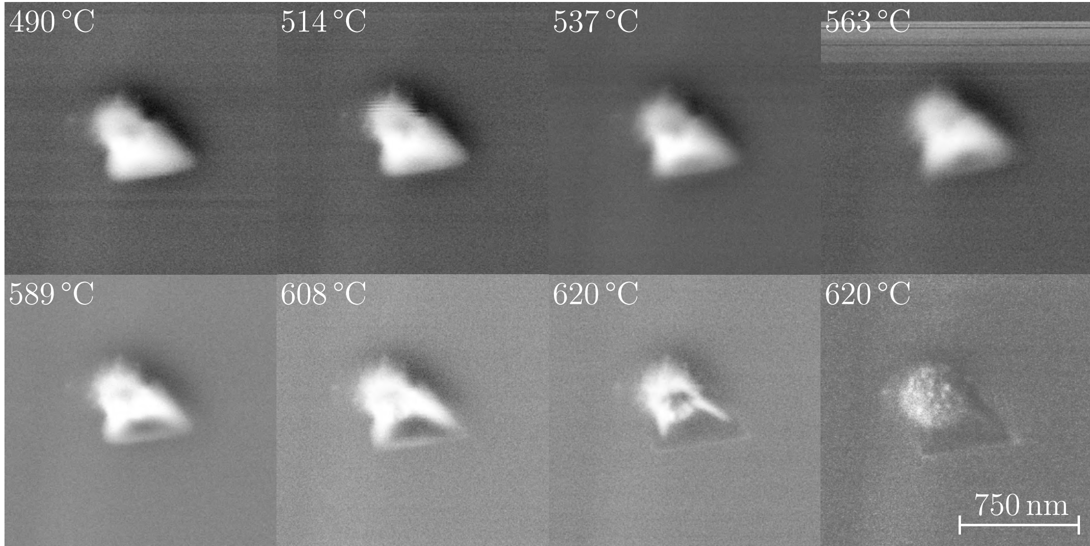

Figure 28: UHV-SEM images capturing the morphological evolution of GaN nanostructures during thermal annealing in the temperature range of 490 °C to 620 °C.

Thermal annealing revealed three key findings: first, that etching can occur even in the absence of nitrogen ions; second, that GaN nanocrystals exhibit relative thermal instability; and third, that the lateral dimensions of the nanostructures change significantly as a result of the annealing process.

Two possible etching mechanisms were considered: physical etching induced by nitrogen ions and thermally driven etching. The results presented in Section 4.2 demonstrate that varying the energy of nitrogen ions leads to etching of both the nanocrystal and the Si(111) 7×7 surface, even when the temperature remains constant at 210 °C. Remarkably, similar etch pits in the substrate were observed under two distinct conditions—at low temperature (210 °C) with 50 eV nitrogen ions, and in the absence of ions at elevated temperatures ranging from 500 °C to 620 °C. This suggests that both mechanisms can independently induce comparable surface modifications.

In comparison with bulk GaN, which exhibits thermal stability up to 900 °C [180, 181] depending on the substrate used, the thermal stability of 2D GaN nanostructures grown by the LTDE method is significantly lower. The GaN nanostructures on the Si(111) 7×7 surface remain stable only up to approximately 500 °C and degrade rapidly once the temperature exceeds 600 °C. To our knowledge, no experimental or theoretical studies have yet reported on the thermal stability of 2D GaN, making these findings particularly unique and noteworthy.

Supporting the hypothesis presented in Section 4.3.1, the GaN nanocrystal exhibited a maximum length of approximately 500 nm prior to annealing and the onset of morphological degradation. As shown in Figure 29, the nanostructure after the annealing process reaches a maximum length of approximately 630 nm. This observation suggests that etching also occurs beyond the original boundaries of the GaN nanocrystal. These intriguing findings require further experimental investigation and theoretical analysis.

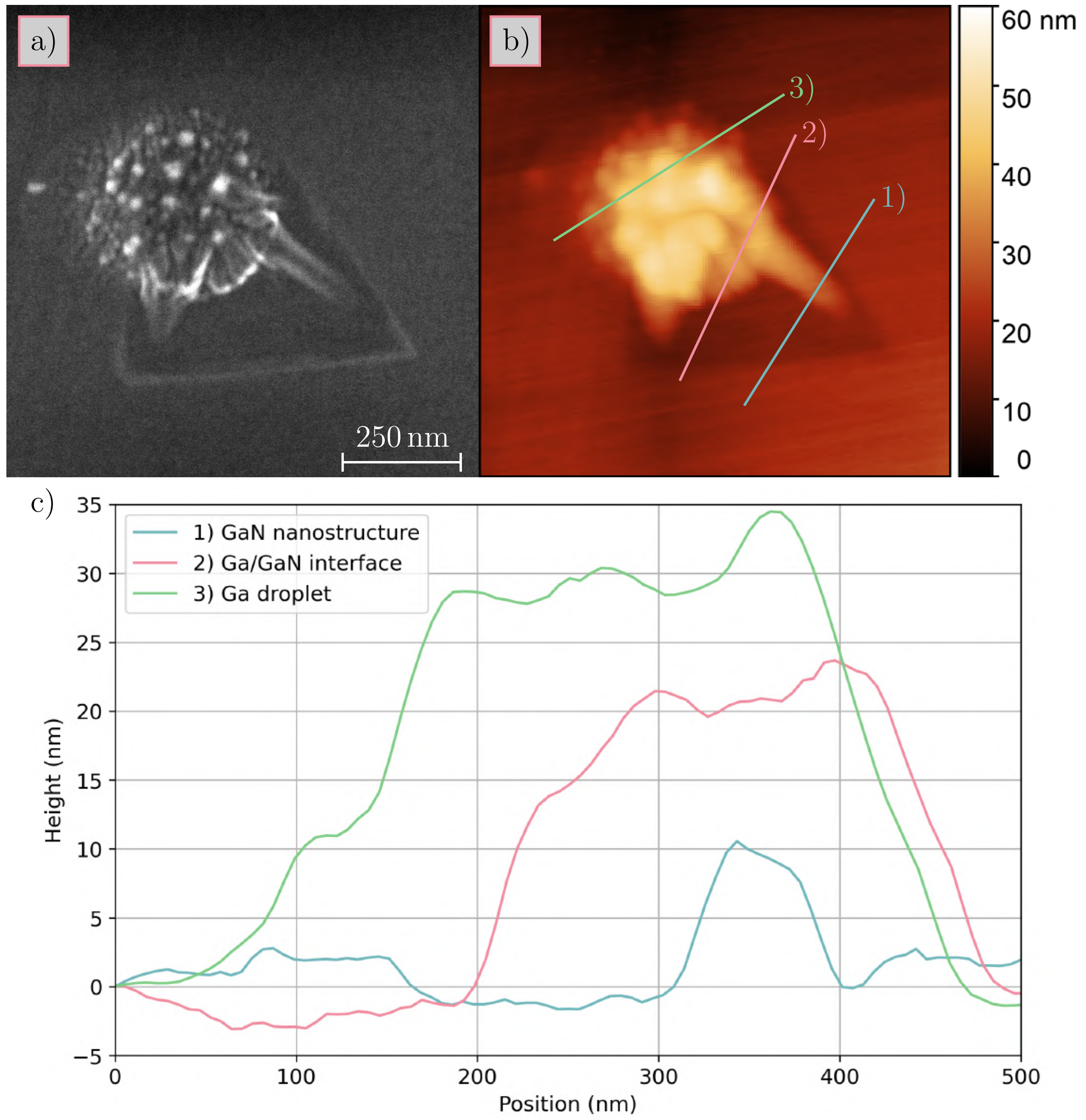

Figure 29: Morphology of annealed GaN nanostructure: a) SEM image, b) AFM measurement with highlighted lines showing c) extracted height profiles.

5. The transfer of GaN nanocrystals

In the previous chapters, the growth of GaN nanocrystals on Si(111) substrates was described in detail. While silicon is well-suited for epitaxial growth, its semiconducting nature [182] makes it unsuitable for electrical measurements of LTDE-grown GaN nanostructures. Therefore, transferring the nanocrystals from the original silicon substrate to an insulating substrate becomes necessary. Moreover, if such a transfer proves successful, it would open the door to integrating 2D GaN into a wide range of practical applications. To our knowledge, no literature covered the transfer of 2D GaN nanocrystals from Si(111).

Transfer methods typically rely either on adhesion forces, as in dry-transfer techniques, or on chemical etching of the underlying substrate, as in wet-transfer approaches, both of which were described in Section 1.4. The Si(111) substrate is chemically stable and thus difficult to etch. While etching methods of Si(111) using KOH [183] or NaOH [184] have been reported, they are unsuitable for the transfer of GaN nanocrystals due to the low etch rate of Si(111) and the unknown chemical resilience of LTDE-grown GaN under such conditions. Consequently, dry-transfer methods appeared to be a more feasible and less invasive alternative for this system.

Three different dry-transfer approaches were attempted on the GaN nanocrystals: transfer using transparent adhesive tape, PDMS stamps, and common nail polish. All three methods are described in more detail in the corresponding sections above.

Even before initiating the experiment, several notable challenges appeared. As previously discussed, the formation of holes in the substrate indicates a strong interaction between the GaN nanocrystals and the Si(111) 7×7 surface. If the adhesion to the substrate exceeds that to the transfer medium, the transfer will likely fail. These interactions suggest that the GaN nanostructures are strongly anchored to the substrate, presenting a significant obstacle. A further limitation is the small size of the nanostructures. Their low dimensions make them difficult to detect using an optical microscope, complicating the transfer process, as it provides no immediate visual confirmation of success. In the following sections, the various dry-transfer approaches are described in detail, and their outcomes are discussed.

The target substrate chosen for the transfer of GaN nanocrystals was SiO_2. The first transfer attempt employed transparent tape, conducted both at room temperature and at elevated temperatures up to 90 °C. Subsequently, both the original Si(111) substrate and the target SiO_2 substrate were examined using SEM. However, no nanocrystals were detected on the SiO_2 surface, and the original substrate showed the presence of impurities surrounding the nanocrystals. These impurities are most likely residues of adhesive from the transparent tape.

To improve the outcome, a second experiment was performed using PDMS stamps and a more advanced setup. Figure 30 displays the configuration of the 4-probe station Cascade Microtech MPS 150, which includes an optical microscope, a heated stage, and a glass slide manipulator. A fresh and clean PDMS stamp (5×5) mm was placed on the glass slide and mounted on the manipulator. The pick-up procedure followed the method described in Section 1.4. Transfers were attempted first at room temperature,

then at elevated temperatures up to 90 °C. As with the tape method, the nanocrystals were not removed from the original substrate. However, less contamination was observed (see Figure 31) on the GaN nanostructures following the PDMS experiment.

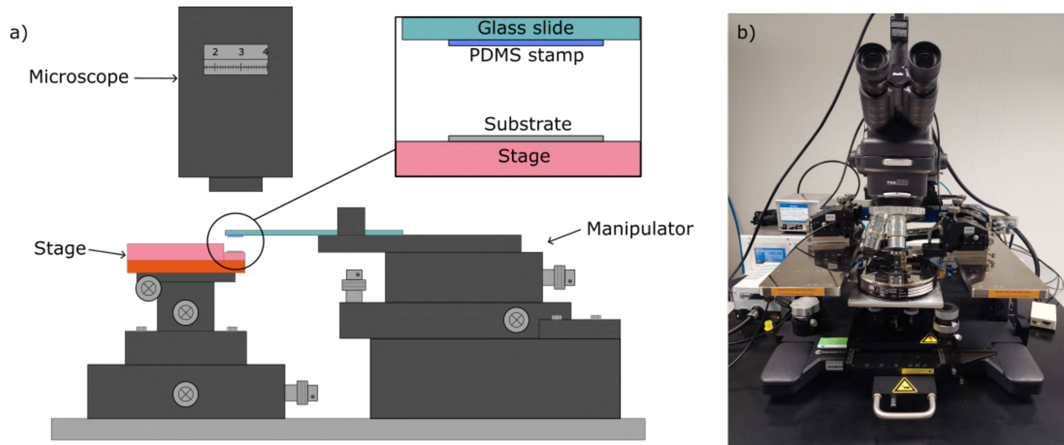

Figure 30: a) The schematic of the transfer setup consisting of a microscope, a heated stage, and a manipulator. b) The photography of the Cascade Microtech MPS 150 4-probe station, used in this work.

To enhance the adhesion between the transfer medium and the GaN nanocrystals, a small droplet of transparent nail polish was applied to the PDMS stamp and cured on a hot plate at 90 °C for three hours. Following this preparation, the glass slide was re-mounted onto the manipulator, and the stage was heated to 50 °C. After aligning the contact point, the droplet was gently brought into contact with the nanocrystal-covered region, spreading arbitrarily over the largest possible area. After several minutes of contact, the glass slide was swiftly retracted, and the droplet was transferred onto the SiO_2 substrate. The stage was subsequently heated to 90 °C to facilitate detachment of the droplet from the PDMS stamp, leaving it adhered to the SiO_2 surface.

To remove the nail polish, the sample was immersed in an acetone bath and left overnight. SEM images presented in Figure 31 reveal complete removal of the nail polish droplet from the SiO_2 surface, and no GaN nanocrystals were observed. Furthermore, all GaN nanocrystals remained intact on the original Si(111) substrate, confirming the failure of the transfer process.

However, the temperature during the pick-up process was later increased up to 80 °C in an attempt to enhance adhesion. At this elevated temperature, the nail polish droplet prematurely detached from the PDMS stamp during contact, contaminating the Si(111) surface. Subsequent cleaning with acetone was insufficient to remove the residue completely. Despite the failure of the transfer, this experiment provided valuable insight: the GaN nanocrystals remained intact after exposure to acetone and IPA, indicating their chemical stability in common solvents used during lithographic processing. This observation is significant for the potential future integration of LTDE-grown GaN nanocrystals into device fabrication workflows.

To enable higher temperatures during the pick-up process, a piece of tape was fixed to the PDMS stamp before applying the nail polish droplet. The adhesion between the

nail polish and the tape was greater than that between the nail polish and the PDMS, which allowed the transfer process to be performed at temperatures up to 80 °C without premature detachment. For the subsequent transfer of the nail polish droplet from the tape to the target substrate, sharp tweezers were used to lift the droplet and place it onto a fresh PDMS stamp mounted on a glass slide. This step was intended to reduce the adhesion of the droplet to the transfer medium and facilitate successful release onto the SiO_2 substrate. Nevertheless, the transfer attempt was ultimately unsuccessful once again. However, compared to the PDMS stamp method, contamination of both the original and target substrates was significantly lower, as visible in Figure 31. This is likely because the nail polish droplet made contact with only a limited area of the surface.

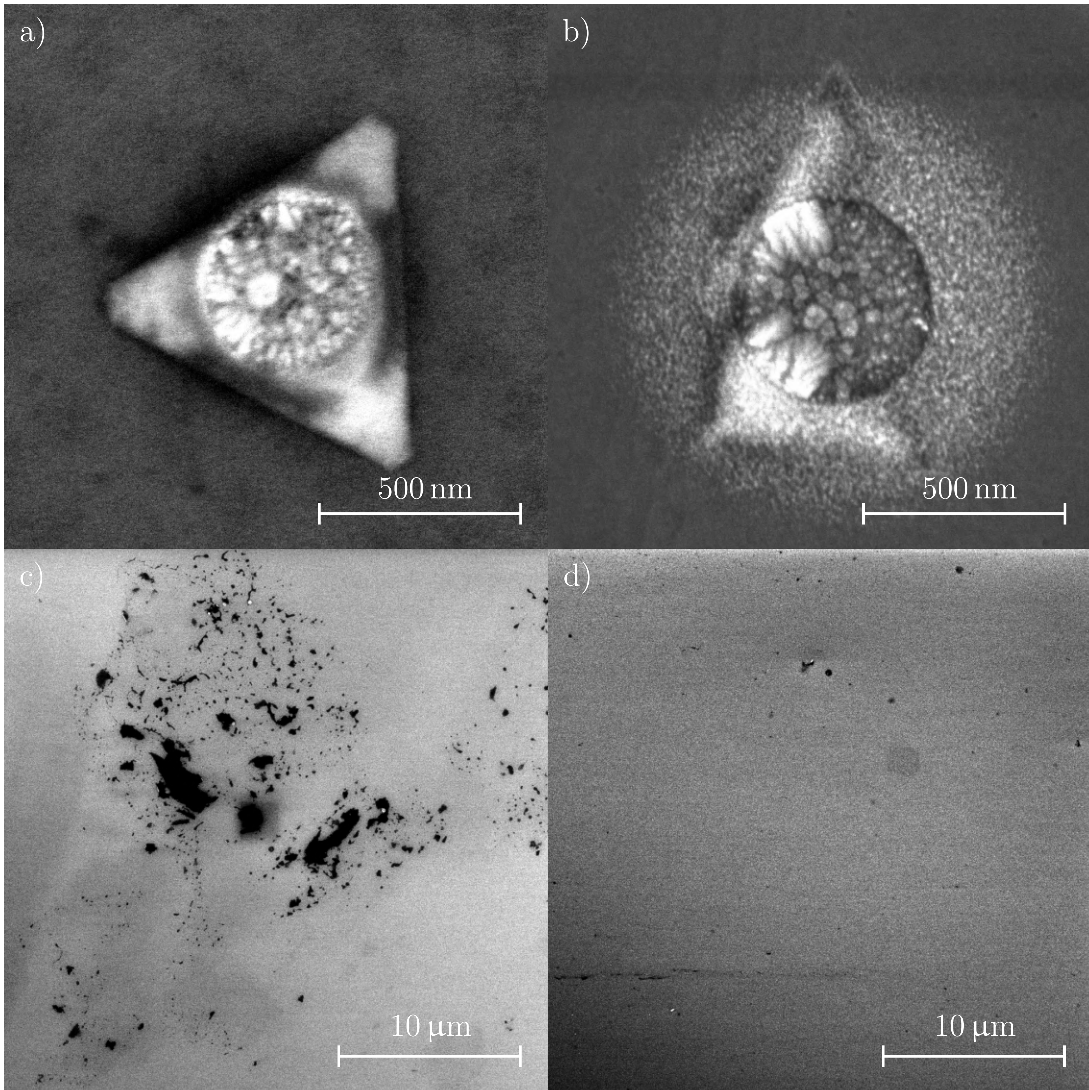

Figure 31: SEM images of the unsuccessful transfer of GaN nanocrystals from a Si(111) substrate to a SiO_2 substrate: a) detail of a GaN nanocrystal on Si(111) after the attempted PDMS transfer, b) detail of a GaN nanocrystal on Si(111) after the attempted nail polish transfer, c)–d) the SiO_2 substrate after contact with the PDMS stamp and after removal of the nail polish droplet, respectively.

None of the dry-transfer methods were successful in transferring the GaN nanocrystals from the Si(111) substrate to the SiO_2 substrate. This may be due to the limitations discussed earlier in this section or the inherently strong adhesion of GaN to the Si(111) surface. Nevertheless, both wet-transfer and dry-transfer approaches require further investigation to better understand the transferability of LTDE-grown GaN nanocrystals.

Conclusion

This thesis focused on the study of 2D GaN nanocrystals grown on the Si(111) 7×7 surface via low-temperature droplet epitaxy (LTDE) based on the findings of Manis et al. [28]. A range of growth parameters was investigated, with particular emphasis on the effect of the incident angle of low-energy nitrogen ions during the nitridation process and the different energies of the nitrogen ions. The first part of this work extended previous findings from the author's bachelor's thesis [33], which explored nitridation angles of 0°, 25°, 35°, 55°, and 80°, by introducing additional angles of 5°, 10°, and 15°.

The resulting nanostructures were analysed using scanning electron microscopy (SEM) and atomic force microscopy (AFM) to evaluate trends in morphology. It was found that the incident angle of nitrogen ions had no significant influence on the lateral size or height of the GaN nanocrystals.

It was found that nitrogen ions with energies around 40–50 eV can induce etching of GaN, this work confirmed that under low-angle nitridation (0°–10°), nanocrystals were not only etched but also left behind 2–4 nm deep holes in the substrate, precisely matching the shape of the original crystals. In contrast, nitridation at higher angles (25°) preserved the nanocrystal structure entirely. Interestingly, at 25°, residual Ga was still observed, indicating incomplete nitridation. This suggests that etching of both GaN and the Si substrate may occur only after full depletion of the Ga reservoir.

For the intermediate case at 15°, the GaN nanocrystals showed signs of etching, but no corresponding holes were observed in the substrate. These findings contribute valuable insight into the role of ion incidence angle in controlling not just the formation, but also the preservation or degradation of GaN nanostructures on silicon substrates.

In addition, the effect of nitrogen ion energy on the nitridation process was also investigated. GaN nanocrystals were formed using nitrogen ions with energies ranging from 20 eV to 50 eV. It was found that the lateral size (reaching approximately 830 nm) and height (reaching above 50 nm) of the nanocrystals were primarily determined by the size of the initial Ga droplets, rather than by the ion energy. However, the quality of the underlying Si(111) 7×7 surface proved to be a critical factor for the successful LTDE growth of uniform and well-defined GaN nanocrystals. In cases where the flashing routine failed to remove carbon contaminants, the formation of large, atomically flat terraces was inhibited, which limited the growth and quality of the nanostructures. The surface cleanliness was verified via x-ray photoelectron spectroscopy (XPS), which also confirmed the successful transformation of Ga droplets into GaN nanocrystals.

Furthermore, etching behaviour was found to correlate with ion energy. Etching of the nanocrystals was observed only at the highest energy studied (50 eV). At lower ion energies, the resulting nanocrystals remained mostly intact, with only minor signs of damage visible in their thinnest regions, as revealed by AFM and SEM imaging.

To investigate the optical properties of LTDE-grown GaN nanocrystals, several characterisation techniques were employed, including Raman spectroscopy, photoluminescence (PL), and cathodoluminescence (CL). However, none of these methods yielded a detectable signal from the nanocrystals. This is most likely due to the low surface cov-

erage, which averaged only 3.5 %, or due to the intrinsically low optical activity of the nanocrystals. Structural characterisation was also attempted using 4D scanning transmission electron microscopy (4D-STEM). Unfortunately, a suitable high-quality lamella could not be prepared, and as a result, no conclusive information on the internal crystalline structure of the GaN nanocrystals was obtained.

To explore the etching mechanism and the parameters that influence it, two additional experiments were conducted: time-dependent nitridation and thermal annealing of GaN nanostructures. Three samples were prepared by nitridising Ga droplets with 50 eV nitrogen ions for 20, 40, and 60 minutes. These experiments revealed the rapid progression of both the nitridation and etching processes. After 60 minutes, the nanocrystals appeared almost identical to those nitridised for 120 minutes. In the case of 40-minute nitridation, damage was observed only at the thinner edges of the nanocrystals, suggesting that the etching process had just begun. After 20 minutes, the nanocrystals appeared undamaged and retained a notable Ga reservoir, supporting the hypothesis that etching begins only after Ga is fully consumed. These findings significantly reduce the required preparation time for GaN nanocrystals.

The thermal annealing experiment revealed that GaN nanocrystals begin to degrade when heated above 500 °C. At 600 °C, the nanocrystals were rapidly etched away, leaving behind shallow triangular holes in the Si(111) substrate. This indicates a relatively low thermal stability of LTDE-grown GaN nanostructures. Importantly, this etching occurred without ion bombardment, yet produced holes with the same triangular shape as those formed by ion-induced etching at lower temperatures. Additionally, an increase in nanostructure size was observed after annealing, further supporting the idea that GaN grows beneath the Si(111) 7×7 surface, making the edges particularly susceptible to etching.

To enable electrical characterisation or integration into heterostructures and nanodevices, attempts were made to transfer the 2D GaN nanocrystals from the Si(111) substrate to a SiO_2 target substrate. Three dry-transfer techniques were explored: transparent adhesive tape, PDMS stamps, and nail polish. The experiments were conducted at both room temperature and elevated temperatures up to 90 °C. However, none of the methods resulted in a successful transfer, likely due to several limiting factors: the strong adhesion between GaN and the Si(111) surface, the partial embedding of the nanocrystals into the substrate, and their small lateral dimensions. These findings suggest that alternative transfer approaches must be developed in future work to overcome these challenges.

In summary, this thesis provides a detailed investigation of the growth, morphology, stability, and transferability of 2D GaN nanocrystals prepared via LTDE on Si(111) 7×7. These findings extend the current understanding of low-energy nitrogen ion nitridation, revealing unique insights into the etching phenomenon and the impact of growth parameters on nanocrystal preservation. Although the optical and structural characterisation was limited, and transfer techniques were unsuccessful, these results offer valuable guidance for optimising LTDE growth and highlight important challenges for further research.

Literature

[1] I. Osborne, M. Lavine, and R. Coontz. "Looking Beyond Silicon". In: *Science* 327.5973 (2010-03-26), pp. 1595–1595. ISSN: 0036-8075. DOI: 10.1126/science.327.5973.1595.

[2] N. P. Guisinger and M. S. Arnold. "Beyond Silicon. Carbon-Based Nanotechnology". In: *MRS Bulletin* 35.4 (2010), pp. 273–279. ISSN: 0883-7694. DOI: 10.1557/mrs2010.729.

[3] K. S. Novoselov, A. K. Geim, S. V. Morozov, D. Jiang, Y. Zhang, S. V. Dubonos, I. V. Grigorieva, and A. A. Firsov. "Electric Field Effect in Atomically Thin Carbon Films". In: *Science* 306.5696 (2004-10-22), pp. 666–669. ISSN: 0036-8075. DOI: 10.1126/science.1102896.

[4] H. Qiu, Z. Yu, T. Zhao, Q. Zhang, M. Xu, P. Li, T. Li, W. Bao, Y. Chai, S. Chen, Y. Chen, H.-M. Cheng, D. Dai, Z. Di, and Z. Dong. "Two-dimensional materials for future information technology. status and prospects". In: *Science China Information Sciences* 67.6 (2024). ISSN: 1674-733X. DOI: 10.1007/s11432-024-4033-8.

[5] M. C. Lemme, D. Akinwande, C. Huyghebaert, and C. Stampfer. "2D materials for future heterogeneous electronics". In: *Nature Communications* 13.1 (2022). ISSN: 2041-1723. DOI: 10.1038/s41467-022-29001-4.

[6] M. Chhowalla, D. Jena, and H. Zhang. "Two-dimensional semiconductors for transistors". In: *Nature Reviews Materials* 1.11 (2016). ISSN: 2058-8437. DOI: 10.1038/natrevmats.2016.52.

[7] Y. Shen, Z. Dong, Y. Sun, H. Guo, F. Wu, X. Li, J. Tang, J. Liu, X. Wu, H. Tian, and T.-L. Ren. "The Trend of 2D Transistors toward Integrated Circuits. Scaling Down and New Mechanisms". In: *Advanced Materials* 34.48 (2022). ISSN: 0935-9648. DOI: 10.1002/adma.202201916.

[8] M. Long, P. Wang, H. Fang, and W. Hu. "Progress, Challenges, and Opportunities for 2D Material Based Photodetectors". In: *Advanced Functional Materials* 29.19 (2019). ISSN: 1616-301X. DOI: 10.1002/adfm.201803807.

[9] A. G. Ricciardulli and P. W. M. Blom. "Solution-Processable 2D Materials Applied in Light-Emitting Diodes and Solar Cells". In: *Advanced Materials Technologies* 5.8 (2020). ISSN: 2365-709X. DOI: 10.1002/admt.201900972.

[10] S. Suragtkhuu, S. Sunderiya, P. Myagmarsereejid, S. Purevdorj, A. S. R. Bati, B. Bold, Y. L. Zhong, S. Davaasambuu, and M. Batmunkh. "Graphene-Like Monoelemental 2D Materials for Perovskite Solar Cells". In: *Advanced Energy Materials* 13.12 (2023). ISSN: 1614-6832. DOI: 10.1002/aenm.202204074.

[11] A. Vaidyanathan, M. Mathew, S. Radhakrishnan, C. S. Rout, and B. Chakraborty. "Theoretical Insight on the Biosensing Applications of 2D Materials". In: *The Journal of Physical Chemistry B* 124.49 (2020-12-10), pp. 11098–11122. ISSN: 1520-6106. DOI: 10.1021/acs.jpcb.0c08539.

[12] Z.-L. Lei and B. Guo. “2D Material-Based Optical Biosensor. Status and Prospect”. In: *Advanced Science* 9.4 (2022). ISSN: 2198-3844. DOI: 10.1002/advs.202102924.

[13] F. Chen, Q. Tang, T. Ma, B. Zhu, L. Wang, C. He, X. Luo, S. Cao, L. Ma, and C. Cheng. “Structures, properties, and challenges of emerging 2D materials in bioelectronics and biosensors”. In: *InfoMat* 4.5 (2022). ISSN: 2567-3165. DOI: 10.1002/inf2.12299.

[14] H. Du, X. Zhang, Z. Liu, and F. Qu. “A supersensitive biosensor based on MoS 2 nanosheet arrays for the real-time detection of H 2 O 2 secreted from living cells”. In: *Chemical Communications* 55.65 (2019-08-8), pp. 9653–9656. ISSN: 1359-7345. DOI: 10.1039/C9CC03502H.

[15] M. Liu, W. Liu, X. Liu, Y. Wang, and Z. Wei. “Application of transition metal dichalcogenides in mid-infrared fiber laser”. In: *Nano Select* 2.1 (2021), pp. 37–46. ISSN: 2688-4011. DOI: 10.1002/nano.202000047.

[16] H. Ribeiro, J. P. Trigueiro, P. S. Owuor, L. D. Machado, C. F. Woellner, J. J. Pedrotti, Y. M. Jaques, S. Kosolwattana, A. Chipara, W. M. Silva, C. J. Silva, D. S. Galvão, N. Chopra, I. N. Odeh, and C. S. Tiwary. “Hybrid 2D nanostructures for mechanical reinforcement and thermal conductivity enhancement in polymer composites”. In: *Composites Science and Technology* 159 (2018), pp. 103–110. ISSN: 02663538. DOI: 10.1016/j.compscitech.2018.01.032.

[17] K. S. Chavali, D. A. Pethsangave, K. C. Patankar, R. V. Khose, P. H. Wadekar, S. Maiti, R. V. Adivarekar, and S. Some. “Graphene-based intumescent flame retardant on cotton fabric”. In: *Journal of Materials Science* 55.29 (2020), pp. 14197–14210. ISSN: 0022-2461. DOI: 10.1007/s10853-020-04989-6.

[18] H. Liu, A. T. Neal, Z. Zhu, Z. Luo, X. Xu, D. Tománek, and P. D. Ye. “Phosphorene. An Unexplored 2D Semiconductor with a High Hole Mobility”. In: *ACS Nano* 8.4 (2014-04-22), pp. 4033–4041. ISSN: 1936-0851. DOI: 10.1021/nn501226z.

[19] M. Batmunkh, M. Bat-Erdene, and J. G. Shapter. “Phosphorene and Phosphorene-Based Materials – Prospects for Future Applications”. In: *Advanced Materials* 28.39 (2016), pp. 8586–8617. ISSN: 0935-9648. DOI: 10.1002/adma.201602254.

[20] M. Kan, J. Y. Wang, X. W. Li, S. H. Zhang, Y. W. Li, Y. Kawazoe, Q. Sun, and P. Jena. “Structures and Phase Transition of a MoS 2 Monolayer”. In: *The Journal of Physical Chemistry C* 118.3 (2014-01-23), pp. 1515–1522. ISSN: 1932-7447. DOI: 10.1021/jp4076355.

[21] P. Yang, S. Zhang, S. Pan, B. Tang, Y. Liang, X. Zhao, Z. Zhang, J. Shi, Y. Huan, Y. Shi, S. J. Pennycook, Z. Ren, G. Zhang, Q. Chen, and X. Zou. “Epitaxial Growth of Centimeter-Scale Single-Crystal MoS 2 Monolayer on Au(111)”. In: *ACS Nano* 14.4 (2020-04-28), pp. 5036–5045. ISSN: 1936-0851. DOI: 10.1021/acsnano.0c01478.

[22] D. Jiang, Z. Liu, Z. Xiao, Z. Qian, Y. Sun, Z. Zeng, and R. Wang. “Flexible electronics based on 2D transition metal dichalcogenides”. In: *Journal of Materials Chemistry A* 10.1 (2021-12-21), pp. 89–121. ISSN: 2050-7488. DOI: 10.1039/D1TA06741A.

[23] K. Hantanasirisakul and Y. Gogotsi. “Electronic and Optical Properties of 2D Transition Metal Carbides and Nitrides (MXenes)”. In: *Advanced Materials* 30.52 (2018). ISSN: 0935-9648. DOI: 10.1002/adma.201804779.

[24] Y. Lin, T. V. Williams, and J. W. Connell. “Soluble, Exfoliated Hexagonal Boron Nitride Nanosheets”. In: *The Journal of Physical Chemistry Letters* 1.1 (2010-01-07), pp. 277–283. ISSN: 1948-7185. DOI: 10.1021/jz9002108.

[25] M. Naguib, V. N. Mochalin, M. W. Barsoum, and Y. Gogotsi. “25th Anniversary Article. MXenes: A New Family of Two-Dimensional Materials”. In: *Advanced Materials* 26.7 (2014), pp. 992–1005. ISSN: 0935-9648. DOI: 10.1002/adma.201304138.

[26] T. K. Sahu, S. P. Sahu, K. P. S. S. Hembram, J.-K. Lee, V. Biju, and P. Kumar. “Free-standing 2D gallium nitride for electronic, excitonic, spintronic, piezoelectric, thermoplastic, and 6G wireless communication applications”. In: *NPG Asia Materials* 15.1 (2023). ISSN: 1884-4057. DOI: 10.1038/s41427-023-00497-6.

[27] G. Zhang, L. Chen, L. Wang, Z. Lu, H. Dong, Z. Cheng, X. Zhang, X. Xu, B. Wang, and S. Chen. “Subnanometer-thick 2D GaN film with a large bandgap synthesized by plasma enhanced chemical vapor deposition”. In: *Journal of Materials Chemistry A* 10.8 (2022), pp. 4053–4059. ISSN: 2050-7496. DOI: 10.1039/d1ta10450k.

[28] J. Maniš, J. Mach, M. Bartošík, T. Šamořil, M. Horák, V. Čalkovský, D. Nezval, L. Kachtik, M. Konečný, and T. Šikola. “Low temperature 2D GaN growth on Si(111) 7×7 assisted by hyperthermal nitrogen ions”. In: *Nanoscale Advances* 4.17 (2022), pp. 3549–3556. ISSN: 2516-0230. DOI: 10.1039/d2na00175f.

[29] Z. Y. A. Balushi, K. Wang, R. K. Ghosh, R. A. Vilá, S. M. Eichfeld, J. D. Caldwell, X. Qin, Y.-C. Lin, P. A. DeSario, G. Stone, S. Subramanian, D. F. Paul, R. M. Wallace, S. Datta, and J. M. Redwing. “Two-dimensional gallium nitride realized via graphene encapsulation”. In: *Nature Materials* 15.11 (2016), pp. 1166–1171. ISSN: 1476-1122. DOI: 10.1038/nmat4742.

[30] C. Sun, M. Yang, T. Wang, Y. Shao, Y. Wu, and X. Hao. “Graphene-Oxide-Assisted Synthesis of GaN Nanosheets as a New Anode Material for Lithium-Ion Battery”. In: *ACS Applied Materials & Interfaces* 9.32 (2017), pp. 26631–26636. ISSN: 1944-8252. DOI: 10.1021/acsami.7b07277.

[31] Y. Chen, K. Liu, J. Liu, T. Lv, B. Wei, T. Zhang, M. Zeng, Z. Wang, and L. Fu. “Growth of 2D GaN Single Crystals on Liquid Metals”. In: *Journal of the American Chemical Society* 140.48 (2018), pp. 16392–16395. ISSN: 1520-5126. DOI: 10.1021/jacs.8b08351.

[32] H. Zhao, E. Li, Z. Cui, C. Liu, Y. Shen, P. Shen, and D. Ma. "Two-dimensional GaN nanosheets realized via hydrothermal reaction and ammoniation two-step method". In: *Vacuum* 203 (2022), p. 111329. ISSN: 0042-207X. DOI: 10.1016/j.vacuum.2022.111329.

[33] J. Šťastný. *Deposition of GaN nanostructures on Si(111) 7x7*. Bachelor's thesis. 2023.

[34] The Nobel Prize Committee. *The Nobel Prize in Physics 2010*. Accessed: 26.04.2025. 2010.

[35] C. Soldano, A. Mahmood, and E. Dujardin. "Production, properties and potential of graphene". In: *Carbon* 48.8 (2010), pp. 2127–2150. ISSN: 00086223. DOI: 10.1016/j.carbon.2010.01.058.

[36] R. Fei, A. Faghaninia, R. Soklaski, J.-A. Yan, C. Lo, and L. Yang. "Enhanced Thermoelectric Efficiency via Orthogonal Electrical and Thermal Conductances in Phosphorene". In: *Nano Letters* 14.11 (2014-11-12), pp. 6393–6399. ISSN: 1530-6984. DOI: 10.1021/nl502865s.

[37] R. G. Dickinson and L. Pauling. "THE CRYSTAL STRUCTURE OF MOLYBDENITE". In: *Journal of the American Chemical Society* 45.6 (1923), pp. 1466–1471. ISSN: 0002-7863. DOI: 10.1021/ja01659a020.

[38] N. D. Mermin. "Crystalline Order in Two Dimensions". In: *Physical Review* 176.1 (1968), pp. 250–254. ISSN: 0031-899X. DOI: 10.1103/PhysRev.176.250.

[39] H. Zhang. "Introduction. 2D Materials Chemistry". In: *Chemical Reviews* 118.13 (2018-07-11), pp. 6089–6090. ISSN: 0009-2665. DOI: 10.1021/acs.chemrev.8b00278.

[40] H. Li, J. Wu, Z. Yin, and H. Zhang. "Preparation and Applications of Mechanically Exfoliated Single-Layer and Multilayer MoS 2 and WSe 2 Nanosheets". In: *Accounts of Chemical Research* 47.4 (2014-04-15), pp. 1067–1075. ISSN: 0001-4842. DOI: 10.1021/ar4002312.

[41] M. Yi and Z. Shen. "A review on mechanical exfoliation for the scalable production of graphene". In: *Journal of Materials Chemistry A* 3.22 (2015), pp. 11700–11715. ISSN: 2050-7488. DOI: 10.1039/C5TA00252D.

[42] B. Jayasena and S. Subbiah. "A novel mechanical cleavage method for synthesizing few-layer graphenes". In: *Nanoscale Research Letters* 6.1 (2011). ISSN: 1556-276X. DOI: 10.1186/1556-276X-6-95.

[43] S. Bhowmik and A. G. Rajan. "Chemical vapor deposition of 2D materials. A review of modeling, simulation, and machine learning studies". In: *IScience* 25.3 (2022). ISSN: 25890042. DOI: 10.1016/j.isci.2022.103832.

[44] K. Yan, L. Fu, H. Peng, and Z. Liu. "Designed CVD Growth of Graphene via Process Engineering". In: *Accounts of Chemical Research* 46.10 (2013-10-15), pp. 2263–2274. ISSN: 0001-4842. DOI: 10.1021/ar400057n.

[45] X. Xu, T. Guo, H. Kim, M. K. Hota, R. S. Alsaadi, M. Lanza, X. Zhang, and H. N. Alshareef. “Growth of 2D Materials at the Wafer Scale”. In: *Advanced Materials* 34.14 (2022). ISSN: 0935-9648. DOI: 10.1002/adma.202108258.

[46] B. Radisavljevic, A. Radenovic, J. Brivio, V. Giacometti, and A. Kis. “Single-layer MoS2 transistors”. In: *Nature Nanotechnology* 6.3 (2011), pp. 147–150. ISSN: 1748-3387. DOI: 10.1038/nnano.2010.279.

[47] C. Kittel. *Introduction to solid state physics*. 8th ed. Hoboken, N.J.: John Wiley & Sons, c2005. ISBN: 047141526X.

[48] S. M. Sze and K. K. Ng. *Physics of semiconductor devices*. 3rd ed. Hoboken: Wiley-Interscience, c2007. ISBN: 978-0-471-14323-9.

[49] D. Akinwande, C. J. Brennan, J. S. Bunch, P. Egberts, J. R. Felts, H. Gao, R. Huang, J.-S. Kim, T. Li, Y. Li, K. M. Liechti, N. Lu, H. S. Park, E. J. Reed, and P. Wang. “A review on mechanics and mechanical properties of 2D materials—Graphene and beyond”. In: *Extreme Mechanics Letters* 13 (2017), pp. 42–77. ISSN: 23524316. DOI: 10.1016/j.eml.2017.01.008.

[50] L. Patra and R. Pandey. “Mechanical properties of 2D materials. A review on molecular dynamics based nanoindentation simulations”. In: *Materials Today Communications* 31 (2022). ISSN: 23524928. DOI: 10.1016/j.mtcomm.2022.103623.

[51] A. K. Geim and I. V. Grigorieva. “Van der Waals heterostructures”. In: *Nature* 499.7459 (2013), pp. 419–425. ISSN: 0028-0836. DOI: 10.1038/nature12385.

[52] K. S. Novoselov, A. Mishchenko, A. Carvalho, and A. H. C. Neto. “2D materials and van der Waals heterostructures”. In: *Science* 353.6298 (2016-07-29). ISSN: 0036-8075. DOI: 10.1126/science.aac9439.

[53] K. F. Mak, C. Lee, J. Hone, J. Shan, and T. F. Heinz. “Atomically Thin MoS : A New Direct-Gap Semiconductor”. In: *Physical Review Letters* 105.13 (2010), p. 136805. DOI: 10.1103/PhysRevLett.105.136805.

[54] W. Zhao, Z. Ghorannevis, L. Chu, M. Toh, C. Kloc, P.-H. Tan, and G. Eda. “Evolution of Electronic Structure in Atomically Thin Sheets of WS and WSe ”. In: *ACS Nano* 7.1 (2013), pp. 791–797. DOI: 10.1021/nn3049662.

[55] G. W. Mudd, S. A. Svatek, T. Ren, A. Patanè, O. Makarovsky, L. Eaves, P. H. Beton, K. S. Novoselov, Z. D. Kovalyuk, G. V. Lashkarev, Z. R. Kudrynskyi, and A. Mishchenko. “Indirect-to-Direct Band Gap Crossover in Few-Layer InSe as Probed by Optical Second-Harmonic Generation”. In: *Advanced Materials* 25.40 (2013), pp. 5714–5718. DOI: 10.1002/adma.201301772.

[56] W. D. Callister and D. G. Rethwisch. *Materials science and engineering. an introduction*. 9th ed. Hoboken, NJ.: Wiley, 2014. ISBN: 978-1-118-32457-8.

[57] Y. Liu, C. Xiao, Z. Li, and Y. Xie. “Vacancy Engineering for Tuning Electron and Phonon Structures of Two-Dimensional Materials”. In: *Advanced Energy Materials* 6.23 (2016). ISSN: 1614-6832. DOI: 10.1002/aenm.201600436.

[58] R. Kumar, S. Sahoo, E. Joanni, R. Pandey, and J.-J. Shim. "Vacancy designed 2D materials for electrodes in energy storage devices". In: *Chemical Communications* 59.41 (2023-05-18), pp. 6109–6127. ISSN: 1359-7345. DOI: 10.1039/D3CC00815K.

[59] A. Mondal and A. Vomiero. "2D Transition Metal Dichalcogenides-Based Electrocatalysts for Hydrogen Evolution Reaction". In: *Advanced Functional Materials* 32.52 (2022). ISSN: 1616-301X. DOI: 10.1002/adfm.202208994.

[60] J. Wang, X. Zhao, G. Zou, L. Zhang, S. Han, Y. Li, D. Liu, C. Fernandez, L. Li, L. Ren, and Q. Peng. "Crystal-defect engineering of electrode materials for energy storage and conversion". In: *Materials Today Nano* 22 (2023). ISSN: 25888420. DOI: 10.1016/j.mtnano.2023.100336.

[61] "Doping in 2D". In: *Nature Electronics* 4.10 (2021), pp. 699–699. ISSN: 2520-1131. DOI: 10.1038/s41928-021-00668-9.

[62] D. Lee, J. J. Lee, Y. S. Kim, Y. H. Kim, J. C. Kim, W. Huh, J. Lee, S. Park, H. Y. Jeong, Y. D. Kim, and C.-H. Lee. "Remote modulation doping in van der Waals heterostructure transistors". In: *Nature Electronics* 4.9 (2021), pp. 664–670. ISSN: 2520-1131. DOI: 10.1038/s41928-021-00641-6.

[63] S.-Y. Seo, G. Moon, O. F. N. Okello, M. Y. Park, C. Han, S. Cha, H. Choi, H. W. Yeom, S.-Y. Choi, J. Park, and M.-H. Jo. "Reconfigurable photo-induced doping of two-dimensional van der Waals semiconductors using different photon energies". In: *Nature Electronics* 4.1 (2021), pp. 38–44. ISSN: 2520-1131. DOI: 10.1038/s41928-020-00512-6.

[64] Y. Qi, M. A. Sadi, D. Hu, M. Zheng, Z. Wu, Y. Jiang, and Y. P. Chen. "Recent Progress in Strain Engineering on Van der Waals 2D Materials. Tunable Electrical, Electrochemical, Magnetic, and Optical Properties". In: *Advanced Materials* 35.12 (2023). ISSN: 0935-9648. DOI: 10.1002/adma.202205714.

[65] H. Li, F. Carrascoso, A. Borrás, G. P. Moreno, F. J. Aparicio, Á. Barranco, and A. C. Gómez. "Towards efficient strain engineering of 2D materials. A four-points bending approach for compressive strain". In: *Nano Research* 17.6 (2024), pp. 5317–5325. ISSN: 1998-0124. DOI: 10.1007/s12274-023-6402-7.

[66] G. H. Ahn, M. Amani, H. Rasool, D.-H. Lien, J. P. Mastandrea, J. W. A. III, M. Dubey, D. C. Chrzan, A. M. Minor, and A. Javey. "Strain-engineered growth of two-dimensional materials". In: *Nature Communications* 8.1 (2017). ISSN: 2041-1723. DOI: 10.1038/s41467-017-00516-5.

[67] Z. Peng, X. Chen, Y. Fan, D. J. Srolovitz, and D. Lei. "Strain engineering of 2D semiconductors and graphene. from strain fields to band-structure tuning and photonic applications". In: *Light: Science & Applications* 9.1 (2020). ISSN: 2047-7538. DOI: 10.1038/s41377-020-00421-5.

[68] E. Scalise, M. Houssa, G. Pourtois, V. Afanas'ev, and A. Stesmans. "Strain-induced semiconductor to metal transition in the two-dimensional honeycomb structure of MoS2". In: *Nano Research* 5.1 (2012), pp. 43–48. ISSN: 1998-0124. DOI: 10.1007/s12274-011-0183-0.

[69] G. Cocco, E. Cadelano, and L. Colombo. "Gap opening in graphene by shear strain". In: *Physical Review B* 81.24 (2010). ISSN: 1098-0121. DOI: 10.1103/PhysRevB.81.241412.

[70] A. Yadav, C. M. Acosta, G. M. Dalpian, and O. I. Malyi. "First-principles investigations of 2D materials. Challenges and best practices". In: *Matter* 6.9 (2023), pp. 2711–2734. ISSN: 25902385. DOI: 10.1016/j.matt.2023.05.019.

[71] S. K. Chakraborty, B. Kundu, B. Nayak, S. P. Dash, and P. K. Sahoo. "Challenges and opportunities in 2D heterostructures for electronic and optoelectronic devices". In: *IScience* 25.3 (2022). ISSN: 25890042. DOI: 10.1016/j.isci.2022.103942.

[72] Z. Zhang, X. Yang, K. Liu, and R. Wang. "Epitaxy of 2D Materials toward Single Crystals". In: *Advanced Science* 9.8 (2022). ISSN: 2198-3844. DOI: 10.1002/advs.202105201.

[73] A. K. Katiyar and J.-H. Ahn. "Strain-Engineered 2D Materials. Challenges, Opportunities, and Future Perspectives". In: *Small Methods* 9.3 (2025). ISSN: 2366-9608. DOI: 10.1002/smtd.202401404.

[74] A. Molle, C. Grazianetti, L. Tao, D. Taneja, M. H. Alam, and D. Akinwande. "Silicene, silicene derivatives, and their device applications". In: *Chemical Society Reviews* 47.16 (2018), pp. 6370–6387. ISSN: 0306-0012. DOI: 10.1039/C8CS00338F.

[75] A. Acun, L. Zhang, P. Bampoulis, M. Farmanbar, A. van Houselt, A. N. Rudenko, M. Lingenfelder, G. Brocks, B. Poelsema, M. I. Katsnelson, and H. J. W. Zandvliet. "Germanene. the germanium analogue of graphene". In: *Journal of Physics: Condensed Matter* 27.44 (2015-11-11). ISSN: 0953-8984. DOI: 10.1088/0953-8984/27/44/443002.

[76] S. Manzeli, D. Ovchinnikov, D. Pasquier, O. V. Yazyev, and A. Kis. "2D transition metal dichalcogenides". In: *Nature Reviews Materials* 2.8 (2017). ISSN: 2058-8437. DOI: 10.1038/natrevmats.2017.33.

[77] K. S. Novoselov, A. K. Geim, S. V. Morozov, D. Jiang, M. I. Katsnelson, I. V. Grigorieva, S. V. Dubonos, and A. A. Firsov. "Two-dimensional gas of massless Dirac fermions in graphene". In: *Nature* 438.7065 (2005), pp. 197–200. ISSN: 0028-0836. DOI: 10.1038/nature04233.

[78] Y. Zhang, Y.-W. Tan, H. L. Stormer, and P. Kim. "Experimental observation of the quantum Hall effect and Berry's phase in graphene". In: *Nature* 438.7065 (2005), pp. 201–204. ISSN: 0028-0836. DOI: 10.1038/nature04235.

[79] K. Bolotin, K. Sikes, Z. Jiang, M. Klima, G. Fudenberg, J. Hone, P. Kim, and H. Stormer. “Ultrahigh electron mobility in suspended graphene”. In: *Solid State Communications* 146.9-10 (2008), pp. 351–355. ISSN: 00381098. DOI: 10.1016/j.ssc.2008.02.024.

[80] X. Du, I. Skachko, A. Barker, and E. Y. Andrei. “Approaching ballistic transport in suspended graphene”. In: *Nature Nanotechnology* 3.8 (2008), pp. 491–495. ISSN: 1748-3387. DOI: 10.1038/nnano.2008.199.

[81] S. K. Krishnan, N. Nataraj, M. Meyyappan, and U. Pal. “Graphene-Based Field-Effect Transistors in Biosensing and Neural Interfacing Applications. Recent Advances and Prospects”. In: *Analytical Chemistry* 95.5 (2023-02-07), pp. 2590–2622. ISSN: 0003-2700. DOI: 10.1021/acs.analchem.2c03399.

[82] A. Béraud, M. Sauvage, C. M. Bazán, M. Tie, A. Bencherif, and D. Bouilly. “Graphene field-effect transistors as bioanalytical sensors. design, operation and performance”. In: *The Analyst* 146.2 (2021-01-25), pp. 403–428. ISSN: 0003-2654. DOI: 10.1039/D0AN01661F.

[83] Y. Y. Illarionov, T. Knobloch, B. Uzlu, A. G. Banshchikov, I. A. Ivanov, V. Sverdlov, M. Otto, S. L. Stoll, M. I. Vexler, M. Waltl, Z. Wang, B. Manna, D. Neumaier, M. C. Lemme, and N. S. Sokolov. “Variability and high temperature reliability of graphene field-effect transistors with thin epitaxial CaF2 insulators”. In: *Npj 2D Materials and Applications* 8.1 (2024). ISSN: 2397-7132. DOI: 10.1038/s41699-024-00461-0.

[84] X. Wang, L. Zhi, and K. Müllen. “Transparent, Conductive Graphene Electrodes for Dye-Sensitized Solar Cells”. In: *Nano Letters* 8.1 (2008-01-01), pp. 323–327. ISSN: 1530-6984. DOI: 10.1021/nl072838r.

[85] P. Blake, P. D. Brimicombe, R. R. Nair, T. J. Booth, D. Jiang, F. Schedin, L. A. Ponomarenko, S. V. Morozov, H. F. Gleeson, E. W. Hill, A. K. Geim, and K. S. Novoselov. “Graphene-Based Liquid Crystal Device”. In: *Nano Letters* 8.6 (2008-06-01), pp. 1704–1708. ISSN: 1530-6984. DOI: 10.1021/nl080649i.

[86] K. Cao, S. Feng, Y. Han, L. Gao, T. H. Ly, Z. Xu, and Y. Lu. “Elastic straining of free-standing monolayer graphene”. In: *Nature Communications* 11.1 (2020). ISSN: 2041-1723. DOI: 10.1038/s41467-019-14130-0.

[87] F. Liu, P. Ming, and J. Li. “Ab initio calculation of ideal strength and phonon instability of graphene under tension”. In: *Physical Review B* 76.6 (2007). ISSN: 1098-0121. DOI: 10.1103/PhysRevB.76.064120.

[88] W. Zhang, X. Zhang, L. K. Ono, Y. Qi, and H. Oughaddou. “Recent Advances in Phosphorene. Structure, Synthesis, and Properties”. In: *Small* 20.4 (2024). ISSN: 1613-6810. DOI: 10.1002/smll.202303115.

[89] F. Xia, H. Wang, and Y. Jia. “Rediscovering black phosphorus as an anisotropic layered material for optoelectronics and electronics”. In: *Nature Communications* 5.1 (2014-12-17). ISSN: 2041-1723. DOI: 10.1038/ncomms5458.

[90] L. Li, Y. Yu, G. J. Ye, Q. Ge, X. Ou, H. Wu, D. Feng, X. H. Chen, and Y. Zhang. "Black phosphorus field-effect transistors". In: *Nature Nanotechnology* 9.5 (2014), pp. 372–377. ISSN: 1748-3387. DOI: 10.1038/nnano.2014.35.

[91] N. Liu, G. Bo, Y. Liu, X. Xu, Y. Du, and S. X. Dou. "Recent Progress on Germanene and Functionalized Germanene. Preparation, Characterizations, Applications, and Challenges". In: *Small* 15.32 (2019). ISSN: 1613-6810. DOI: 10.1002/smll.201805147.

[92] D. Jose and A. Datta. "Structures and Chemical Properties of Silicene. Unlike Graphene". In: *Accounts of Chemical Research* 47.2 (2014-02-18), pp. 593–602. ISSN: 0001-4842. DOI: 10.1021/ar400180e.

[93] A. Acun, B. Poelsema, H. J. W. Zandvliet, and R. van Gastel. "The instability of silicene on Ag(111)". In: *Applied Physics Letters* 103.26 (2013-12-23). ISSN: 0003-6951. DOI: 10.1063/1.4860964.

[94] T. Hartman and Z. Sofer. "Beyond Graphene. Chemistry of Group 14 Graphene Analogues: Silicene, Germanene, and Stanene". In: *ACS Nano* 13.8 (2019-08-27), pp. 8566–8576. ISSN: 1936-0851. DOI: 10.1021/acsnano.9b04466.

[95] S. Trivedi, A. Srivastava, and R. Kurchania. "Silicene and Germanene. A First Principle Study of Electronic Structure and Effect of Hydrogenation-Passivation". In: *Journal of Computational and Theoretical Nanoscience* 11.3 (2014-03-01), pp. 781–788. ISSN: 15461955. DOI: 10.1166/jctn.2014.3428.

[96] D. S. Dhungana, C. Massetti, C. Martella, C. Grazianetti, and A. Molle. "All-around encapsulation of silicene". In: *Nanoscale Horizons* 8.10 (2023-09-26), pp. 1428–1434. ISSN: 2055-6756. DOI: 10.1039/D3NH00309D.

[97] N. S. Arul and V. D. Nithya. *Two Dimensional Transition Metal Dichalcogenides*. Singapore: Springer Singapore, 2019. ISBN: 978-981-13-9044-9. DOI: 10.1007/978-981-13-9045-6.

[98] R. Yang, Y. Fan, Y. Zhang, L. Mei, R. Zhu, J. Qin, J. Hu, Z. Chen, Y. H. Ng, D. Voiry, S. Li, Q. Lu, Q. Wang, J. C. Yu, and Z. Zeng. "2D Transition Metal Dichalcogenides for Photocatalysis". In: *Angewandte Chemie International Edition* 62.13 (2023-03-20). ISSN: 1433-7851. DOI: 10.1002/anie.202218016.

[99] H. M. Hill, A. F. Rigosi, K. T. Rim, G. W. Flynn, and T. F. Heinz. "Band Alignment in MoS 2 /WS 2 Transition Metal Dichalcogenide Heterostructures Probed by Scanning Tunneling Microscopy and Spectroscopy". In: *Nano Letters* 16.8 (2016-08-10), pp. 4831–4837. ISSN: 1530-6984. DOI: 10.1021/acs.nanolett.6b01007.

[100] S. Yang, C. Wang, H. Sahin, H. Chen, Y. Li, S.-S. Li, A. Suslu, F. M. Peeters, Q. Liu, J. Li, and S. Tongay. "Tuning the Optical, Magnetic, and Electrical Properties of ReSe 2 by Nanoscale Strain Engineering". In: *Nano Letters* 15.3 (2015-03-11), pp. 1660–1666. ISSN: 1530-6984. DOI: 10.1021/nl504276u.

[101] M. Xu, T. Liang, M. Shi, and H. Chen. “Graphene-Like Two-Dimensional Materials”. In: *Chemical Reviews* 113.5 (2013-05-08), pp. 3766–3798. ISSN: 0009-2665. DOI: 10.1021/cr300263a.

[102] Y. Cai, Y. Liu, Y. Xie, Y. Zou, C. Gao, Y. Zhao, S. Liu, H. Xu, J. Shi, S. Guo, and C. Sun. “Band structure, effective mass, and carrier mobility of few-layer h -AlN under layer and strain engineering”. In: *APL Materials* 8.2 (2020-02-01). ISSN: 2166-532X. DOI: 10.1063/1.5139664.

[103] D. H. Ozbey, M. E. Kilic, and E. Durgun. “Promising anisotropic mechanical, electronic, and charge transport properties of 2D InN alloys for photocatalytic water splitting”. In: *Applied Surface Science* 638 (2023). ISSN: 01694332. DOI: 10.1016/j.apsusc.2023.157982.

[104] M. Kolos and F. Karlický. “Accurate many-body calculation of electronic and optical band gap of bulk hexagonal boron nitride”. In: *Physical Chemistry Chemical Physics* 21.7 (2019-02-13), pp. 3999–4005. ISSN: 1463-9076. DOI: 10.1039/C8CP07328G.

[105] X. D. Pu, J. Chen, W. Z. Shen, H. Ogawa, and Q. X. Guo. “Temperature dependence of Raman scattering in hexagonal indium nitride films”. In: *Journal of Applied Physics* 98.3 (2005-08-01). ISSN: 0021-8979. DOI: 10.1063/1.2006208.

[106] L. Liu, Y. P. Feng, and Z. X. Shen. “Structural and electronic properties of h -BN”. In: *Physical Review B* 68.10 (2003). ISSN: 0163-1829. DOI: 10.1103/PhysRevB.68.104102.

[107] K. Zhang, Y. Feng, F. Wang, Z. Yang, and J. Wang. “Two dimensional hexagonal boron nitride (2D-hBN). synthesis, properties and applications”. In: *Journal of Materials Chemistry C* 5.46 (2017), pp. 11992–12022. ISSN: 2050-7526. DOI: 10.1039/C7TC04300G.

[108] F. Yang, A. D. McQuain, A. Kumari, D. Gundurao, H. Liu, and L. Li. “Understanding the Intrinsic Water Wettability of Hexagonal Boron Nitride”. In: *Langmuir* 40.12 (2024-03-26), pp. 6445–6452. ISSN: 0743-7463. DOI: 10.1021/acs.langmuir.3c04035.

[109] M. N. Ivanova, Y. A. Vorotnikov, E. E. Plotnikova, M. V. Marchuk, A. A. Ivanov, I. P. Asanov, A. R. Tsygankova, E. D. Grayfer, V. E. Fedorov, and M. A. Shestopalov. “Hexamolybdenum Clusters Supported on Exfoliated h-BN Nanosheets for Photocatalytic Water Purification”. In: *Inorganic Chemistry* 59.9 (2020-05-04), pp. 6439–6448. ISSN: 0020-1669. DOI: 10.1021/acs.inorgchem.0c00528.

[110] N. Kostoglou, K. Polychronopoulou, and C. Rebholz. “Thermal and chemical stability of hexagonal boron nitride (h-BN) nanoplatelets”. In: *Vacuum* 112 (2015), pp. 42–45. ISSN: 0042207X. DOI: 10.1016/j.vacuum.2014.11.009.

[111] S. Ali, P. M. Ismail, M. Humayun, and M. Bououdina. “Hexagonal boron nitride. From fundamentals to applications”. In: *Desalination* 599 (2025). ISSN: 00119164. DOI: 10.1016/j.desal.2024.118442.

[112] J. Ghosh, S. Mazumdar, M. Das, S. Ghatak, and A. Basu. "Microstructural characterization of amorphous and nanocrystalline boron nitride prepared by high-energy ball milling". In: *Materials Research Bulletin* 43.4 (2008), pp. 1023–1031. ISSN: 00255408. DOI: 10.1016/j.materresbull.2007.04.022.

[113] H. Yurdakul, Y. Göncü, O. Durukan, A. Akay, A. T. Seyhan, N. Ay, and S. Turan. "Nanoscopic characterization of two-dimensional (2D) boron nitride nanosheets (BNNSs) produced by microfluidization". In: *Ceramics International* 38.3 (2012), pp. 2187–2193. ISSN: 02728842. DOI: 10.1016/j.ceramint.2011.10.064.

[114] A. Falin, Q. Cai, E. J. Santos, D. Scullion, D. Qian, R. Zhang, Z. Yang, S. Huang, K. Watanabe, T. Taniguchi, M. R. Barnett, Y. Chen, R. S. Ruoff, and L. H. Li. "Mechanical properties of atomically thin boron nitride and the role of interlayer interactions". In: *Nature Communications* 8.1 (2017-08-30). ISSN: 2041-1723. DOI: 10.1038/ncomms15815.

[115] L. Song, L. Ci, H. Lu, P. B. Sorokin, C. Jin, J. Ni, A. G. Kvashnin, D. G. Kvashnin, J. Lou, B. I. Yakobson, and P. M. Ajayan. "Large Scale Growth and Characterization of Atomic Hexagonal Boron Nitride Layers". In: *Nano Letters* 10.8 (2010-08-11), pp. 3209–3215. ISSN: 1530-6984. DOI: 10.1021/nl1022139.

[116] Y. Shi, C. Hamsen, X. Jia, K. K. Kim, A. Reina, M. Hofmann, A. L. Hsu, K. Zhang, H. Li, Z.-Y. Juang, M. S. Dresselhaus, L.-J. Li, and J. Kong. "Synthesis of Few-Layer Hexagonal Boron Nitride Thin Film by Chemical Vapor Deposition". In: *Nano Letters* 10.10 (2010-10-13), pp. 4134–4139. ISSN: 1530-6984. DOI: 10.1021/nl1023707.

[117] C. A. Klein and G. F. Cardinale. "Young's modulus and Poisson's ratio of CVD diamond". In: *Diamond and Related Materials* 2.5-7 (1993), pp. 918–923. ISSN: 09259635. DOI: 10.1016/0925-9635(93)90250-6.

[118] F. Schwierz. "Graphene transistors". In: *Nature Nanotechnology* 5.7 (2010), pp. 487–496. ISSN: 1748-3387. DOI: 10.1038/nnano.2010.89.

[119] G. Shen and Z. Fan. *Flexible electronics. from materials to devices*. New Jersey: World Scientific, [2016]. ISBN: 978-981-4651-98-1.

[120] G. Malucelli. "The Role of Graphene in Flame Retardancy of Polymeric Materials. Recent Advances". In: *Current Graphene Science* 2.1 (2018-10-09), pp. 27–34. ISSN: 24522732. DOI: 10.2174/2452273202666180706145545.

[121] J. Zhou, L. Shen, M. D. Costa, K. A. Persson, S. P. Ong, P. Huck, Y. Lu, X. Ma, Y. Chen, H. Tang, and Y. P. Feng. "2DMatPedia, an open computational database of two-dimensional materials from top-down and bottom-up approaches". In: *Scientific Data* 6.1 (2019). ISSN: 2052-4463. DOI: 10.1038/s41597-019-0097-3.

[122] K. S. Novoselov and A. H. C. Neto. "Two-dimensional crystals-based heterostructures. materials with tailored properties". In: *Physica Scripta* T146 (2012-01-31). ISSN: 0031-8949. DOI: 10.1088/0031-8949/2012/T146/014006.

[123] V. León, A. M. Rodriguez, P. Prieto, M. Prato, and E. Vázquez. “Exfoliation of Graphite with Triazine Derivatives under Ball-Milling Conditions via Selective Noncovalent Interactions. Preparation of Few-Layer Graphene via Selective Noncovalent Interactions”. In: *ACS Nano* 8.1 (2014-01-28), pp. 563–571. ISSN: 1936-0851. DOI: 10.1021/nn405148t.

[124] Y.-C. Lin, B. Jariwala, B. M. Bersch, K. Xu, Y. Nie, B. Wang, S. M. Eichfeld, X. Zhang, T. H. Choudhury, Y. Pan, R. Addou, C. M. Smyth, J. Li, K. Zhang, and M. A. Haque. “Realizing Large-Scale, Electronic-Grade Two-Dimensional Semiconductors”. In: *ACS Nano* 12.2 (2018-02-27), pp. 965–975. ISSN: 1936-0851. DOI: 10.1021/acsnano.7b07059.

[125] C. Muratore, A. A. Voevodin, and N. R. Glavin. “Physical vapor deposition of 2D Van der Waals materials. a review”. In: *Thin Solid Films* 688 (2019). ISSN: 00406090. DOI: 10.1016/j.tsf.2019.137500.

[126] C. Kim, M. Yoon, B. Jang, J. Kim, and K. Kim. “Review on Transfer Process of Two-dimensional Materials”. In: *Tribology and Lubricants* 36.1 (2020-01-01), pp. 1–10. ISSN: 2713-8011. DOI: 10.9725/kts.2020.36.1.1.

[127] H. Li, X. Xiong, F. Hui, D. Yang, J. Jiang, W. Feng, J. Han, J. Duan, Z. Wang, and L. Sun. “Constructing van der Waals heterostructures by dry-transfer assembly for novel optoelectronic device”. In: *Nanotechnology* 33.46 (2022-08-30). ISSN: 0957-4484. DOI: 10.1088/1361-6528/ac5f96.

[128] A. J. Watson, W. Lu, M. H. D. Guimarães, and M. Stöhr. “Transfer of large-scale two-dimensional semiconductors. challenges and developments”. In: *2D Materials* 8.3 (2021-05-03). ISSN: 2053-1583. DOI: 10.1088/2053-1583/abf234.

[129] X. Li, Y. Zhu, W. Cai, M. Borysiak, B. Han, D. Chen, R. D. Piner, L. Colombo, and R. S. Ruoff. “Transfer of Large-Area Graphene Films for High-Performance Transparent Conductive Electrodes”. In: *Nano Letters* 9.12 (2009-12-09), pp. 4359–4363. ISSN: 1530-6984. DOI: 10.1021/nl902623y.

[130] J. S. Lee, S. H. Choi, S. J. Yun, Y. I. Kim, S. Boandoh, J.-H. Park, B. G. Shin, H. Ko, S. H. Lee, Y.-M. Kim, Y. H. Lee, K. K. Kim, and S. M. Kim. “Wafer-scale single-crystal hexagonal boron nitride film via self-collimated grain formation”. In: *Science* 362.6416 (2018-11-16), pp. 817–821. ISSN: 0036-8075. DOI: 10.1126/science.aau2132.

[131] L. Wang, X. Xu, L. Zhang, R. Qiao, M. Wu, Z. Wang, S. Zhang, J. Liang, Z. Zhang, Z. Zhang, W. Chen, X. Xie, J. Zong, Y. Shan, and Y. Guo. “Epitaxial growth of a 100-square-centimetre single-crystal hexagonal boron nitride monolayer on copper”. In: *Nature* 570.7759 (2019), pp. 91–95. ISSN: 0028-0836. DOI: 10.1038/s41586-019-1226-z.

[132] S. M. Shinde, T. Das, A. T. Hoang, B. K. Sharma, X. Chen, and J.-H. Ahn. "Surface-Functionalization-Mediated Direct Transfer of Molybdenum Disulfide for Large-Area Flexible Devices". In: *Advanced Functional Materials* 28.13 (2018). ISSN: 1616-301X. DOI: 10.1002/adfm.201706231.

[133] A. Pirkle, J. Chan, A. Venugopal, D. Hinojos, C. W. Magnuson, S. McDonnell, L. Colombo, E. M. Vogel, R. S. Ruoff, and R. M. Wallace. "The effect of chemical residues on the physical and electrical properties of chemical vapor deposited graphene transferred to SiO2". In: *Applied Physics Letters* 99.12 (2011-09-19). ISSN: 0003-6951. DOI: 10.1063/1.3643444.

[134] Y.-C. Lin, C. Jin, J.-C. Lee, S.-F. Jen, K. Suenaga, and P.-W. Chiu. "Clean Transfer of Graphene for Isolation and Suspension". In: *ACS Nano* 5.3 (2011-03-22), pp. 2362–2368. ISSN: 1936-0851. DOI: 10.1021/nn200105j.

[135] X. Liang, B. A. Sperling, I. Calizo, G. Cheng, C. A. Hacker, Q. Zhang, Y. Obeng, K. Yan, H. Peng, Q. Li, X. Zhu, H. Yuan, A. R. H. Walker, Z. Liu, and L.-m. Peng. "Toward Clean and Crackless Transfer of Graphene". In: *ACS Nano* 5.11 (2011-11-22), pp. 9144–9153. ISSN: 1936-0851. DOI: 10.1021/nn203377t.

[136] C. Gong, H. C. Floresca, D. Hinojos, S. McDonnell, X. Qin, Y. Hao, S. Jandhyala, G. Mordi, J. Kim, L. Colombo, R. S. Ruoff, M. J. Kim, K. Cho, R. M. Wallace, and Y. J. Chabal. "Rapid Selective Etching of PMMA Residues from Transferred Graphene by Carbon Dioxide". In: *The Journal of Physical Chemistry C* 117.44 (2013-11-07), pp. 23000–23008. ISSN: 1932-7447. DOI: 10.1021/jp408429v.

[137] H. H. Kim, B. Kang, J. W. Suk, N. Li, K. S. Kim, R. S. Ruoff, W. H. Lee, and K. Cho. "Clean Transfer of Wafer-Scale Graphene via Liquid Phase Removal of Polycyclic Aromatic Hydrocarbons". In: *ACS Nano* 9.5 (2015-05-26), pp. 4726–4733. ISSN: 1936-0851. DOI: 10.1021/nn5066556.

[138] H. V. Ngoc, Y. Qian, S. K. Han, and D. J. Kang. "PMMA-Etching-Free Transfer of Wafer-scale Chemical Vapor Deposition Two-dimensional Atomic Crystal by a Water Soluble Polyvinyl Alcohol Polymer Method". In: *Scientific Reports* 6.1 (2016-12-16). ISSN: 2045-2322. DOI: 10.1038/srep33096.

[139] S. Shin, S. Kim, T. Kim, H. Du, K. S. Kim, S. Cho, and S. Seo. "Graphene transfer with self-doping by amorphous thermoplastic resins". In: *Carbon* 111 (2017), pp. 215–220. ISSN: 00086223. DOI: 10.1016/j.carbon.2016.09.077.

[140] W. S. Leong, H. Wang, J. Yeo, F. J. Martin-Martinez, A. Zubair, P.-C. Shen, Y. Mao, T. Palacios, M. J. Buehler, J.-Y. Hong, and J. Kong. "Paraffin-enabled graphene transfer". In: *Nature Communications* 10.1 (2019). ISSN: 2041-1723. DOI: 10.1038/s41467-019-08813-x.

[141] Z. Zhang, J. Du, D. Zhang, H. Sun, L. Yin, L. Ma, J. Chen, D. Ma, H.-M. Cheng, and W. Ren. "Rosin-enabled ultraclean and damage-free transfer of graphene for large-area flexible organic light-emitting diodes". In: *Nature Communications* 8.1 (2017-04-28). ISSN: 2041-1723. DOI: 10.1038/ncomms14560.

[142] Y. Lee, S. Bae, H. Jang, S. Jang, S.-E. Zhu, S. H. Sim, Y. I. Song, B. H. Hong, and J.-H. Ahn. “Wafer-Scale Synthesis and Transfer of Graphene Films”. In: *Nano Letters* 10.2 (2010-02-10), pp. 490–493. ISSN: 1530-6984. DOI: 10.1021/nl903272n.

[143] A. Jain, P. Bharadwaj, S. Heeg, M. Parzefall, T. Taniguchi, K. Watanabe, and L. Novotny. “Minimizing residues and strain in 2D materials transferred from PDMS”. In: *Nanotechnology* 29.26 (2018-06-29). ISSN: 0957-4484. DOI: 10.1088/1361-6528/aabd90.

[144] K. T. Lim, S. E. Webber, and K. P. Johnston. “Synthesis and Characterization of Poly(dimethyl siloxane)−Poly[alkyl (meth)acrylic acid] Block Copolymers”. In: *Macromolecules* 32.9 (1999-05-01), pp. 2811–2815. ISSN: 0024-9297. DOI: 10.1021/ma981658o.

[145] M.-A. Kang, S. J. Kim, W. Song, S.-j. Chang, C.-Y. Park, S. Myung, J. Lim, S. S. Lee, and K.-S. An. “Fabrication of flexible optoelectronic devices based on MoS2/graphene hybrid patterns by a soft lithographic patterning method”. In: *Carbon* 116 (2017), pp. 167–173. ISSN: 00086223. DOI: 10.1016/j.carbon.2017.02.001.

[146] K. Kinoshita, R. Moriya, M. Onodera, Y. Wakafuji, S. Masubuchi, K. Watanabe, T. Taniguchi, and T. Machida. “Dry release transfer of graphene and few-layer h-BN by utilizing thermoplasticity of polypropylene carbonate”. In: *Npj 2D Materials and Applications* 3.1 (2019). ISSN: 2397-7132. DOI: 10.1038/s41699-019-0104-8.

[147] K. L. Haley, J. A. Cloninger, K. Cerminara, R. M. Sterbentz, T. Taniguchi, K. Watanabe, and J. O. Island. “Heated Assembly and Transfer of Van der Waals Heterostructures with Common Nail Polish”. In: *Nanomanufacturing* 1.1 (2021), pp. 49–56. ISSN: 2673-687X. DOI: 10.3390/nanomanufacturing1010005.

[148] I. G. Rebollo, F. C. Rodrigues-Machado, W. Wright, G. J. Melin, and A. R. Champagne. “Thin-suspended 2D materials. facile, versatile, and deterministic transfer assembly”. In: *2D Materials* 8.3 (2021-05-03). ISSN: 2053-1583. DOI: 10.1088/2053-1583/abf98c.

[149] D.-Y. Wang, I.-S. Huang, P.-H. Ho, S.-S. Li, Y.-C. Yeh, D.-W. Wang, W.-L. Chen, Y.-Y. Lee, Y.-M. Chang, C.-C. Chen, C.-T. Liang, and C.-W. Chen. “Clean-Lifting Transfer of Large-area Residual-Free Graphene Films”. In: *Advanced Materials* 25.32 (2013-08-27), pp. 4521–4526. ISSN: 0935-9648. DOI: 10.1002/adma.201301152.

[150] J. Seo, C. Kim, B. S. Ma, T.-I. Lee, J. H. Bong, J. G. Oh, B. J. Cho, and T.-S. Kim. “Direct Graphene Transfer and Its Application to Transfer Printing Using Mechanically Controlled, Large Area Graphene/Copper Freestanding Layer”. In: *Advanced Functional Materials* 28.26 (2018). ISSN: 1616-301X. DOI: 10.1002/adfm.201707102.

[151] G. Zhang, A. G. Güell, P. M. Kirkman, R. A. Lazenby, T. S. Miller, and P. R. Unwin. “Versatile Polymer-Free Graphene Transfer Method and Applications”. In: *ACS Applied Materials & Interfaces* 8.12 (2016-03-30), pp. 8008–8016. ISSN: 1944-8244. DOI: 10.1021/acsami.6b00681.

[152] F. Roccaforte and M. Leszczynski. *Nitride Semiconductor Technology*. Wiley, 2020-09-15. ISBN: 9783527347100. DOI: 10.1002/9783527825264.

[153] H. Xing, S. Keller, Y.-F. Wu, L. McCarthy, I. P. Smorchkova, D. Buttari, R. Coffie, D. S. Green, G. Parish, S. Heikman, L. Shen, N. Zhang, J. J. Xu, B. P. Keller, and S. P. DenBaars. “Gallium nitride based transistors”. In: *Journal of Physics: Condensed Matter* 13.32 (2001-08-13), pp. 7139–7157. ISSN: 0953-8984. DOI: 10.1088/0953-8984/13/32/317.

[154] K. Miwa and A. Fukumoto. “First-principles calculation of the structural, electronic, and vibrational properties of gallium nitride and aluminum nitride”. In: *Physical Review B* 48.11 (1993), pp. 7897–7902. ISSN: 0163-1829. DOI: 10.1103/PhysRevB.48.7897.

[155] S. Mohammad, A. Salvador, and H. Morkoc. “Emerging gallium nitride based devices”. In: *Proceedings of the IEEE* 83.10 (), pp. 1306–1355. ISSN: 00189219. DOI: 10.1109/5.469300.

[156] H. D. Jabbar, M. A. Fakhri, and M. J. AbdulRazzaq. “Synthesis Gallium Nitride on Porous Silicon Nano-Structure for Optoelectronics Devices”. In: *Silicon* 14.18 (2022), pp. 12837–12853. ISSN: 1876-990X. DOI: 10.1007/s12633-022-01999-8.

[157] R. C. Sharma, R. Nandal, N. Tanwar, R. Yadav, J. Bhardwaj, and A. Verma. “Gallium Arsenide and Gallium Nitride Semiconductors for Power and Optoelectronics Devices Applications”. In: *Journal of Physics: Conference Series* 2426.1 (2023-02-01). ISSN: 1742-6588. DOI: 10.1088/1742-6596/2426/1/012008.

[158] S. Denbaars. “Gallium-nitride-based materials for blue to ultraviolet optoelectronics devices”. In: *Proceedings of the IEEE* 85.11 (), pp. 1740–1749. ISSN: 00189219. DOI: 10.1109/5.649651.

[159] The Royal Swedish Academy of Sciences. *The Nobel Prize in Physics 2014 - Press Release*. Awarded to Isamu Akasaki, Hiroshi Amano, and Shuji Nakamura for the invention of efficient blue light-emitting diodes. 2014-10-07.

[160] Y. Liu, H. Wu, K. Zhang, Q. Wang, J. Peng, F. Wu, C. He, and H. Dong. “The electronic and mechanical properties of two dimensional multilayered GaN: A first-principles study”. In: *Materials Today Communications* 37 (2023), p. 107425. ISSN: 2352-4928. DOI: 10.1016/j.mtcomm.2023.107425.

[161] N. Sanders, D. Bayerl, G. Shi, K. A. Mengle, and E. Kioupakis. “Electronic and Optical Properties of Two-Dimensional GaN from First-Principles”. In: *Nano Letters* 17.12 (2017-12-13), pp. 7345–7349. ISSN: 1530-6984. DOI: 10.1021/acs.nanolett.7b03003.

[162] H. Qin, X. Luan, C. Feng, D. Yang, and G. Zhang. “Mechanical, Thermodynamic and Electronic Properties of Wurtzite and Zinc-Blende GaN Crystals”. In: *Materials* 10.12 (2017), p. 1419. ISSN: 1996-1944. DOI: 10.3390/ma10121419.

[163] A. V. Kolobov, P. Fons, J. Tominaga, B. Hyot, and B. André. “Instability and Spontaneous Reconstruction of Few-Monolayer Thick GaN Graphitic Structures”. In: *Nano Letters* 16.8 (2016-08-10), pp. 4849–4856. ISSN: 1530-6984. DOI: 10.1021/acs.nanolett.6b01225.

[164] Y. Dai, S. Xia, H. Shi, Y. Wang, X. Wu, and Y. Diao. “Two-dimensional GaN of wurtzite hexagonal and haeckelite (4|8) structure with multiple layers. A first principle DFT study on structural and optoelectronic properties”. In: *Physica E: Low-dimensional Systems and Nanostructures* 168 (2025). ISSN: 13869477. DOI: 10.1016/j.physe.2025.116193.

[165] J. Mach, T. Šamořil, S. Voborný, M. Kolíbal, J. Zlámal, J. Spousta, L. Dittrichová, and T. Šikola. “An ultra-low energy (30–200 eV) ion-atomic beam source for ion-beam-assisted deposition in ultrahigh vacuum”. In: *Review of Scientific Instruments* 82.8 (2011). ISSN: 1089-7623. DOI: 10.1063/1.3622749.

[166] C. G. Van de Walle. “Effects of impurities on the lattice parameters of GaN”. In: *Physical Review B* 68.16 (2003). ISSN: 1095-3795. DOI: 10.1103/physrevb.68.165209.

[167] S. Zhang, J. Zhou, Q. Wang, X. Chen, Y. Kawazoe, and P. Jena. “Penta-graphene: A new carbon allotrope”. In: *Proceedings of the National Academy of Sciences* 112.8 (2015), pp. 2372–2377. ISSN: 1091-6490. DOI: 10.1073/pnas.1416591112.

[168] A. Zavabeti, J. Z. Ou, B. J. Carey, N. Syed, R. Orrell-Trigg, E. L. H. Mayes, C. Xu, O. Kavehei, A. P. O’Mullane, R. B. Kaner, K. Kalantar-zadeh, and T. Daeneke. “A liquid metal reaction environment for the room-temperature synthesis of atomically thin metal oxides”. In: *Science* 358.6361 (2017), pp. 332–335. ISSN: 1095-9203. DOI: 10.1126/science.aao4249.

[169] B. J. Carey, J. Z. Ou, R. M. Clark, K. J. Berean, A. Zavabeti, A. S. R. Chesman, S. P. Russo, D. W. M. Lau, Z.-Q. Xu, Q. Bao, O. Kavehei, B. C. Gibson, M. D. Dickey, R. B. Kaner, T. Daeneke, and K. Kalantar-Zadeh. “Wafer-scale two-dimensional semiconductors from printed oxide skin of liquid metals”. In: *Nature Communications* 8.1 (2017). ISSN: 2041-1723. DOI: 10.1038/ncomms14482.

[170] V. Lakhotia, D. A. Neumayer, A. H. Cowley, R. A. Jones, and J. G. Ekerdt. “GaN Film Growth Using Single-Source Precursors”. In: *Chemistry of Materials* 7.3 (1995), pp. 546–552. ISSN: 1520-5002. DOI: 10.1021/cm00051a016.

[171] J.-W. Zhao, Y.-F. Zhang, Y.-H. Li, C.-h. Su, X.-M. Song, H. Yan, and R.-Z. Wang. “A low cost, green method to synthesize GaN nanowires”. In: *Scientific Reports* 5.1 (2015). ISSN: 2045-2322. DOI: 10.1038/srep17692.

[172] N. F. Patel, S. A. Bhakhar, G. K. Solanki, K. D. Patel, V. M. Pathak, C. K. Zankat, P. M. Pataniya, J. D. Gohil, and S. U. Gupta. “Sonochemical exfoliation, characterization and photoresponse of MoS0.5Se1.5 nanosheets”. In: *Journal of Materials Science: Materials in Electronics* 32.9 (2021), pp. 11805–11812. ISSN: 1573-482X. DOI: 10.1007/s10854-021-05810-z.

[173] N. K. Nobuyuki Koguchi and K. I. Keiko Ishige. “Growth of GaAs Epitaxial Microcrystals on an S-Terminated GaAs Substrate by Successive Irradiation of Ga and As Molecular Beams”. In: *Japanese Journal of Applied Physics* 32.5R (1993), p. 2052. ISSN: 1347-4065. DOI: 10.1143/jjap.32.2052.

[174] J. Stangl, V. Holý, and G. Bauer. “Structural properties of self-organized semiconductor nanostructures”. In: *Reviews of Modern Physics* 76.3 (2004), pp. 725–783. ISSN: 1539-0756. DOI: 10.1103/revmodphys.76.725.

[175] M. L. V. GAYLER. “Melting Point of High-Purity Silicon”. In: *Nature* 142.3593 (1938-09-10), pp. 478–478. ISSN: 0028-0836. DOI: 10.1038/142478a0.

[176] J. Mach, T. Šamořil, S. Voborný, M. Kolíbal, J. Zlámal, J. Spousta, L. Dittrichová, and T. Šikola. “An ultra-low energy (30–200 eV) ion-atomic beam source for ion-beam-assisted deposition in ultrahigh vacuum”. In: *Review of Scientific Instruments* 82.8 (2011-08-01). ISSN: 0034-6748. DOI: 10.1063/1.3622749.

[177] M. Khoury, O. Tottereau, G. Feuillet, P. Vennéguès, and J. Zúñiga-Pérez. “Evolution and prevention of meltback etching. Case study of semipolar GaN growth on patterned silicon substrates”. In: *Journal of Applied Physics* 122.10 (2017-09-14). ISSN: 0021-8979. DOI: 10.1063/1.5001914.

[178] S. Zhao, H. Wang, L. Niu, W. Xiong, Y. Chen, M. Zeng, S. Yuan, and L. Fu. “2D GaN for Highly Reproducible Surface Enhanced Raman Scattering”. In: *Small* 17.45 (2021). ISSN: 1613-6810. DOI: 10.1002/smll.202103442.

[179] V. Bajo. *Application of four-dimensional scanning transmission electron microscopy in the scanning electron microscopy.* Master’s thesis. 2025.

[180] Y. Song, X. Wu, W. Wang, W. Yuan, and X. Chen. “Thermal stability and electronic specific heat of GaN”. In: *Journal of Alloys and Compounds* 370.1-2 (2004), pp. 65–68. ISSN: 09258388. DOI: 10.1016/j.jallcom.2003.09.110.

[181] H. Ishikawa, K. Yamamoto, T. Egawa, T. Soga, T. Jimbo, and M. Umeno. “Thermal stability of GaN on (1 1 1) Si substrate”. In: *Journal of Crystal Growth* 189-190 (1998), pp. 178–182. ISSN: 00220248. DOI: 10.1016/S0022-0248(98)00223-1.

[182] J. Low, M. Kreider, D. Pulsifer, A. Jones, and T. Gilani. “Band Gap Energy in Silicon”. In: *American Journal of Undergraduate Research* 7.1 (2008-6-20). ISSN: 15364585. DOI: 10.33697/ajur.2008.010.

[183] R. Oosterbroek, J. Berenschot, H. Jansen, A. Nijdam, G. Pandraud, A. van den Berg, and M. Elwenspoek. “Etching methodologies in 111-oriented silicon wafers”. In: *Journal of Microelectromechanical Systems* 9.3 (2000), pp. 390–398. ISSN: 1057-7157. DOI: 10.1109/84.870065.

[184] P. Allongue, V. Costa-Kieling, and H. Gerischer. “Etching of Silicon in NaOH Solutions. II . Electrochemical Studies of n-Si(111) and (100) and Mechanism of the Dissolution”. In: *Journal of The Electrochemical Society* 140.4 (1993-04-01), pp. 1018–1026. ISSN: 0013-4651. DOI: 10.1149/1.2056190.

List of Abbreviations

γ-Ga_2O_3 gamma gallium oxide

2D two-dimensional

2D GaN two-dimensional gallium nitride

4D-STEM four-dimensional scanning transmission electron microscopy

AFM atomic force microscopy

Ag_2Te silver telluride

AlN aluminium nitride

BN boron nitride

$C_2H_2O_4$+($2H_2O$) oxalic acid dihydrate

CH_4N_2O urea

CL cathodoluminescence

CVD chemical vapor deposition

DE droplet epitaxy

DFT density functional theory

DI deionised

DMF N N-dimethylformamide

DMSO dimethyl sulfoxide

DOS density of states

EDX energy-dispersive x-ray spectroscopy

FETs field-effect transistors

$Ga(CH_3)_3$ trimethylgallium

$Ga(OH)_3$ gallium hydroxide

$GaCl_3$ gallium chloride

GaN gallium nitride

GaOOH gallium oxyhydroxide

GaS gallium sulfide

GaSe gallium selenide

GeSe germanium selenide

GO graphene oxide

H_2O_2 hydrogen peroxide

h-BN hexagonal boron nitride

h-InN hexagonal indium nitride

HCl hydrogen chloride

HfS_2 hafnium disulfide

HRTEM high-resolution transmission electron microscopy

InN indium nitride

IPA isopropyl alcohol

LEDs light-emmiting devices

LEED low-energy electron diffraction

LTDE low temperature droplet epitaxy

MBE molecular beam epitaxy

MEEG migration-enhanced encapsulated growth

MOCVD metal-oxide chemical vapor deposition

MoS_2 molybdenum disulfide

$MoSe_2$ molybdenum diselenide

$MoTe_2$ molybdenum ditelluride

NbS_2 niobium disulfide

NH_3 ammonia

PBN pyrolytic boron nitride

PDMS polydimethylsiloxane

PECVD plasma-enhanced chemical vapor deposition

PL photoluminescence

PLD pulse laser deposition

PMMA polymethyl methacrylate

PVA polyvinyl alcohol

PVD physical vapor deposition

PVP polyvinylpyrrolidone

SEM scanning electron microscopy

STM scanning tunnelling microscopy

TMDs transition metal dichalcogenides

TMNs transition metal nitrides

UHV ultra-high vacuum

UHV-SEM ultra-high vacuum scanning electron microscope

UV ultraviolet

VSe_2 vanadium diselenide

WS_2 tungsten disulfide

WSe_2 tungsten diselenide

XPS x-ray photoelectron spectroscopy